2024

Journal of JART

—English edition—

2024

The Japan Association of Radiological Technologists

Journal of JART —English edition—
2024
The Japan Association of Radiological Technologists

CONTENTS

Note: The contents of this magazine are those that have been published in JART magazine.

Overview of the Japan Association of Radiological Technologists

The Japan Association of Radiological Technologists, a public interest incorporated association under the jurisdiction of the Ministry of Health, Labour and Welfare, was established in 1947 with the purpose of contributing to the health of citizens through raising the professional ethics of members, improving and furthering the study of medical radiology and medical radiological technology, and enhancing public health.

In light of the startling progress being made in the fields of image diagnostics and radiation therapy where radiological technologists work, it is necessary to stay constantly aware of the latest know-how and technology. JART collaborates with other certification agencies to enhance the capacity of all radiological technologists in general through providing lifelong learning seminars, short courses, academic conferences and numerous other learning opportunities. We believe that such activities constitute our obligation as medical professionals to the general public.

As the only medical profession that has “radiological” in its name, we strive to limit medical exposure, to raise the standing of our profession, and to realize a profession of specialist technologists that can be advertised. And we are committed to promoting services with you all for the provision of safe and secure medical care.

general principles

We will render our services to those in need of health care.

We will act as individual members of a health care team.

We will perform our duties in our field of specialty.

We will continue to study for the benefit of mankind.

We will respect and practice the policy of informed consent.

Regarding Publication of the English Edition

UEDA Katsuhiko (President)

The journal of the JART English version issues every year. It has a favorable reception for we members of the world and general people. As well as this issue, 12 articles to be useful for radiological technologists are issued.

We will feature clinical, educational, and research-based achievements by radiological technologists in the monthly issues of the JART journal, and continually work to improve the magazine. I truly hope that this English edition will benefit radiological technicians worldwide.

To give our radiological technologists from across the globe an insight into our business, I will briefly explain the history of the JART. In March 1896, we succeeded in taking the first X-ray image in Japan. In 1897, Shimadzu Corporation released an X-ray generator for educational use. In 1925, there were approximately 1,500 X-ray technicians. In 1927, the first Shimadzu X-ray Technician Training Institute was established, and evidence-based education was put in place. The JART was founded in 1947 to make “radiological technologist” a national qualification. Since its establishment, we have worked towards broad acceptance of this national qualification, in collaboration with the government, the Diet, the Japanese Medical Association, and occupational military authorities.

As a result in June 1951, we were finally able to see the promulgation of the Radiology X-ray Technicians Act, Act No.226 of 1951. Since then, we have responded to the changing needs of the society, revising the original act to get the Radiology X-ray Technicians Act of 1968 passed, and partially revising that to get the Radiology Technicians Act and Radiology X-ray Technicians Act of 1983 passed, and finally getting the Radiology Technicians Act, which is in place currently, passed. Back then, the scope of work was limited to general X-ray testing, television X-ray testing, angiography, X-ray computed tomography scanning, RI scanning, and radiation therapy. In 1993, the Radiology Technicians Act was further revised, and MRI scanning, ultrasonic testing, and non-mydriatic fundus camera examination were added to the list. In 2010, image interpretation assistance, radiation examination explanation, and consultation work were added. In April 2015, intravenous contrast agent injection using automated contrast injectors, needle removal and hemostasis, lower digestive tract examination (anal catheter insertion and administration of contrast medium), anal catheter insertion, and oxygen inhalation during radiation therapy were added as operations that could be performed by radiological technologists.

In October 2021, the needle insertion for examinations of contrasting of the examination for CT, MRI, Ultrasound and Radioisotope are added as the new operation that can be performed by radiological technologists.

The JART will continue to respond to the needs of the medical industry, and we hope to broaden the operational scope of radiological technologists based on our foundation in scientific evidence.

History of The Japan Association of Radiological Technologists (JART)

1947
- Establishment of JART (July 13)

1951
- Promulgation of the Act on Medical Radiographers (June 11)
- Authorization for Establishment of the Japan Association of Radiographers (June 13)

1954
- First national examination for Medical Radiographers (May 30)

1956
- Event to commemorate the 10th anniversary of founding, attended by Her Imperial Highness Princess Chichibunomiya

1962
- Event to commemorate the 15th anniversary of founding and 10th anniversary of enactment of the Act on Medical Radiographers, attended by Her Imperial Highness Princess Chichibunomiya

1968
- Promulgation of the Act to Partially Revise the Act on Medical Radiographers (establishment of two professions) (May 23)
- First national examination for radiological technologists

1969
- Renaming as the JART
- Staging of the 4th International Society of Radiographers & Radiological Technologist (ISRRT) World Congress at Tokyo Palace Hotel, attended by Her Imperial Highness Princess Chichibunomiya

1975
- Event to commemorate the 80th anniversary of the discovery of X-rays, attended by Her Imperial Highness Princess Chichibunomiya

1979
- Completion of the Education Center for JART

1983
- Partial revision of the Act on Medical Radiographers and the Act on Radiological Technologists (unification of the professions)

1985
- Event to commemorate the 90th anniversary of the discovery of X-rays, attended by Her Imperial Highness Princess Chichibunomiya
- Staging of the 1st Japan Conference of Radiological Technologists

1987
- General assembly resolution for establishment of the New Education Center and a four-year university

1989
- Completion of the New Education Center (Suzuka City)

1991
- Opening of Suzuka University of Medical Science

1993
- The Act to Partially Revise the Act on Radiological Technologists, and Ministerial Ordinance to Partially Revise the Enforcement Orders (April 28)

1994
- Appointment of the President of JART as the 11th President of ISRRT

1995
- Event to commemorate the 100th anniversary of the discovery of X-ray, attended by Her Imperial Highness Prince Akishinomiya

1996
- Start of the Medical Imaging and Radiologic Systems Manager certification system

1998
- Staging of the 11th ISRRT World Congress at Makuhari

1999
- Start of the Radiation Safety Manager certification system

2000

- "Presentation of the Medical Exposure Guidelines (Reduction Targets)" for patients

2001

- Start of the Radiological Technologists Liability Insurance System

2003

- Enactment of X-Ray Week

2004

- Relocation of offices to the World Trade Center Building in Tokyo

2005

- Start of the Medical Imaging Information Administrator certification system

2006

- Staging of a joint academic conference between Japan, South Korea, and Taiwan
- Revision of the Medical Exposure Guidelines

2008

- Establishment of the committee on Autopsy imaging (Ai)

2009

- Revision to the national examination for radiological technologists
- Launch of the Team Medicine Promotion Conference, with the President of JART as its representative
- Appointment of the President of JART as chairperson of the Central Social Insurance Medical Council specialist committee

2010

- Health Policy Bureau Director's notification concerning promotion of team medicine

2011

- Support activities following the Great East Japan Earthquake
- Staging of an extraordinary general meeting concerning transition to a public interest incorporated association

2012

- Registration of transition to a public interest incorporated association (April 1)
- Event to mark the 65th anniversary of founding and transition to a public interest incorporated association (June 2)
- Renaming as public interest incorporated association JART
- Launch of the Radiological Technologists Liability Insurance System with participation by all members

2013

- Signing of the Comprehensive Mutual Cooperation Agreement on Prevention of Radiation Exposure (September 21)

2014

- Consignment of work to measure personal exposure of residents
- Revision of the Act on Radiological Technologists, Government Ordinance to Partially Revise the Enforcement Orders, and Revision of the Enforcement Regulations (June 25)
- Launch of the radiation exposure advisor certification system

2015

- Event to commemorate the 120th anniversary of the discovery of X-rays

2017

- Event to mark the 70th anniversary of founding (June 2)

2018

- Notice from the Regional Medical Care Planning Division Director, Health Policy Bureau, Ministry of Health, Labour and Welfare, and Director of the Economic Affairs Division regarding Operational Considerations for Securing a System for Safety Management pertaining to Medical Equipment

2019

- Notice from the Health Policy Bureau on a Safety Management System for Medicinal Use of Radiation

2020

- Partial revision of the Ordinance on Prevention of Ionizing Radiation Hazards

2021

- Relocation of offices to the Mita Kokusai Building in Tokyo
- Revision of the Radiological Technologists Act expanded the scope of practice.
- Holding the 23th AACRT with 37th JCRT in Tokyo

2022

- Event to mark the 75th anniversary of founding (July 16)

Received May 24, 2021; accepted May 30, 2022

Experiential learning of managerial responsibilities in radiological technologists: Implications for career development through a qualitative analysis of narratives

KOBAYASHI Hideyuki[1)], SAKATA Yusuke[2)], NAKAMURA Maki[3)], KATO Ken[4)], YONEMOTO Kuramoto[5)]

1) M.S./Department of Radiation, Radiological Technologist, Seirei Hamamatsu General Hospital
2) Fellow, M.S./Fujita Health University Graduate School
3) Clinical Laboratory Technician, M.S./Clinical Laboratory, Chunichi Hospital
4) Ph.D./Faculty of Health and Medical Sciences, Aichi Shukutoku University
5) Ph.D./Department of Medical Management and Information Science, Fujita Health University Graduate School

Note: This paper is secondary publication, the first paper was published in the JART, vol. 70 no. 843: 16-23, 2023.

Key words: Radiological technologist, Management, Career development, Modified grounded theory approach, Relationship with people

【Abstract】
This study aimed to clarify the career development process of radiological technologist managers in the radiology department. Nine managers of the radiology department were interviewed, and data were analyzed using the modified grounded theory approach. Consequently, career development comprised 9 categories, 13 subcategories, and 83 concepts. Managers gained the information and experience necessary for them through interaction with doctors, bosses, and senior engineers at their facilities, and engineers at other facilities through activities, such as radiological technologists' associations. Career and management learning opportunities are relatively few. To improve the careers of radiological technologists in managerial positions, systematically developing learning opportunities that transcend organizational boundaries is essential.

1. Introduction

The advancement of radiographic imaging equipment promotes the specialization of medical radiology technicians; however, simultaneously, the role of managers who systematically integrate differentiated tasks and information and promote team medical care is becoming increasingly significant. However, to date, the career development of managerial positions in clinical radiological technologists has relied on the so-called apprenticeship relationship between superiors and subordinates as well as seniors and juniors, and training has not necessarily been conducted in a scientific and systematic manner. Conversely, in other industries, instead of forcing students to unilaterally learn a uniform managerial style, "iperiential learning career development" was promoted, wherein students autonomously learn their path to growth from diverse experiences through work and repeat reflections.[1)] However, whether the career development of clinical radiological technologist managers is progressing remains inconclusive.

Conversely, much research on career development in the medical profession has accumulated in the area of nurses. For example, in nursing, career development education and training based on the clinical ladder model is commonly performed.[2)] Moreover, as part of lifelong learning, several studies on human resource development through the fusion of academia and pragmatism have been conducted, including a study on support systems collaborating with university teachers and hospital

nurses.[3] Although only a few studies on career development in radiology departments are available, there is one called "Basic Attitudes of Managerial Skills" by Higashimura et al.[4] However, this study is concerned with the technical responsibilities that medical radiology technicians have acquired from their experience in radiography work, the career development process, which includes the content of these responsibilities, has not yet been clarified as to what kind of experiences excellent medical radiology department managers have learned, acquired, and grown the ability to fulfill their responsibilities, there is a lack of information when considering methodologies for managerial training.

Therefore, this study aimed to obtain useful knowledge for the career development methodology of excellent radiology department managers who can demonstrate leadership in team medical care and clarify through qualitative research based on interview data the process by which managers in clinical radiology departments learn and acquire the ability to fulfill their responsibilities and develop independently. Furthermore, this study aimed to present a model of the characteristic career development process of radiological technologist managers.

2. Method

1) Definition of terms

The word n of termhas various definitions; however, in this study, based on previous research, Douglas Hall defined it as "a series of work-related experiences and activities over a lifetime, as well as the attitudes and actions an individual takes."

2) Survey target

The target participant is a member of the "Japan Association of Radiological Technologists" and "Japanese Society of Radiological technology," which are public interest incorporated associations; has worked at a hospital with >200 beds; and has experienced working as a radiological technologist at the facility. The participants included nine radiological technologists appointed by the facility director as managers of medical radiology services, or persons with equivalent responsibilities, who agreed to participate in the study.

3) Data collection

The survey was conducted over a 2-month period from June to July 2018. The interviews were conducted in a way that asked participants to speak freely according to the following four semistructured questions: "what are the experiences and events that have helped me grow as a manager," "what aspects of that experience/event led to your growth, ha "what abilities (e.g., knowledge and skills) did you gain from it, dand "ddid opportunities that you believe would be best to experience to become a manager in the medical radiology department," owhich are listed in the request form in advance. The interviewee specified the time and place of the interview, which was conducted in a quiet place where only the researcher and the interviewee were allowed to enter and where the content of the conversation could not be overheard by others. The interview time was approximately 60 min, and consent for recording and subsequent processing was obtained before the interview began. The interview was conducted, and audio data were recorded using an IC recorder.

4) Data analysis

For the analysis, all audio data obtained was transcribed and the text data was analyzed based on Kinoshita's modified grounded theory approach (hereinafter referred to as M-GTA). M-GTA is a qualitative research method developed by Kinoshita to make it easier to put into practice the grounded theory approach devised in the 1960s by sociologists Glaser and Strauss. The grounded theory is related to di-

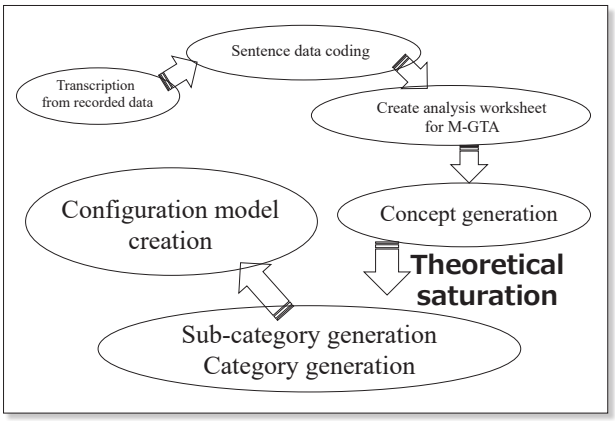

Fig. 1 Flow until configuration model creation

rect interaction between humans, that is, social interaction, and is effective in explaining and predicting human behavior, and researchers have clearly confirmed its significance.[5)]

The procedure is shown in Figure 1. The specific procedure was to transcribe the recorded voice data and repeatedly read the interviewee'n narrative, thereby encoding the text data as a meaningful group. The worksheet comprised concept names, definitions, variations, and theoretical notes. To provide an example of an analysis worksheet, first, carefully observe the coded data, consider similarities and polarities, and create data variations, such as "Subsequently, I showed him the direction of leading him in that direction worksheet interaction, and is effective in expl wouldn't be a bad idea to be the chief engineer (1-19)" showed him the direc. When creating variation, ensure including an interpretation of the meaning of the data and a theoretical memo, such as "The chief engineer tried it and believed it was not bad (1-19)" based on this, we defined it as "It is better to have a higher position to express your thoughts." Subsequently, this process is repeated until all the coded data have been classified into an analysis worksheet, and a concept such as bThe exercise of communication power due to a high position" eis generated. The concept generation ends after confirming theoretical saturation where no new concepts can be extracted. Furthermore, from multiple concepts generated from the analysis worksheet, subcategories are created using related concepts as superordinate concepts. Furthermore, a category is generated as a superordinate concept of that subcategory.[5)]

3. Results

1) Target person attributes

The participant characteristics are presented in Table 1. All nine participants from eight facilities were male. The average age of the participants was 56.0 years, with the youngest and oldest being 51 and 63 years, respectively. The average number of years of experience of clinical radiology technicians was 34.6 years of ranging from a minimum of 29 years to a maximum of 42 years. The number of years of managerial experience ranged from a minimum of <1 nyear to a maximum of 10 years, with an average of 5.0 years, including two with <1 nyear.

Table 1 Outline of the target person

Target Person	age	TechnicianHistory	Management Career	Facility Trancefer Histor
A	60s	Over 40 years	5 years or more	
B	50s	30 ～ 39 years	Less than 5 years	
C	50s	30 ～ 39 years	Less than 5 years	
D	50s	30 ～ 39 years	5 years or more	
E	50s	30 ～ 39 years	5 years or more	Yes
F	50s	30 ～ 39 years	5 years or more	
G	50s	30 ～ 39 years	5 years or more	Yes
H	50s	30 ～ 39 years	Less than 5 years	Yes
I	50s	29 Years or less	5 years or more	Yes
Average	56.0	34.6 years	5.0 years	

In addition, four participants had a work experience outside their facility. The duration of the interview survey ranged from a minimum of 55 min to a maximum of 85 min per participant.

2) Analysis results

The analysis results of the career development process of radiological technologist managers are shown in Tables 2 and 3. The components of career development for managers in clinical radiology departments, extracted by creating an analysis worksheet, were 83 concepts, 13 subcategories, and 9 categories. Furthermore, below, categories are indicated in 【 】, subcategories in『 』, concepts in〔 〕, and the narratives of the interviewees in「 」.

(1) Relationship with people

Relationship with people comprised 16 concepts. Managers in radiology departments realized the need for teamwork from the relationships with other professions inside and outside the hospital, rather than receiving advice from nearby superiors or training where they could obtain information themselves; it was believed that managers acquired the communication skills necessary for a managerial position. In particular, in the process of『Relationship with

Table 2　Analysis results of the career development process of radiological technologist managers ①

Category	Sub-category	Theory
① Relationship with people	・Relationship with doctors	・Awareness of behavior based on opinions from doctors ・Knowledge and inspiration from working with a doctor ・Confidence with doctors deepens by producing results
	・In-hospital involvement	・Thanks to the environment blessed with the surrounding staff ・Conflict with lack of understanding of managers from others ・Difficulty in selecting staff ・Difficulty in treating staff equally ・Efforts to build relationships with other departments
	・Out-of-hospital involvement	・Difficulty in taking on a position in the Engineers' Association ・Activeness to get out of the workplace ・Awareness through interaction with out-of-hospital technicians
	・Teamwork	・The importance of working with colleagues ・The importance of trusting staff
		・Need for bargaining skills ・The importance of team ・The importance of communication
② Concept of human resource development	・Skills for human resource development	・Have a theory of human resource development ・Feedback and disclosure of my experience ・Acquire knowledge of labor regulations ・Knowledge and leadership in medical safety ・Management resources that can be used by oneself in human resource development ・Attitude to think about training from a broad perspective ・Take advantage of interviews ・Bachelor's degree acquisition and its utilization ・Improvements to inadequate goal management ・Management learning that supplements management experience ・Workplace culture with little need for leader development
	・Utilization of human resources	・Utilization of learning in training ・Awareness of becoming a manager
	・A place to learn	・Human resource development system not yet constructed ・Lack of opportunities to acquire management skills
		・Possession for the significance of learning ・The theory about educational methods ・Student experience ・Guidance from the boss ・Experience of all modality
③ Satisfaction from the fact that played a role	・Joy of action	・The joy of returning good results to patients ・The joy of management ・The joy of working as a manager ・The joy of feeling results as an administrator
	・Superiority complex from joy	・Superiority complex to be entrusted with work ・Superiority complex of being recognized by a doctor ・Superiority complex of being recognized by your boss ・Superiority complex recognized by staff at other facilities ・Satisfaction relied on in the workplace ・Self-satisfaction that fulfilled my role

doctors,』the professional identity of radiological technologists was confirmed,[6] and the following experience was described in which that sense of self-efficacy led to motivation for growth.

「*It is not our strength in being able to return images. I think it could be an image, or it could be a number (with increased motivation). (For doctors) When you give something that exceeds expectations, it makes them (doctors) happy*」. (1–12)

Moreover, they stated that starting out-of-hospital involvement at an early stage in one's career, before becoming a manager, and forming several connections through engineering associations and other institutions from a young age are significant.

Regarding『Teamwork』, he mentioned regarding the significance of being aware of the limits of individual ability as well as the need for organizational strength, and of delegating tasks by forming relationships of trust with the surrounding staff.

「*(Collaborative work by teams) is voluntary or based on the needs of the hospital. I must do it. Well, I am thinking of purchasing a new radiation device (in the future); therefore, I have to do this. But I don't have to handle everything myself, Ummu. Didn't I say that my subordinates are in charge of everything? Leave everything to those people. Everything, or to some extent, document creation. I try to leave things like that to them. Well, I think I've got a little better at using people that way*」. (8–40)

(2) Concept of human resource development

The concept of human resource development comprised 20 concepts. Here, along with

Table 3　Analysis results of the career development process of radiological technologist managers ②

Category	Sub-category	Theory
④ The ideal way of the personnel system	・What the evaluation system should be	・Questions about promotion by seniority ・Worries about underdeveloped personnel evaluation system ・Current situation where management results are ambiguous ・Trouble that the expected role of the administrator is not clear ・The gap between the ideal and reality of personnel changes ・Current status of lack of strategic personnel system
	・Anxiety about the system	・A sense of crisis toward oneself due to distrust of the hospital organization ・Anxiety about the introduction of a new management system
⑤ Necessary actions from the standpoint	・What your organization needs	・Organizational culture that considers human resource development important ・Permeation and thorough management philosophy ・Visualization of management for subordinates ・Transparency of grounds in staffing ・Work style reform of female engineers
	・What you need	・Show the results of management as a manager ・Self-control of emotional ups and downs ・Tolerant posture
⑥ Actions you want to take as an administrator		・Acquiring business initiatives ・Formulation and clarification of vision ・Coordinator of organizational management ・Awareness and responsible behavior as an administrator ・A perspective that sees a change of management as an opportunity ・Appropriate interpretation of past boss's behavior
⑦ Way of thinking about management		・Objective understanding of hospital management ・Worries about lack of understanding of the site of management ・Difficulty in balancing medical care and management
⑧ Information handling		・Thorough information management and proper handling ・Information gathering activities required as an administrator ・Demonstrate the role of information dissemination on behalf of the department ・Ability to appeal the department
⑨ The underlying idea as a medical professional		・Maintaining a strong sense of mission as an engineer ・Confidence through accumulated experience ・Achievements of skilled skills ・Words and deeds that keep your beliefs ・Demonstrate the spirit of challenge ・Make use of experience different from other staff ・Patient-first thinking
⑩ other		・Anxiety due to lack of knowledge and experience in management

their experience, most respondents believed that having an attitude of going through the management cycle of P (planning), D (execution), C (confirmation), and A (review) when dealing with issues at their facility was important. Specifically, in『Skills for human resource development』technical skills including〔Acquire knowledge of labor regulations〕and〔Knowledge and leadership in medical safety〕are introduced. Furthermore, nontechnical skills including〔Feedback and disclosure of my experience〕,〔Take advantage of interviews〕, and〔Improvements to inadequate goal management〕were cited. Moreover, they considered〔Utilization of learning in training〕an effective learning opportunity. In addition, a respondent discussed〔Awareness of becoming a manager〕as a way of preparing himself. The respondent reported that being aware of the role expected of the organization helps maintain motivation. Furthermore, in『A place to learn』, he stated the following about〔Human resource development system being not yet constructed〕.

「*I do not know myself. It is natural for medical radiology technicians to improve their skills by themselves, and they do not have to be told what to do by others. Study by yourself, (Whether you do it or not) is up to you. I've spent my time thinking that people who want to study, study on their own, and present at an academic conference should do so*」. (2–48)

The respondent discussed the organizational culture of radiology technicians. Conversely, based on my experience, I believe that the future should be「*(Omitted) I was able to take care of my subordinates, because there was an education system in place, If such things can be evaluated, (In other words) Maybe if we had a system where we could say, oh, this guy will get better if he does it this way, so let us do that for him, You will be able to change into the person you want to be more quickly*」. (8–23) and the need for systematic career development.

(3) Satisfaction from the fact that played a role

【Satisfaction from the fact that played a role】comprised 10 concepts. As an experience that provides you the joy of fulfilling your role, a participant discussed his sense of role accomplishment with respect to『Joy of action』in two situations as follows: the joy of achieving results for patients and the joy of achieving results as a manager. Moreover, the participant stated that this『Superiority complex from joy』has satisfied the need for approval from others.

(4) The ideal way of the personnel system

【The ideal way of the personnel system】comprised eight concepts. Two subcategories were raised that spoke openly regarding『What the evaluation system should be』. A respondent discussed his sense of crisis over an outdated personnel system based on seniority that poorly reflects abilities and results; conversely,『Anxiety about the system』, although I feel that the system must be changed, I find it difficult to take active steps to address it.

(5) Necessary actions from the standpoint

【Necessary actions from the standpoint】comprised eight concepts. Here, items considered to be essential regarding the functions within the organization that administrators are responsible for are listed as『What your organization needs』. Moreover, it was classified into the following two subcategories:『What you need』, wherein managers discuss their personal theories on the basis of their experiences about the actions they should take to perform their functions within the organization.

(6) Actions you want to take as an administrator

【Actions you want to take as an administrator】comprised six concepts. Here, the respondents discussed the knowledge and skills that they are currently using to perform their duties as managers, and what they are especially aware of and what they pay close attention to daily.

(7) Way of thinking about management

【Way of thinking about management】comprised three concepts. Several managers discussed how hospitals should be run while managing the front lines. One manager stated that rI realized that I could gain a different understanding if I looked at management issues not only from the perspective of those in the field but also from the perspective of higher-level hospital managers." The following statement explains the significance of an objective understanding of hospital management to grow as a manager.

「*Also, the hospital's management goals and numbers, after all, things like that can be seen at a glance (you can see the whole thing), well, anyone (even if you're not a manager) can see it if they want to. Well, that'e what we need to do directly by getting together with only managers (looking at it in detail from a management perspective). Well, there was a meeting today as well. Well, because you hear things directly from management (you get the perspective of management). It was very exciting, and I learned a lot. Well, I think this is where I could grow.*」(8–35)

(8) Information handling

【Information handling】comprised four concepts. Here, as managers, they were required to not only play the role of communicating information collection and handling subordinates and other departments but also the ability to quickly, appropriately, and simultaneously disseminate information.

(9) The underlying idea as a medical professional

【The underlying idea as a medical professional】comprised seven concepts. Here, the participants discussed professionalism that perseveres through a unified sense of ethics, which should be maintained as a medical professional regardless of one'r position within the organization and whether one is a manager or not.

(10) Others

The concept of〔Anxiety due to lack of knowledge and experience in management〕refers to the reality that managers of clinical radiological technologists have not had the opportunity to learn management, and even if they want to learn, they are highly busy with their daily work that they do not have the time. In reality, several managers do not learn about legitimate management when performing management. One manager mentioned that "As a manager who lacks knowledge and experience, I feel guilty, and I feel that I am not really suitable as a manager." Furthermore, the manager discussed his feelings of anxiety owing to his〔lack of management knowledge and experience〕, as he wonders if he can evaluate his subordinates and take responsibility for them.

3) Configuration model for managerial career development

On the basis of the abovementioned results, we modeled the career development storyline for managers in the medical radiology department, as shown in Figure 2. Rather than formal

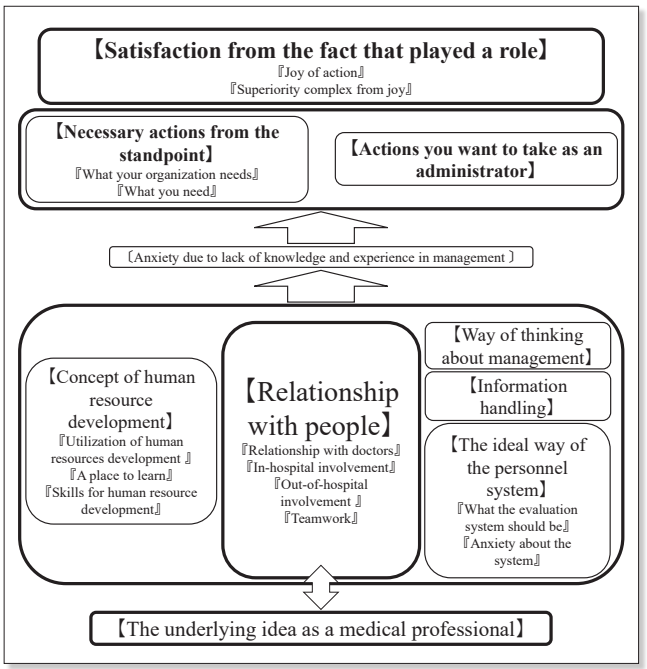

Fig. 2 Career development configuration model for radiological technologist managers

learning opportunities provided by the organization, the career development of a medical radiological technologist manager involves self-growth through repeated self-reflection and self-directed practice of learning from interpersonal relationships with individuals inside and outside the workplace, including informal ones. In addition to the technical skills required for managerial positions, students have the opportunity to acquire the human skills required for leaders and conceptual skills for decision-making. Their personal interaction with other individuals was driven by their underlying idea as medical professionals, that is, their desire to contribute to the medical field, which formed the basis for their career development throughout their lives. Moreover, the significance of【Way of thinking about management】, 【Information handling】, and 【The ideal way of the personnel system】 was shown as skills that are particularly necessary for managerial positions to acquire from【Relationship with people】. Furthermore, in departmental operations, participation and management of corporate or facility management is necessary for managerial works; therefore, information handling for smooth functional collaboration between organizations is required. The personnel systems that support them differ depending on the corporation or facility. Therefore, collecting information about other facilities and the neighborhood and recognizing personnel systems that increase motivation are essential to maintain competitiveness in acquiring human resources. Particularly in a business environment where work style reforms are beginning to take hold, individuals may feel『Anxiety about the system』at their facility; however, such anxieties can be controlled by【Relationship with people】. Conversely, the【Concept of human resource development】 is a significant factor within the department, and the development of staff within the department will lead to the achievement of the next goals and the growth of the organization. However, internally, managers felt anxious owing to a〔lack of management knowledge and experience〕. In this regard,【Relationship with people】 provided emotional support, and they perceived this in a positive manner as【Necessary actions from the standpoint】 and【Actions you want to take as an administrator】. In this manner, radiological technologists in managerial positions develop their careers by using【Satisfaction from the fact that played a role】 as motivation for their next actions. Soon after joining the company, we conducted a cycle of observation, experimentation, and reflection on managers inside and outside the organization.

4. Consideration

Rather than through formal training, managers in medical radiology departments tended to develop their careers as individuals through【Relationship with people】 inside and outside the organization. In particular, the process of interacting with radiologists at one'I institution, with whom one has a close professional relationship, strongly influences the acquisition of human skills, such as interpersonal communication, in addition to technical skills, such as specialized knowledge. The influence of this relationship with radiologists on the career development of radiology technicians is believed to be a characteristic of their work, unlike the nursing profession, which interacts with physicians from various medical departments. This suggests that facilities without radiologists can only interact with part-time physicians from other facilities, and the degree of career development can be influenced by that radiologist despite the presence of a full-time physician. Therefore, to overcome the educational environment that tends to lead to closed on-the-job training, having specific doctors, hospital staff, seniors, and superiors at work along with actively engaging with out-of-hospital activities such as with radiological technologists' associ-

ations and connecting with managers and organizational cultures of other facilities are necessary; subsequently, they become aware of diverse perspectives and values. Creating situations for self-reflection is particularly significant for career development for managers. In other words, an effective way to systematically develop the career of clinical radiology technicians is to support opportunities to interact with others outside the workplace where they can discover individuals who can serve as role models for the leadership they aspire to and make them aware of 〔Activeness to get out of the workplace〕.[7] Furthermore, 【Relationship with people】 consists of the concepts of 〔Need for bargaining skills〕, 〔The importance of team〕, and 〔The importance of communication〕. This is because it is an ability that can be acquired through accumulated experience rather than through classroom training or knowledge from books. Combining this with "experience in other games" such as being transferred to other facilities or off-the-job training is necessary.

To systematically conduct career development for the next generation on the basis of 【Relationship with people】 within the hospital over a medium-to-long term, a change in the mindset of the management who supports this is required regarding the 【Concept of human resource development】; however, in response to the current immaturity such as 〔Human resource development system not yet constructed〕 and 〔Lack of opportunities to acquire management skills〕, 【Necessary actions from the standpoint】 【Actions you want to take as an administrator】 it seems that there is a growing need within current managers to take action themselves, rather than passing the responsibility on to management.[8] In addition, the reflective experiential learning cycle[9] based on human interactions for radiological technologists, 【Relationship with people】 was observed to be a significant educational method to acquire the ability to create improvement plans for career development in managerial positions in the medical radiology department, as in other industries. Additionally, repeating active new 【Relationship with people】 creates continuity in motivation for career development and stimulates the identity of medical radiological technologists as a sense of 【Satisfaction from the fact that played a role】 and that it is interesting to be a manager.[10] Simultaneously, the identity that stimulates this motivation includes a strong sense of mission, which is the 【The underlying idea as a medical professional】. Of note, this is an indispensable foundation for the career development of medical radiology technicians, who are involved in medical care among other professions. In other words, if you actually become a manager with management responsibilities, you may face conflicts in balancing medical services with medical fees and costs. In making decisions in such cases, radiological technologists must cultivate career anchors,[11] which are beliefs that they have as individuals, on the basis of their reflective experience of connecting with patients' diverse values. Moreover, a sense of insecurity arises from the fact that these abilities as managers are opinions based on limited experience. To eliminate this anxiety, organizations require systematic education based on management theory.

Although this study shows that informal 【Relationships with people】 inside and outside the hospital are important, the issue of how managers can promote 【Relationships with people】 has once again come to light, considering that the radiology department is characterized by a closed organizational culture with small staff and self-contained work. In contrast, career development through one-on-one communication has been recently introduced in some companies.[12] The theoretical notes under 〔Need for bargaining skills〕 include 「I recognize that the ability to see and observe subordinates is important」, 「First, listen to the other party's wishes」, and 「top-down action is not an

option」. One-on-one communication is a method of face-to-face interviews between superiors and subordinates,[13] and the role of the superior is to provide support for solving problems experienced by subordinates and help subordinates achieve their goals.[14] We believe that this will be useful for career development in the radiology department, where job characteristics such as that in the nursing department make it difficult to gain experience in deep interaction with other people within the organization, such as other occupations, patients, and families. Build relationships of trust with everyone we interact with, both inside and outside the organization. Furthermore, managers must possess skills that allow them to create【Relationships with people】so that they can engage in a cycle of experiential learning. In nursing, a management ladder for managers has been added to the lifelong education system based on the clinical ladder method, and its effectiveness has been confirmed.[3] However, by adding the acquisition of one-on-one communication skills for managerial training to the Japan Society of Radiological Technologists' Clinical Ladder,[15] promoting experience in【Relationships with people】and enabling more effective career development are possible.

5. Conclusion

From interacting with radiology specialists, superiors, and senior technicians at your facility, and technicians at other facilities through technical association activities in the career development of clinical radiological technologists in managerial positions, it was suggested that career development should be based on the core concept of【Relationships with people】to obtain the information and experience necessary for managerial positions. However, in several cases, this【Relationships with people】is not performed through formal career development in an organization, particularly in radiology departments, where organizations tend to be small, and they tend to rely on motivation based on individual career anchors and identity. Therefore, promoting career development from a new perspective on the basis of job characteristics such as incorporating the acquisition of one-on-one communication skills into the organizational career development of managers in medical radiology departments is desirable.

Research limitations and future challenges

The participants of this study were managers who worked in a hospital with more than 200 beds and were employees who achieved significant results in a limited environment. Therefore, the information obtained from only nine managers may be biased or insufficient. In the future, conducting quantitative research with a wider range of participant to verify whether career development can be achieved using the configuration model constructed in this study will be necessary. Furthermore, to examine novel continuous career development for managers, the development of not only the managers but also their teams and organizations as well as the growth and satisfaction of their subordinates must be considered. The subordinates' growth and satisfaction level must also be considered.

References

1) Atsushi Nakahara (editor): Introduction to corporate human resource development Learn the basic theories of psychology and pedagogy for developing people. Diamond Inc., 2006.
2) Reiko Hara: How to create and utilize a nursing career development ladder linked to goal management. Japanese Nursing Association Press, 2015.
3) Kyoko Kojima, Kaneko Noji (eds.): Continuing nursing education to develop nurses as professionals: Clinical ladder and management ladder in practice. Ishiyaku Publishing, 2005.
4) Kyoji Higashimura (ed.): Professional guide for radiological technologists. Bunkodo, 2008.
5) Yasuhito Kinoshita: Live lecture M-GTA practical qualitative research methods: All about the revised grounded theory approach. Kobundo, 2011.
6) Sachiko Ochiai, et al.: Lifelong development process of professional identity of radiological technologists. Bulletin of Ibaraki Prefectural Medical University, ASVPI Volume 11; 23-32, 2006.
7) Takako Murai, Hiroko Harada: Structure of career development of nursing managers with certified nursing manager qualifications. 7, 17-25; 151-159, 2017.
8) P Hershey et al.: Seiji Yamamoto, Azusa Yamamoto translation: From introduction to application: Development of behavioral science. Productivity Publishing, 2000.
9) Mutsumi Matsuo: Learning from experience: The process of professional growth. Dobunkan Publishing, 2006.
10) Mutsumi Matsuo: An introduction to “experiential learning” that helps people thrive in the workplace Diamond Inc., 2011.
11) Career anchor by Edgar H. Schein, translated by Toshihiro Kanai Discover your true worth. Hakuto Shobo, 2003.
12) HR Vision: Japanese human resources department editorial department: Japanese human resources department human resources white paper 2018. HR Vision, 2018.
13) Atsushi Nakahara: Introduction to feedback: Techniques to rebuild your subordinates and the workplace by communicating what hurts.
14) Kosuke Honma, Jun Nakahara: The company is full of dilemmas: Training for on-site managers to make decisions. Kobunsha Shinsho, 2016.
15) Academic Education Committee of the Japanese Society of Radiological Technologists: Overview of lifelong education system. The Japan Association of Radiological Technologists, 68, 77-91; 413-427, 2021.

Received February 25, 2022; accepted June 24, 2022

Human Resource Development for Radiological Technologists who can Respond to Nuclear Accident-Experience and Lessons Learned from the Fukushima Daiichi Nuclear Power Station Accident

OHBA Takashi, Ph.D.[1), 2)], MABUNE Koichi, M.Sc.[3)], KANNO Shuichi, M.Sc.[4)], SATOH Kenichi, Ph.D.[5)], HASEGAWA Arifumi, M.D., Ph.D.[6)]

1) Department of Radiological Sciences, Fukushima Medical University, School of Health Sciences
2) Department of Radiation Health Management, Fukushima Medical University, School of Medicine
3) Department of Radiation Technology, Iwase Hospital
4) Miyakoji Clinic 5) Faculty of Data Science, Shiga University
6) Department of Radiation Disaster Medicine, Fukushima Medical University, School of Medicine

Note: This paper is secondary publication, the first paper was published in the JART, vol. 70 no. 844: 19-28, 2023.

Key words: Education, Fukushima Daiichi nuclear power station accident, Qualitative analysis, Radiation protection, Radiological Technologists

【Abstract】
This paper aims to analyse the disaster response experiences of radiological technologists during the Fukushima Daiichi nuclear power station (FDNPS) accident by participants' backgrounds, and to suggest outcomes for human resource development. We conducted focus group interviews with 23 radiological technologists in Fukushima Prefecture (divided into 5 groups), who differed in terms of work location, position, and gender. Comparison of the coded phrase rates and correspondence analysis of notable words took place. Our results showed characteristics of phrases and words depending on participants' workplace distance from the FDNPS, and in the same area, gender differences were noted. We consider that the content of human resource development for radiological technologists in the event of a nuclear accident should include flexible education based on the distance from a nuclear power plant, and radiation protection measurements needed in daily life, including of family members, in addition to the existing content.

1. Introduction

Effective radiation protection methods for the affected population in the event of a nuclear disaster include evacuation, temporary relocation and indoor evacuation (sheltering)[1)]. Human resource development to ensure radiation protection for affected populations is being carried out in Japan and globally. For example, the Radiation Emergency Assistance Centre/Training Site (REAC/TS) in the United States is an international human resource development facility for nuclear disaster response[2)] and in Japan, the Nuclear Regulation Authority (NRA) is taking the lead in human resource development activities related to a nuclear disaster[3, 4)].

In addition, international organisations such as the International Commission on Radiological Protection (ICRP) expect medical personnel to be involved in the radiation protection of the affected population in the event of a nuclear disaster[5)]. Radiological technologists hold national medical licenses in Japan and are required to play an important role in body surface contamination measurement and ambient dose measurement at their facilities in a nuclear disaster[3, 6)]. However, the content of human resource development for radiological technologists who are expected to work in such situations is uniform and does not necessarily consider the background of each radiological technologist (e.g. their work area, job position, and gender).

Radiological technologists played diverse roles in the Fukushima Daiichi nuclear power station (FDNPS) accident that occurred in March 2011 related to the Great East Japan Earthquake (GEJE), including measurement of body surface contamination and decontamination for radiation protection of the affected population [7, 8]. The lessons learned from the FDNPS accident by radiological technologists have been reported in many activity records, but this information has been fragmentary. Many radiological technologists experienced the FDNPS accident while working at medical facilities in Fukushima Prefecture, and systematically organising the activities of these radiological technologists at that time may provide an important perspective for improving the content of human resource development.

Based on this background, we set out to systematically organise the experiences of radiological technologists at the time of the FDNPS accident based on their individual backgrounds, such as their work area, job position, and gender at the time of the accident. The results of this study may be applied to the human resource development of radiological technologists who are responsible for responding to a nuclear disaster, and will have implications for their effective human resource development in the future.

2. Materials and methods

2-1. Study design and participants

This study was a recall cross-sectional study using a qualitative research approach with text-mining, targeting radiological technologists who were working in Fukushima Prefecture at the time of the FDNPS accident. The participants resided in three regions of Fukushima Prefecture (Aizu, Naka-dori and Hama-dori areas) and were engaged in medical work at their facilities on 11 March 2011. Fukushima Prefecture is geographically divided into three main regions: the Hama-dori area (Area 1), the Naka-dori area (Area 2), and the Aizu area (Area 3) (Fig. 1). The Hama-dori area (Area 1) is located on the Pacific coast, where the FDNPS was located. In this study, radiological technologists working at medical facilities within 20 to 30 km of the FDNPS were considered as the Area 1 group. Those working at medical facilities within 30 to 80 km were the Area 2 group, and those in medical facilities outside the 80 km radius were in the Area 3 group (Fig. 1).

A total of 23 participants were classified into five groups in the three areas of Fukushima Prefecture based on their work area, job position, age, and gender. Table 1 shows the details of the participants and these groups. The Area 1 group consisted of four males in their 40s and 50s as department managers and section chiefs. The Area 2 group comprised five males in their 50s as department managers (hereafter, Area 2 department manager), five females in their 30s and 40s as section chiefs (Area 2 female section chief), and five males in their 30s and 40s as section chiefs (Area 2 male section chief). The

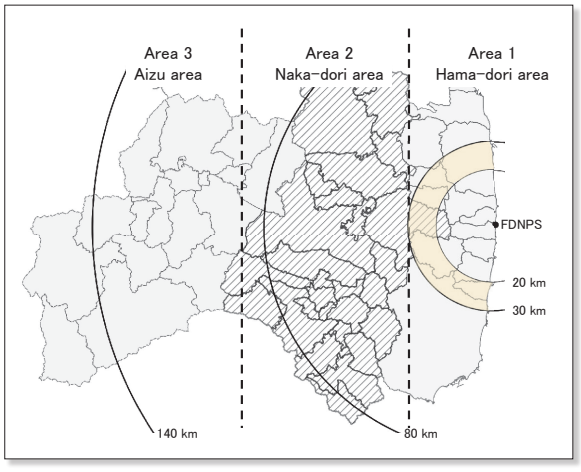

Fig. 1 Three local areas (Area 1: Hama-dori area, Area 2: Naka-dori area, and Area 3: Aizu area) in Fukushima Prefecture are clarified by the dotted lines. Distance lines from the Fukushima Daiichi nuclear power station (FDNPS) are the zone from 20 km to 140 km. The light-yellow marker on this map depicts the zone of 20-30 km radius from the FDNPS. The detailed municipalities of Naka-dori area (Area 2) are shown as the diagonal line.

Area 3 group consisted of four men in their 20s to 50s in a variety of positions, including department managers, section chiefs, and section staff.

2-2. Focus group interviews

Focus group interviews (FGIs) were conducted with the participants in Table 1. The FGIs took place from October to November 2017 with groups of four to six interviewees. We aimed for the interview process to be synergistic, with a snowball effect, stimulating, reassuring, and spontaneous. FGIs are useful for uncovering latent factors within participants and for collecting narrative information compared with one-to-one interviews [9]. The duration of each FGI was 90 minutes per group in this study.

The FGIs focused on two main items: (1) the GEJE and their roles at work and in private, and (2) the GEJE and their health. Participants' opinions were sought separately for two time periods: the early GEJE phase (immediately after the FDNPS accident) and six years after the GEJE (at the time of the interview) [10]. We asked about two other aspects: (3) activities remembered during the GEJE, and (4) experiences of being relied upon, which focused on their opinions regardless of the time period such as the early or recovery phases. FGI facilitators asked open-ended questions and avoided leading participants to respond in a particular way. Participants were encouraged to discuss the topics freely as they saw fit in any chronological order. An assistant was present during the FGIs and responsible for audio- and video-recording the sessions.

2-3. Data analysis

2-3-1. Coding the utterance content

Fig. 2 shows an overview of the analytical procedures in this study. First, the recorded FGI utterances of each group were transcribed and converted into textual information. Next, the textual transcription was corrected for any Japanese notational errors (e.g. survey: "サーベイ" or "サーベー", and radiological technologists: "診療放射線技師", "放射線技師", or "技師") and proper nouns were processed so that participants could not be identified. Finally, each sentence was coded. Two authors of this article (T.O. and K.M.) individually examined the content of each sentence of each utterance and assigned each sentence to a subtopic based on its intended meaning. Each subtopic was then classified into a larger concept – the main topic – so that every utterance was coded with two main topics {A, B} and six subtopics {a, b, c, d, e, f}, with the aim of grasping the content of the utterance (Fig. 2). Next, the results of the two coders were collated and, in case of discrepancies, the codes for the subtopics were assigned after consultation between two authors (T.O. and K.M.), referring to the sentences before and after.

NVivo Release 1.1 (QSR International Inc., MA, US) Computer Assisted/Aided Qualitative-Data-Analysis Software (CAQDAS) was used for the analysis [11]. To assess the coding concordance between the two authors, a test of con-

Table 1 General characteristics of the participants

Working area in Fukushima Prefecture	Position at the time of the FDNPS accident	Gender	Age group (number of participants)
Area 1	Department manager and section chief	Male	40s (2), 50s (2)
Area 2	Department manager	Male	50s (5)
	Section chief	Male	30s (3), 40s (2)
	Section chief	Female	30s (3), 40s (2)
Area 3	Department manager, section chief, and section staff	Male	20s (1), 40s (1), 50s (2)

FDNPS, Fukushima Daiichi nuclear power station

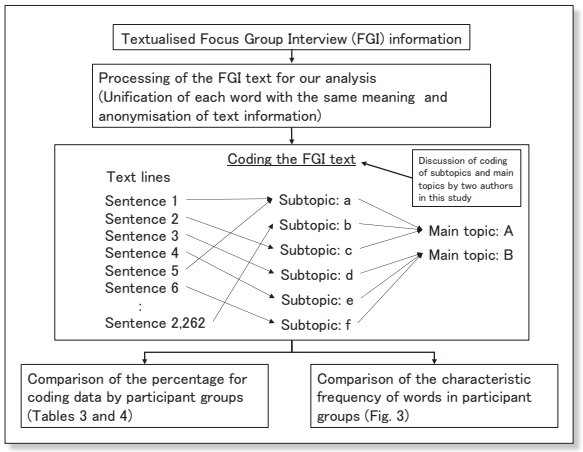

Fig. 2 Flow of our research methods

cordance was conducted using SPSS version 28 (IBM Corp., IL, US). The significance level for this study was set at 5%.

2-3-2. Analysis of the relationship between utterance content and interview groups based on coding data

The number of relevant sentences and the proportion of occurrences of codes related to the main topic to the total utterances were compared from the following two perspectives for each FGI group: (1) The percentage of occurrence of codes related to the main topic in total utterances among the work areas (Areas 1–3), and (2) the percentage of occurrence of codes related to the main topic in total utterances among the three groups with different job positions and genders, restricting the target to Area 2.

To examine the association between the three main topics (including where the main topic was "Unknown" (Not classifiable)) and the three regions of work or the three groups, a 3 by 3 cross-tabulation table was developed and a Pearson's χ^2 test was applied to obtain *p*-values. The proportion of occurrences in each cell after the χ^2 test was compared with the expected value under independence, and a residual analysis was performed using the z-test. The significance level of this study was 5%, and the adjusted residuals from the z-test used in the residual analysis showed a tendency to be significantly higher or lower if the absolute value was greater than ±1.96. Statistical analysis was performed using SPSS version 28.

2-3-3. Analysis of the relationship between utterance content and groups based on frequent words and phrases

Frequently occurring words and phrases were extracted for each coded main topic. The words analysed were limited to nouns in general (words with two or more characters, including Kanji), nouns in the accusative case, adjectives, organisation names, place names, unknown words, tags, verbs, adjectives, adverbs, and noun C (words with one Kanji character), to avoid confusion associated with ambiguous use. The tags (extraction of designated words) were: radiological technologist, decontamination, Hama-dori, Minamisoma, temporary house, whole body counter, monitoring post, glass badge, and survey meter. Based on the above criteria, the top 100 words with a minimum number of 13 or more occurrences were extracted for each main topic. A cross-tabulation table was then created between the frequently occurring words and interview groups, and visualised using correspondence analysis.

Correspondence analysis was conducted using the free software KH Coder version 3. Beta.01.a (https://khcoder.net/)[12]. Monkin® Reporting for KH Coder 1.0.0 (SCREEN Advanced System Solutions Inc., Kyoto, Japan) was used as a plug-in system for KH Coder to facilitate visual evaluation of the correspondence analysis results.

2-4. Ethical considerations

This study was conducted with the approval of the General Ethics Committee of Fukushima Medical University (Approval No. 2573). We explained the voluntary nature of research cooperation, the freedom to withdraw during the course of the research, the benefits and disad-

vantages associated with research cooperation, ensuring privacy, that identifying information would not be revealed when the results were published, and that no harm would be caused to participants. Informed consent was then obtained from the participants.

3. Results

3-1. Understanding utterance content through coding

The results of the utterance coding carried out through the analysis procedure shown in Fig. 2 are presented in Table 2. The total number of recorded utterances was 2,262 across the five FGI groups. The coding results for the two authors of this article showed that the degree of agreement (kappa coefficient) was 0.82 ($p < 0.01$).

Ninety-six percent of the total utterances were coded as the following topics. The main-topic A: "anxiety about health effects of radiation exposure and changes in their daily life" consisted of 3 items in the subtopic code (the percentage ratio of related sentences in the subtopic against total utterances of the FGI in this study), such as a. "Health effects within their family (25.8%)", b. "Interest in the radiation exposure situation (7.2%)", and c. "Reconstruction and harmful rumours (9.5%)". Notable words and phrases in the subtopic utterances were as follows: a. Relationships with family members, Implementation of evacuation, Anxiety about health effects of radiation exposure, and Risk assessment of radiation exposure; b. Decontamination work, Personal radiation exposure dose, Radioactive contamination of food and water, and Measurement of thyroid dose; c. Fading issues, Changing landscapes by reconstruction, Daily life during the evacuation, and Harmful rumours. The main-topic B: "Changes in their work and the issues faced" also consisted of 3 items in the subtopic code (the percentage ratio in total utterances),

Table 2 The coding list of main and subtopics with frequency in the focus group interviews (FGIs) based on qualitative analysis

Code			Number of sentences relating to subtopics in the overall FGI data (%)
Main-topic	Subtopic	Notable words and phrases during the FGIs	
A: Anxiety about health effects of radiation exposure and changes in their daily life	a. Health effects within their family	Relationships with family members, Implementation of evacuation, Anxiety about health effects of radiation exposure, Risk assessment of radiation exposure	583 (25.8)
	b. Interest in the radiation exposure situation	Decontamination work, Personal radiation exposure dose, Radioactive contamination of food and water, Measurement of thyroid dose	164 (7.2)
	c. Reconstruction and harmful rumours	Fading issues, Changing landscapes by reconstruction, Daily life during the evacuation, Harmful rumours	215 (9.5)
B: Changes in their work and the issues faced	d. GEJE-related works	Work immediately after the GEJE, Evacuation of hospitals, Counselling for medical exposure, Improvement of daily workflows after the GEJE	494 (21.8)
	e. The measurement of radiation exposure dose	Ambient dose rate, Body surface contamination, Internal radiation exposure dose measurement	495 (21.9)
	f. Communication and lessons learned from the accident	Activities to alleviate anxiety about radiation exposure, Dissemination of information using SNSs, Face-to-face talks about radiation knowledge, Lack of knowledge about radiation protection, Evaluation of previous training for a nuclear disaster, Sharing experiences with the next generation	221 (9.8)

FGI: Focus group interview, GEJE: Great East Japan Earthquake, SNS: Social Networking Services

such as d. "GEJE-related works (21.8%)", e. "The measurement of radiation exposure dose (21.9%)", and f. "Communication and lessons learned from the accident (9.8%)". Notable words and phrases in the utterances of the subtopics included: d. Work immediately after the GEJE, Evacuation of hospitals, Counselling for medical exposure, and Improvement of daily workflows after the GEJE; e. Ambient dose rate, Body surface contamination, and Internal radiation exposure dose measurement; f. Activities to alleviate anxiety about radiation exposure, Dissemination of information using social networking services (SNSs), Face-to-face talks about radiation knowledge, Lack of knowledge about radiation protection, Evaluation of previous training for a nuclear disaster, and Sharing experiences with the next generation. In total, 90 sentences (4.0% of the total utterances) involved silent responses and non-codable utterances that were excluded from the coding.

3-2. Comparison of utterance content with a focus on coding

The proportion of utterance occurrences of each main topic to the total utterances is shown by location for Areas 1-3 (Table 3) for the main-topic A: "anxiety about health effects of radiation exposure and changes in their daily life", main-topic B: "Changes in their work and the issues faced", and non-codable utterances "unknown". The proportions of utterance occurrence by location for each main topic showed significantly different trends in the χ^2 test ($p < 0.01$). In particular, the z-test showed that Area 1 group's proportion of all utterances for the main-topic A: "anxiety about health effects of radiation exposure and changes in their daily life" was lower than that of the Area 2 and Area 3 groups ($p < 0.05$). In contrast, for the main-topic B: "Changes in their work and the issues faced", a z-test showed that the proportion of Area 1 group to total FGI utterances tended to be higher than the proportion of Area 2 and Area 3 groups ($p < 0.05$).

The analysis then focused on the Area 2 group, where the backgrounds of participants were diverse. Table 4 shows the comparison of the proportion of each main topic to the total utterances between the three groups with different job positions and gender. For both main topics A and B, the χ^2 test showed that the proportion of the total FGI utterances showed a significantly different trend ($p < 0.01$) between the groups. For the main-topic A: "anxiety about health effects of radiation exposure and changes in their daily life", the z-test showed that the Area 2 female section chiefs' group had the highest percentage trend in the total FGI utterances of the three groups ($p < 0.05$). Regarding the main-topic B: "Changes in their work and the issues faced", the z-test showed that the proportion of occurrences for the Area 2 male section chiefs' group to the total utterances had the highest proportion trend among the three groups ($p < 0.05$).

3-3. Comparison of utterance content focusing on high frequency words

To analyse the relationship between frequently occurring FGI words and the work area, job position, and gender of the participants, the relationship between frequently occurring words and the groups was analysed for each main topic by correspondence analysis (Fig. 3). In the correspondence analysis, the closer the words and FGI groups were located to each other in the diagram, the more characteristic and stronger the association was.

For the main-topic A: "anxiety about health effects of radiation exposure and changes in their daily life", a tendency was observed in Area 1 and Area 3 groups to overlap characteristic frequent words related to evacuation, such as "Minamisoma", "tsunami", and "water" (quadrant 2 in Fig. 3-1). In contrast, words related to the acceptance of evacuees, such as "Hamadori" and "evacuate", were found as characteristic frequent words only in the Area 3 group.

Table 3 The proportion rate of interview sentences related to the main-topics using coding analysis in the three Fukushima Prefecture areas

Category	Group	Area 1	Area 2	Area 3	Total
Main-topic A	Frequency (%)	185 (33.4)	540 (47.2)	237 (42.1)	962 (42.5)
	Adjusted residual (z-test)	−5.01*	4.51*	−0.24	
Main-topic B	Frequency (%)	340 (61.4)	578 (50.4)	292 (51.9)	1,210 (53.5)
	Adjusted residual (z-test)	4.28*	−2.91*	−0.89	
Unknown	Frequency (%)	29 (5.2)	27 (2.4)	34 (6.0)	90 (4.0)
	Adjusted residual (z-test)	1.74	−3.99*	2.89*	
Total	Frequency (%)	554 (100)	1,145 (100)	563 (100)	2,262 (100)

*$p < 0.05$

Table 4 The proportion rate of interview sentences related to the main-topics using coding analysis in relation to the work position and gender of three groups in Area 2

Category	Group	Male section chief	Female section chief	Manager	Total
Main-topic A	Frequency (%)	126 (27.0)	273 (74.6)	141 (45.2)	540 (47.1)
	Adjusted residual (z-test)	−11.4*	12.7*	−0.82	
Main-topic B	Frequency (%)	328 (70.2)	86 (23.5)	164 (52.6)	578 (50.5)
	Adjusted residual (z-test)	11.1*	−12.5*	0.86	
Unknown	Frequency (%)	13 (2.8)	7 (1.9)	7 (2.2)	27 (2.4)
	Adjusted residual (z-test)	0.79	−0.68	−0.16	
Total	Frequency (%)	467 (100)	366 (100)	312 (100)	1,145 (100)

*$p < 0.05$

Words related to the conflict between evacuation and work in relation to "retire" were found to be characteristic of the Area 1 group only (quadrant 2 of Fig. 3-1). The characteristic frequent words of the Area 2 department managers' and the Area 2 male section chiefs' groups had considerable overlap, and "safety", "stress", "life", and "thyroid" were found to indicate sudden changes in participants' daily life and work (quadrant 3 in Fig. 3-1). However, the characteristic frequent words of the Area 2 female section chiefs' group were independent of the other groups, with words reflecting concerns about radiation exposure related to children and families, such as "children", "elementary school", "evacuation", and "home" (quadrants 1 and 4 in Fig. 3-1). In the correspondence analysis of the main-topic B: "Changes in their work and the issues faced", the characteristic frequent words of the Area 2 department managers' and male section chiefs' groups were very similar, and words related to body surface contamination examinations and working facilities, such as "hospital", "self-defence force", and "cpm (count per minute)", were found (quadrants 1 and 2 in Fig. 3-2). A tendency was observed between the Area 1 group and the Area 2 female section chief group to overlap characteristic frequent words for consultation on medical exposure, such as "come", "explanation", "hear", "photo", and "anxiety" (quadrant 4 in Fig. 3-2). The words that were characteristic of the Area 1 group only were "tsunami", "nothing", and "task", which indicate the critical situation of the disaster, and words related to internal exposure measurement such as "whole body counter", "measurement", and "hear" (upper part of quadrant 4 in Fig. 3-2). Furthermore, frequent words characteristic of the Area 2 female section chief group included "radiation," which was close to the word "children", indicating concerns about exposure to family members (upper part of quadrant 3 in Fig. 3-2). In contrast, the frequent words char-

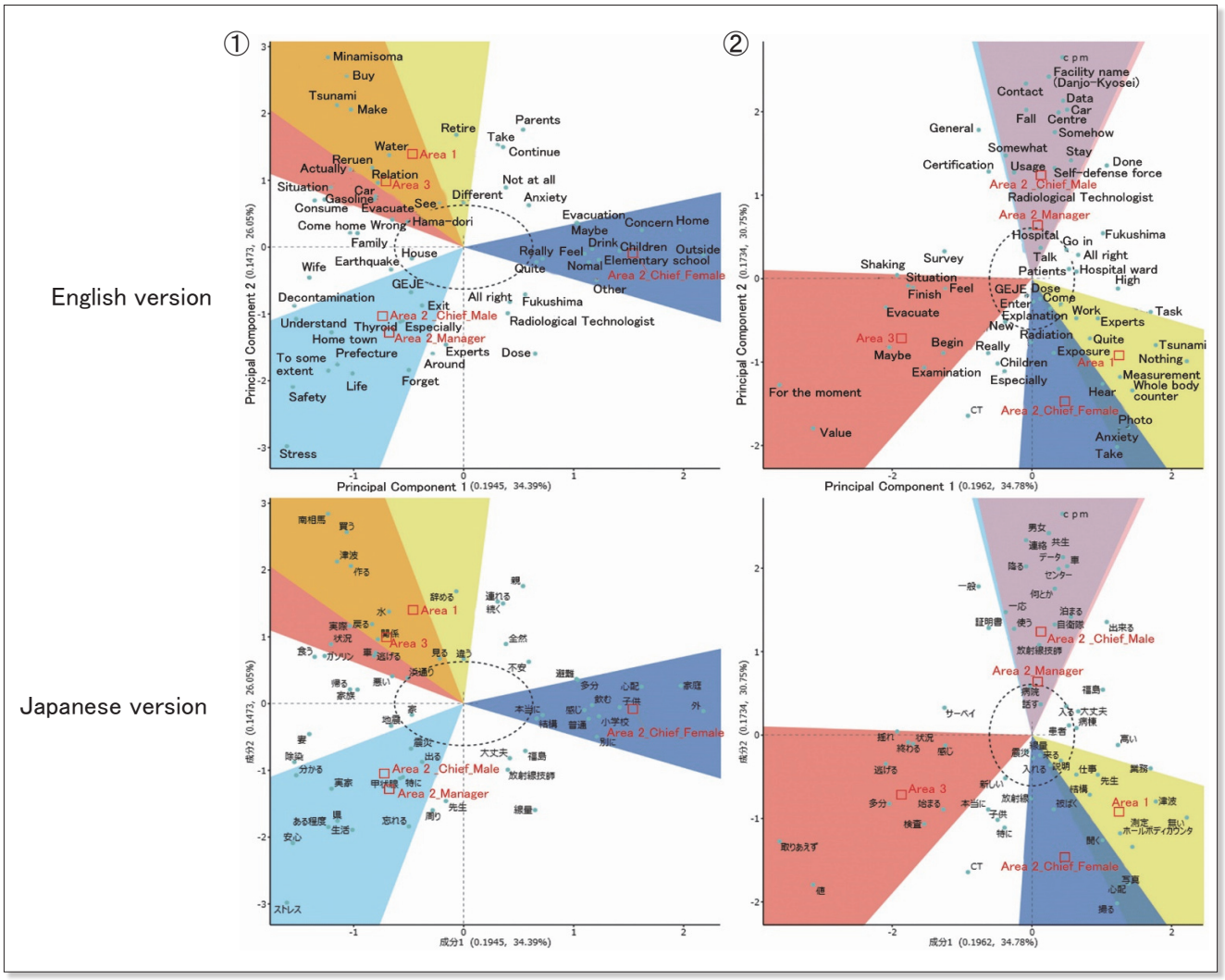

Fig. 3　The correspondence analysis using KH coder in 5 groups

① Anxiety about health effects of radiation exposure and changes in their daily life at the main-topic A
② Changes in their work and the issues faced at the main-topic B

acteristic of the Area 3 group were independent of the other groups and included "evacuate", "examinations", and "value", – all words related to body surface contamination testing (quadrant 3 of Fig. 3-2).

4. Discussion

We examined radiological technologists' experiences of the FDNPS accident from immediately after the accident to the present-day using text mining methodology based on utterance content from five groups of interviewees with different backgrounds. The proportion of statements and utterance content were characteristic of each participant's background, reflecting their experiences and lessons learned from the nuclear disaster – important information for future generations. The results of the study contribute to human resource development contents in Japan to raise awareness of radiological technologists' roles in a future nuclear disaster.

4-1. Regional differences based on the ratio of utterance occurrence by topic

The study found regional characteristics in the work of radiological technologists in response to the FDNPS accident. In the Area 1 group, effects of the accident were reported,

such as hospital evacuation, other GEJE-related tasks and internal exposure measurement examination. The proportion of utterances in the main-topic B: "Changes in their work and the issues faced" in the Area 1 group was 61.4%, which was higher than the proportion in the other groups (Table 3). In the Area 1 group, words related to "critical situation of disaster" and "implementation of internal exposure measurement" appeared as the main-topic B: "Changes in their work and the issues faced" (Fig. 3-2). The Area 1 group was strongly related to the subtopics d. "GEJE-related works" and e. "The measurement of radiation exposure dose" in the main-topic B (Table 2). The Area 1 group was forced to evacuate the hospitals during the GEJE. These medical workers faced extreme stress because they were in a "critical situation of disaster" [13]. The statements suggest that the indoor evacuation of medical facilities was also related to the "critical situation of disaster". Indoor evacuation is an effective measure for radiation protection in the event of a nuclear disaster [1], but it was evident that radiological technologists struggled to facilitate effective indoor evacuation after the nuclear disaster. The frequent occurrence of the term "implementation of internal exposure measurement" suggests that this was because internal exposure examinations using whole body counters had been conducted in the 20–30 km radius from the FDNPS, including Area 1 (Fig. 1), from the early stages of the accident [14]. Thus, the participants in the Area 1 group were required to respond to demands that they had never experienced before, and they were strongly affected by the FDNPS accident. Based on the lessons learned from the accident, the education programme for radiological technologists in municipalities within a 30 km radius of a nuclear power station – that is within the UPZ (Urgent Protective action planning Zone) – should be designed to provide them with the opportunity to perform unexpected and special tasks, such as internal exposure examinations in crisis situations. The need to provide educational content on knowledge and skills for sudden and special work-related tasks was emphasised.

The Area 2 group was required to maintain the in-hospital healthcare delivery capacity in the GEJE, and manage radiation protection for residents and their families outside the hospital. This group had a higher rate of utterance occurrence for the main-topic A: "anxiety about health effects of radiation exposure and changes in their daily life" than the Area 1 group, and a lower rate of utterance occurrence for the main-topic B: "Changes in their work and the issues faced" than those in Area 1 (Table 3). The results of the correspondence analysis (Figs. 3-1 and 2) showed that the characteristic frequent utterances represented the participants' daily life, rapid changes in their work (Area 2 department managers' and the Area 2 male section chiefs' groups) and daily concerns related to children and family (Area 2 female section chiefs' group). These utterances were related to the Table 2 subtopics a. "Health effects within their family", d. "GEJE-related works", and e. "The measurement of radiation exposure dose". The reason for the emergence of "GEJE-related works" was that the localities in Area 2 were not ordered to evacuate even though many medical facilities were affected by the GEJE, and therefore, efforts were made to maintain the normal level of medical care provision despite the excessive burden of maintaining both disaster and routine medical care in that context. Subtopic e. "The measurement of radiation exposure dose" reflected the fact that at the time of the FDNPS accident, body surface contamination examination sites were set up in various municipalities in Area 2 [15], and Area 2 radiological technologists were mobilised as body surface contamination surveyors and decontamination staff [8]. In contrast, a. "Health effects within their family", confirmed that medical personnel were involved with their families and communities away from

the workplace and "needed knowledge of radiation protection to cope with concerns about radiation exposure in their daily lives" even outside of their work. Therefore, it was suggested that in areas outside the 30 km radius of a nuclear power station (outside the UPZ), radiological technologists still need to have knowledge and skills to deal with a nuclear disaster and knowledge about radiation protection for use in their daily lives.

This study showed that the Area 3 group was required to know about radiation protection in the event of a nuclear disaster and to communicate effectively to convey this knowledge. The Area 3 group had a higher rate of occurrence of the main-topic A: "anxiety about health effects of radiation exposure and changes in their daily life" than the Area 1 participants, and a lower rate of occurrence of the main-topic B: "Changes in their work and the issues faced" than the Area 1 group (Table 3). The results of the correspondence analysis (Figs. 3-1 and 2) suggest that words related to "acceptance of evacuees" appeared among the characteristic frequent utterances, originating from the body surface contamination examinations in subtopic e. "The measurement of radiation exposure dose" (Table 2). In fact, in the acute phase of the GEJE, the damage to medical facilities and radioactive contamination in Area 3 was less severe than in Areas 1 and 2, and thus, the "acceptance of evacuees" was needed to establish a system to conduct body surface contamination examinations. In addition, the Area 3 group noted that "there were many questions about how to cope with radiation exposure during the body surface contamination examinations". Therefore, it was considered that the education curriculum in areas relatively far from a nuclear power station (e.g. outside the 80 km zone in the case of the FDNPS accident) should focus on education that includes communication about radiation protection for evacuees with body surface contamination.

In summary, the findings suggest that human resource development for radiological technologists responding to a nuclear disaster needs to be flexible in providing knowledge and technical content with an awareness of the different roles based on the distance from a nuclear power station.

4-2. Occurrence of utterance topics based on job position and gender

Utterance topic occurrence rates were distinctive according to job position and gender, even if the work area was the same.

The Area 2 department managers' group and the Area 2 male section chiefs' group had significantly different frequencies of each main topic in relation to the total utterances (Table 4). However, a correspondence analysis showed that the characteristic words of these two groups were similar and overlapping (Figs. 3-1 and 2). These characteristic tendencies were related to the subtopics d. "GEJE-related works" and e. "The measurement of radiation exposure dose" in Table 2. However, the members of the Area 2 department managers' group in this study were male only (Table 1). Therefore, the strong association between the Area 2 department managers and Area 2 male section chiefs (in Figs. 3-1 and 2) was that, regardless of their job, the men were required to perform duties such as body surface contamination measurement, air radiation dose rate measurement [8], and radiation protection activities for residents and hospital patients and staff at medical facilities following the FDNPS accident.

In contrast, the proportion of occurrences of the main-topic A: "anxiety about health effects of radiation exposure and changes in their daily life" in the Area 2 female section chiefs' group was significantly higher than in the other groups (Table 4). This was strongly related to subtopic a. "Health effects within their family" in Table 2. The correspondence analysis (Figs. 3-1 and 2) showed that the characteristic

frequent utterances of the Area 2 female section chiefs' group were mainly concerns about radiation exposure related to children and family in daily life. The Area 2 female section chiefs in this study were in their 30s and 40s, the age group most concerned about "Health effects within their family" compared with other generations. Previous studies have shown that women working in radiation-related jobs have a more conservative level of radiation exposure tolerance with regard to radiation risk perception than men [16]. The findings of our study suggest that Area 2 female section chiefs were very concerned about radiation protection of their families and children.

Regardless of their position, male radiologists were interested in radiation protection of local residents and medical facility personnel as part of their work. In contrast, women were more interested in radiation protection for their families in their daily lives. Although training related to nuclear disasters has been systematised in recent years [3], it does not necessarily consider health workers' backgrounds, mainly focusing on education and training to carry out radiation protection for local residents and medical facility personnel. The results of this study suggest that human resource development of radiological technologists for future nuclear disasters should consider established educational content and comprehensive knowledge and skills from the viewpoint of affected residents, with an awareness of radiation protection in daily life.

4-3. Limitations and future research

The study has some limitations that should be acknowledged. 1) We reported the experiences of radiological technologists who responded to the FDNPS accident. Therefore, the possibility that the participants' utterances were influenced by regional characteristics specific to Fukushima Prefecture cannot be denied. However, the trend of activities during the FDNPS accident depending on the distance from a nuclear power station can be considered as a reference for human resource development in the event of a nuclear disaster; 2) The study did not include FGIs with female radiological technologists in Areas 1 and 3. Thus, uncertainties in the study of human resource development related to gender remain. However, Area 2 is located between Areas 1 and 3 in terms of distance from the FDNPS and, as shown in Table 3 and Fig. 3-2, it is possible that Area 1 and Area 3 were similar in terms of the activities undertaken. Therefore, comprehensive education on radiation protection measures that can be taken in daily life is necessary regardless of the distance from a nuclear power station; 3) The considerations on distance from a nuclear power station in this study were applicable to some nuclear accidents at facilities for commercial power reactors because of the lessons learned from the FDNPS accident. Flexible modification of education according to the size of the nuclear facility is necessary because the radius of PAZ (Precautionary Action Zones) and UPZ for other nuclear-related facilities varies depending on the type and size of the facility [4]; and 4) The results of this study may not necessarily be generalisable because of the relatively small number of participants and the use of qualitative research methods. In the future, we plan to conduct a questionnaire survey that would allow greater generalisation of the findings and the proposal of an appropriate educational programme for human resource development based on the background of radiological technologists.

5. Conclusion

To effectively manage a future nuclear disaster, human resource development needs to focus on comprehensive educational content that takes differences in work regions into account, based on distance from a nuclear power station. Radiation protection in everyday family

life should also be included when preparing for potential nuclear accidents and emergencies. In Japan, the NRA and other organisations are taking the lead in standardising educational content for the human resource development of responders to a nuclear disaster [3, 6]. They need to reflect the characteristics of the location level based on the experience of the FDNPS accident and ensure these characteristics are passed on to the next generation. This study contributes to the human resource development of radiological technologists who can respond appropriately in the event of a nuclear disaster.

6. Acknowledgements

We would like to thank all the participants in this study. We would also like to express our sincere gratitude to Ms. Mami Nemoto, Secretary of the Department of Radiation Disaster Medicine, Faculty of Medicine, Fukushima Medical University, for her efforts in the smooth conduct of this study. This work was supported by the Research project on the Health Effects of Radiation (JFY 2015-2017) "Proposal of feasible group-tailored risk communication on radiation-related health anxiety" organised by Ministry of the Environment, Japan. We thank Michelle Pascoe, PhD, from Edanz (https://jp.edanz.com/ac) for editing a draft of this manuscript.

References

1) Ohba T, et al.: Evacuation after a nuclear accident: Critical reviews of past nuclear accidents and proposal for future planning. Environ Int, 148, 106379, 2021.
2) U.S. Department of Energy. Radiation emergency assistance center/training site. https://orise.orau.gov/reacts/index.html (22 February 2024, date last accessed).
3) Tominaga T.: Current status of education and training on medical responses in the event of a nuclear disaster (Japanese). Isotope News, 770, 18-20, 2020.
4) Nuclear Regulation Authority.: Guide for Emergency Preparedness and Response (Japanese). https://www.nra.go.jp/activity/bousai/measure/index.html (22 February 2024, date last accessed).
5) ICRP: Application of the commission's recommendations for the protection of people in emergency exposure situations. Ann ICRP, 39(1), 1-67, 2009.
6) Tsujiguchi T, et al.: Survey on training of the nuclear emergency medical assistance team and their educational needs. Radiat Environ Med, 8(1), 16-20, 2019.
7) Tosa T.: Radiation survey initiatives (Special issues:27th Japan Conference of Radiological Technologists) (Japanese). JART, 58(12), 1143-1146, 2011.
8) Yusa T.: Efforts and future responses to the Great East Japan Earthquake by the Fukushimaken Association of Radiological Technologist (Special issues:28th Japan Conference of Radiological Technologists) (Japanese). JART, 59(12), 1541-1545, 2012.
9) Anme T.: Group interview methods in human services-Development of scientifically based qualitative research methods (Japanese). 1-138, Ishiyaku Pub,Inc., Tokyo, 2001.
10) Hasegawa A, et al.: Lexical analysis suggests differences between subgroups in anxieties over radiation exposure in Fukushima. J Radiat Res, 59(2_suppl), ii83-ii90, 2018.
11) Furukawa R.: Introduction to Nvivo for Nursing Research (Japanese). 1-232, Shinyousya, Tokyo, 2019.
12) Higuchi K.: Quantitative text analysis for social research-Inheritance and development of content analysis (Japanese). 1-264, Nakanishiya Shuppan, Kyoto, 2020.
13) Sawano T, et al.: Emergency hospital evacuation from a hospital within 5 km radius of Fukushima Daiichi nuclear power plant: A retrospective analysis of disaster preparedness for hospitalized patients. Disaster Med Public Health Prep, 16(5), 2190-2193, 2022.
14) Hayano RS, et al.: Whole-body counter survey results 4 months after the Fukushima Dai-ichi NPP accident in Minamisoma City, Fukushima. J Radiol Prot, 34(4), 787-799, 2014.
15) Kondo H, et al.: Screening of residents following the Tokyo electric Fukushima Daiichi nuclear power plant accident. Health Phys, 105(1), 11-20, 2013.
16) Miura M, et al.: Perception of radiation risk by Japanese radiation specialists evaluated as a safe dose before the Fukushima nuclear accident. Health Phys, 110(6), 558-562, 2016.

Received February 28, 2022; accepted December 8, 2022

A Prospective Study of Muscle Stiffness Using Ultrasound Shear Wave Elastography in the Biceps Brachii of Patients with Parkinson's Disease

KOBAYASHI Satoshi, RT, PhD[1)], KASAI Kenji, PT, MS[2)], YABE Hitoshi, MS[3)], IMAO Masashi, RT, MS[4)], HASHIMOTO Yuji, MD, PhD[5)], ICHIKAWA Tadashi, MD, PhD[5)]

1) Department of Radiology, Saitama Prefectural Rehabilitation Center
2) Department of Physical Therapy, Saitama Prefectural Rehabilitation Center
3) Department of Radiology, Faculty of Health Sciences, Tsukuba International University
4) School of Radiological Sciences, Faculty of Health Science, Gunma Paz University
5) Department of Neurology, Saitama Prefectural Rehabilitation Center

Note: This paper is secondary publication, the first paper was published in the JART, vol. 70 no. 848: 5-11, 2023.

Key words: Parkinson's disease, biceps brachii muscle, ultrasound shear wave elastography, Movement Disorder Society-Sponsored Revision of the Unified Parkinson's Disease Rating Scale (MDS-UPDRS), rigidity

【Abstract】
In patients with Parkinson's disease (PD), the relationship between biceps brachii muscle stiffness measured using ultrasound shear wave elastography (SWE) and upper extremity rigidity score (indicating severity) evaluated using the Movement Disorder Society-Sponsored Revision of the Unified Parkinson's Disease Rating Scale (MDS-UPDRS) is unclear. This study measured biceps brachii muscle stiffness using SWE and scored upper extremity rigidity based on the MDS-UPDRS in 43 patients with PD. Factors affecting muscle stiffness measured using SWE were identified using multiple regression analysis. Threshold values of muscle stiffness detected on SWE were calculated for each upper extremity rigidity score according to MDS-UPDRS. This study included 43 patients with PD (20 men and 23 women). MDS-UPDRS upper extremity rigidity scores of 2 and 3 were identified as factors affecting muscle stiffness measured using SWE. The results suggest that the threshold values of muscle stiffness measured using SWE in the dominant arm can be used to determine MDS-UPDRS upper extremity rigidity scores of 1, 2, and 3.

1. Introduction

Parkinson's disease (PD) is a progressive neurodegenerative disorder characterized by resting tremors, bradykinesia, rigidity, and postural reflex impairment [1)]. Rigidity refers to an increased state of muscle tonus, which is perceived as resistance when the joints are moved passively. Muscle rigidity is different between the left and right sides in many patients, with the dominant side often remaining unchanged throughout the medical history [2)].

To assess the severity of Parkinson's disease (PD) based on multiple assessment items encompassing both motor and non-motor symptoms, the Unified Parkinson's Disease Rating Scale (UPDRS), proposed by Fahn et al. [3)], and subsequently revised by the Movement Disorder Society (MDS) as the MDS-UPDRS [4)], is widely used in clinical and research settings worldwide. The MDS-UPDRS is composed of parts I–IV [4)], as follows. Part I: nonmotor experiences of daily living, Part II: motor experiences of daily living, Part III: motor examination, and Part IV: motor complications. Part III includes an assessment of the severity of upper extremity rigidity (3.3) [4)]. The severity of upper extremity rigidity is evaluated separately on the left and right sides on a 5-point scale: 0 - normal, 1 - very mild, 2 - mild, 3 - moderate, and 4 - severe (Table 1) [4)].

Rigidity is assessed by the resistance (stiffness) to muscle stretch encountered when the examiner passively moves the patient's joints [4)]. Due to the difficulty in evaluating this resistance quantitatively and the need for expertise,

Table 1 MDS-UPDRS rigidity scoring criteria for upper extremities[4)]

Instructions to examiner: Rigidity is judged on slow passive movement of major joints with the patient in a relaxed position and the examiner manipulating the limbs and neck. First, test without an activation maneuver. Test and rate the neck and each limb separately. For arms, test the wrist and elbow joints simultaneously. For legs, test the hip and knee joints simultaneously. If no rigidity is detected, use an activation maneuver, such as tapping fingers, fist opening/closing, or heel tapping, in a limb not being tested. Explain the patient to go as limp as possible as you test for rigidity. 0: Normal: No rigidity. 1: Slight: Rigidity only detected with activation maneuver. 2: Mild: Rigidity detected without the activation maneuver, but full range of motion is easily achieved. 3: Moderate: Rigidity detected without the activation maneuver; full range of motion is achieved with effort. 4: Severe: Rigidity detected without the activation maneuver and full range of motion not achieved.	SCORE RUE LUE

Note: MDS-UPDRS, Movement Disorder Society-Sponsored Revision of the Unified Parkinson's Disease Rating Scale; RUE, right upper extremity; LUE, left upper extremity.

assessing the rigidity score (severity) is challenging[4)]. Therefore, there is a demand for methods that utilize objective and quantifiable indicators to assess the rigidity score (severity).

Ultrasound shear wave elastography (SWE) can be used to determine tissue stiffness (Young's modulus) based on the propagation speed of the shear waves generated in the body [5), 6)]. The propagation speed of the shear waves varies according to tissue stiffness [7)]. SWE is employed to study the mechanical properties of skeletal muscles, including the assessment of passive stiffness [8-11)] and stiffness changes during voluntary contractions [7), 12)]. Chen et al. investigated muscle stiffness using SWE of the biceps brachii muscle in 10 healthy controls according to sex during 30° flexion and extension of the elbow [13)]. They reported that SWE is reproducible and valid for quantification of biceps brachii stiffness. However, there have been few reports on the quantitative assessment of muscle stiffness in patients with PD [14)]. Du et al. found a relatively strong correlation between muscle stiffness measured using SWE in the biceps brachii of patients with PD and the comprehensive motor symptom score ($r = 0.646$, $P < 0.001$) from 14 assessment items in the UPDRS Part III [14)]. They reported that SWE of the biceps brachii was effective for the quantitative evaluation of muscle stiffness in patients with PD. Additionally, they observed that the higher the muscle rigidity of the upper limb, the higher the measured Young's modulus (muscle stiffness), which directly correlated with a decline in upper limb motor function. Therefore, they stated that "muscle stiffness assessed using SWE in the biceps brachii of patients with PD seems to be closely related to the rigidity score (severity)" [14)]. However, this report did not explicitly elucidate the relationship between muscle stiffness measured using SWE in the biceps brachii of patients with PD and the rigidity score (severity) for the upper limbs, a single evaluation item in the UPDRS for the same location.

The objective of this study was to clarify the relationship between biceps brachii muscle stiffness measured using SWE and the upper extremity rigidity score (severity) evaluated using the MDS-UPDRS in patients with PD. Additionally, this study aimed to clarify thresholds for muscle stiffness using SWE for each rigidity score.

2. Methods

2-1 Participants and Evaluation

This was a single-center prospective investigation conducted at our institution. This study included patients with PD who were admitted to our hospital between January and July 2019. PD was diagnosed in these patients by neurologists based on the widely used clinical diagnostic criteria for Parkinson's disease established by the MDS [15)]. In contrast, the control group consisted of healthy individuals without

a history of neuromuscular disorders or receiving any medication therapy.

For patients with PD, muscle stiffness was measured using SWE in the biceps brachii and upper extremity rigidity was assessed using the MDS-UPDRS. For comparison, healthy controls underwent muscle stiffness measurements using SWE in the biceps brachii.

2-2 Measuring muscle stiffness (Young's modulus) using SWE in biceps brachii

Muscle stiffness (Young's modulus) was measured using SWE in patients with PD and healthy controls separately for the biceps brachii muscles on the left and right sides. All participants were positioned in a supine position with their arms placed at their sides to ensure complete relaxation of the hands and limbs [14]. Muscle stiffness was measured using an Aplio i700 system (Canon Medical Systems, Tochigi, Japan) equipped with a linear probe operating at frequencies of 4.0–18.2 MHz. The scan was initiated with a B-mode image set of skeletal muscles to observe the biceps brachii [16, 17]. Subsequently, the probe orientation was adjusted in the direction of the biceps brachii muscle fibers (longitudinal view) [5, 13, 14, 18]. Furthermore, the probe was gently positioned on the skin overlying the biceps brachii without exerting tissue compression. The middle portion of the muscle belly, where the thickest muscle bundle was located, was identified [11, 14, 19-22]. Thus, our measurement approach closely followed methods with documented research outcomes [11, 14, 19-22]. Subsequently, the measurement mode was switched to SWE to quantify the muscle stiffness. The SWE function offers three image display modes: propagation speed, muscle stiffness, and propagation (arrival-time contours). In Fig. 1, the left side (1a) represents the muscle stiffness display and the right side (1b) illustrates the propagation display. The propagation display presents shear waves propagating within the muscle as moving images (Fig. 1b). Color-coded boxes overlaid on the B-mode image represent the regions of interest (ROI) (Fig. 1a). The color scale within these coded boxes, featuring blue (soft tissue) and red (hard tissue), reflects the values of muscle stiffness within the ROI (Fig. 1a). For the quantitative analysis, a circular ROI with a diameter of 5 mm was placed within the box [14, 23]. This allowed the calculation of muscle stiffness (Young's modulus) within the circle (Fig. 1a). The settings for muscle stiffness measurements included a depth of field of 4 cm, a single focal point, and tissue harmonic imaging. Muscle stiffness measurements were conducted three times separately in the left and right biceps brachii of all participants (patients with PD and healthy controls) [13, 14]. The average value was then calculated, serving as the representative value for muscle stiffness in the left and right biceps brachii separately [13, 14]. These measurements were applied to all par-

(1a) 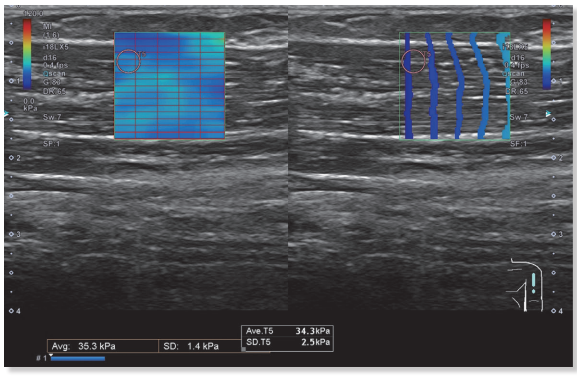

(1b)

Fig. 1 Measuring muscle stiffness using SWE in longitudinal plane of biceps brachii

Muscle stiffness (Young's modulus) was measured at the middle portion of the biceps brachii muscle belly where the muscle bundle was the thickest [14]. SWE has three image display modes: propagation speed, muscle stiffness, and propagation (arrival time contour). The left image (1a) shows the muscle stiffness display mode, and the right image (1b) shows the propagation display mode. The propagation display mode shows the shear wave propagation within the muscle tissue as a moving image (1b). The colored box superimposed on the B-mode scan image represents the region of interest (ROI) (1a). Muscle stiffness (Young's modulus) values are represented by a color scheme in the ROI box: blue indicates soft tissue and red indicates hard tissue (1a). A 5-mm diameter circle was placed within the ROI for quantitative measurement [14, 23], and the muscle stiffness (Young's modulus) was calculated within the circle (1a). Muscle stiffness measurements were conducted three times separately in the left and right biceps brachii of all participants (patients with PD and healthy controls) [13, 14].

ticipants. Muscle stiffness measurements were conducted by a single radiological technologist, a certified sonographer with over 14 years of experience in ultrasound examinations.

The reasons for conducting the measurements in triplicate are as follows. Previous studies on stiffness measurement of the biceps brachii muscle using SWE have reported good intra- and inter-rater reliability even with 2–3 measurements [13), 14), 20), 21)]. In our preliminary study, however, we could not confirm the inter-rater reliability because there was only one examiner; however, the intra-rater reliability was good. Therefore, we adopted three measurements in this study.

2-3 Upper extremity rigidity scores evaluated using the MDS-UPDRS

Rigidity score (severity) was assessed using Part III, 3.3 of MDS-UPDRS to evaluate upper extremity rigidity (Table 1) [4)]. This assessment was performed separately for the left and right upper limbs in all patients with PD. The limb with higher rigidity was designated as the dominant arm, whereas the limb with lower rigidity was considered the non-dominant arm. Muscle rigidity was scored by a physical therapist with > 16 years of experience in physical therapy for patients with PD. Muscle stiffness and rigidity scores were rated on the same day at the same time.

2-4 Statistical analysis

To analyze the factors influencing muscle stiffness measured using SWE, a multiple regression analysis was conducted with muscle stiffness using SWE as the dependent variable. The seven independent variables were age, sex, and MDS-UPDRS rigidity scores ranging from 0 to 4, each for both upper extremities (dominant and non-dominant arms), and the dominant arm. Sex and dominant arm were represented as dummy variables in the analysis. The selection of seven independent variables in the multiple regression analysis was based on the results of previous studies and clinical judgment [14)]. Additionally, the threshold for muscle stiffness in the dominant arm was calculated using Receiver Operating Characteristic (ROC) curve analysis. The intra-rater reliability of SWE muscle stiffness measurements was assessed using the intraclass correlation coefficient (ICC). The significance level was set at 5%, with a P-value < 0.05 considered statistically significant. All analyses were performed using EZR software (Jichi Medical University Saitama Medical Center, Saitama, Japan) [24)].

2-5 Ethical Consideration

This study was approved by the Ethics Committee of our institution (Approval Number: H29-015). Written informed consent was obtained from all the participants. This study was conducted in accordance with the principles of the Declaration of Helsinki.

3. Results

In 43 patients with PD, muscle stiffness measurements using SWE in the biceps brachii and assessments of upper extremity rigidity using the MDS-UPDRS were conducted. Additionally, 12 healthy controls underwent muscle stiffness measurements using SWE in the biceps brachii. The 43 patients included 20 males (40 limbs) and 23 females (46 limbs) (Table 2). The average age was 69.7 years ± 8.3 years. The 12 healthy controls included 5 males (10 limbs) and 7 females (14 limbs), with an average age of 67.9 ± 5.3 years.

Based on the criteria for upper extremity rigidity scores using the MDS-UPDRS assessment (Table 1) [4)], the frequency of each rigidity score in the 43 patients with PD (86 limbs) was as follows: score 0, eight limbs (9.3%); score 1, 23 limbs (26.7%); score 2, 44 limbs (51.2%); score 3, 11 limbs (12.8%); and score 4, 0 limbs (0%).

Fig. 2 illustrates the muscle stiffness (Young's modulus) as measured on SWE for each rigidity score in the MDS-UPDRS upper limb assess-

Table 2 Clinical characteristics of patients with PD and control groups

Item	Control (*n*=12)	PD (*n*=43)	*P*-value
Age, mean±SD	67.9±5.3	69.7±8.3	$p \geqq 0.05$
Female sex, n (%)	7 (58.3%)	23 (53.5%)	$p \geqq 0.05$

Note: PD, Parkinson's disease.

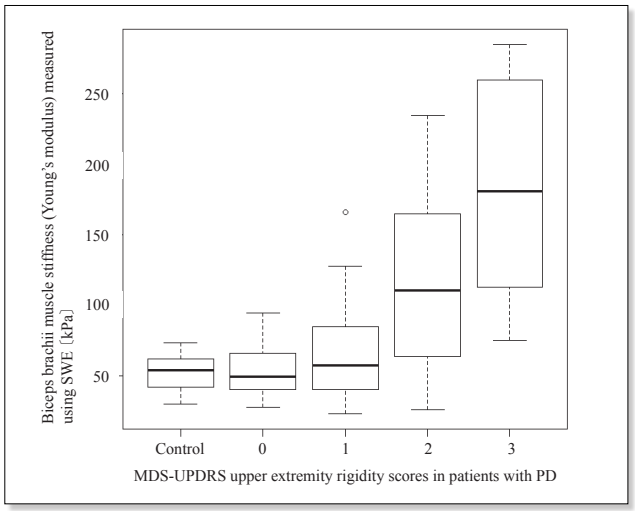

Fig. 2 Muscle stiffness (Young's modulus) measured using SWE for each MDS-UPDRS upper extremity rigidity score in patients with PD.

ment in patients with PD. Specifically, it shows the stiffness of the right biceps brachii with respect to the rigidity score of the right upper limb in patients with PD. Similarly, the stiffness of the left biceps brachii is depicted with respect to the rigidity score of the left upper limb (Fig. 2). Additionally, the figure includes the muscle stiffness measured using SWE in the biceps brachii of healthy controls (control). For patients with PD, the muscle stiffness on SWE in the upper limbs for each rigidity score was as follows: score 0, 49.66 [40.80–61.20] kPa; score 1, 57.81 [40.29–84.93] kPa; score 2, 110.13 [63.69–159.14] kPa; and score 3, 180.75 [112.93–259.84] kPa. The muscle stiffness measured using SWE in the biceps of healthy controls was 53.99 [43.66–61.62] kPa.

Multiple regression analysis for both upper limbs (dominant and non-dominant arms) revealed that the factors influencing muscle stiffness measured using SWE were MDS-UPDRS upper extremity rigidity scores of 2 (P < 0.001) and 3 (P < 0.001), age (P = 0.030), and dominant arm (P = 0.012) (Table 3). Age was excluded as a factor for threshold consideration because its regression coefficient estimate was 1.44, indicating a small effect on muscle stiffness measured using SWE. The threshold for muscle stiffness in the dominant arm of patients with PD was calculated using ROC analysis. The threshold for MDS-UPDRS upper extremity rigidity scores 1 and 2 in the dominant arm was 93.55 kPa, with an area under the curve (AUC) of 0.74, and a 95% confidence interval (CI) of 0.56–0.93 (Fig. 3). For scores 2 and 3, the threshold was 170.53 kPa, with an AUC of 0.78 and a 95% CI of 0.59–0.98 (Fig. 4). The ICC for SWE was 0.94 ($p < 0.05$).

Table 3 Factors affecting muscle stiffness measured using SWE in both upper limbs (dominant and non-dominant arms)

	Regression Coefficient	*t*-value	*p*-value
Constant	−45.515		
Age	1.443	2.202	0.030
Female sex	−1.233	−0.131	0.90
MDS-UPDRS upper extremity rigidity score : 0	0.764	0.037	0.97
MDS-UPDRS upper extremity rigidity score : 1	−0.197	−0.013	0.99
MDS-UPDRS upper extremity rigidity score : 2	50.704	3.793	*P*<0.001
MDS-UPDRS upper extremity rigidity score : 3	98.327	4.839	*P*<0.001
Dominant arm	27.450	2.550	0.012

Note: Analysis of variance $p<0.001$, Coefficient of determination (R^2) = 0.440;
MDS-UPDRS, Movement Disorder Society-Sponsored Revision of the Unified Parkinson's Disease Rating Scale; SWE, shear wave elastography.

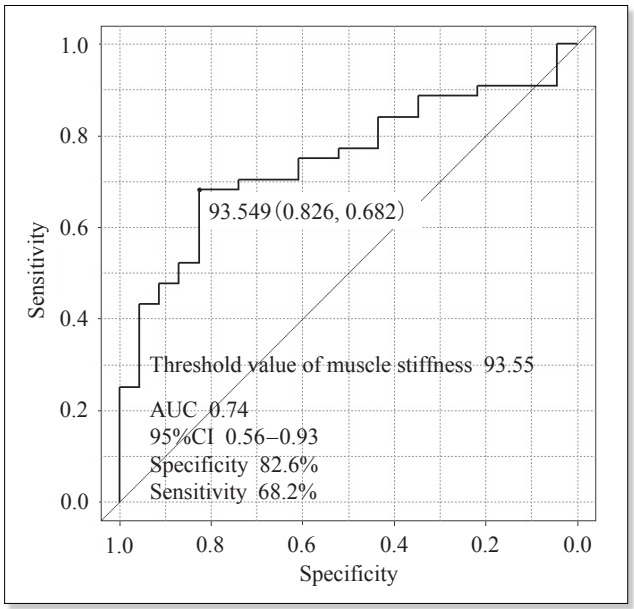

Fig. 3 ROC analysis of patients with PD with an MDS-UPDRS rigidity score of 1 or 2 in the dominant arm

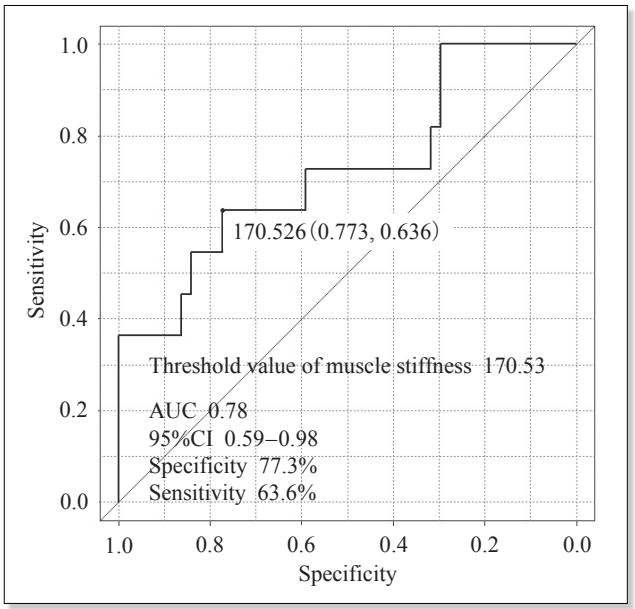

Fig. 4 ROC analysis of patients with PD with an MDS-UPDRS rigidity score of 2 or 3 in the dominant arm

4. Discussion

The objective of this study was to clarify the relationship between biceps brachii muscle stiffness measured using SWE and the upper extremity rigidity score (severity) evaluated using the MDS-UPDRS in patients with PD. Additionally, this study aimed to determine the threshold for muscle stiffness using SWE for each rigidity score.

The results of the multiple regression analysis indicated that MDS-UPDRS upper extremity rigidity scores of 2 and 3, age, and dominant arm (Table 3) were factors affecting muscle stiffness measured using SWE. Furthermore, the use of threshold values for muscle stiffness using SWE in the dominant arm suggests the potential to distinguish between rigidity scores of 1, 2, and 3 in the upper extremities.

Du et al. investigated muscle stiffness using SWE of the biceps brachii in patients with PD and healthy controls [14]. They reported that muscle stiffness in the biceps brachii of patients with PD with noticeable or mild upper limb rigidity was significantly higher than that in healthy controls. However, this study did not examine the relationship between muscle stiffness measured using SWE in the biceps brachii and upper extremity rigidity scores using UPDRS. Therefore, it remains unclear whether rigidity scores affect muscle stiffness as measured using SWE.

As a result of our multiple regression analysis, we identified that upper extremity rigidity scores of 2 and 3 were factors affecting muscle stiffness measured using SWE. Although age was also detected as a factor influencing muscle stiffness, the regression coefficient estimate was 1.44 (Table 3), suggesting that age had a minor impact on muscle stiffness. We focused on other factors that strongly influence muscle stiffness.

In the subsequent multiple regression analysis of both upper limbs (dominant and non-dominant arms), the coefficient of determination was 0.440 (Table 3). In contrast, the coefficient of determination for the dominant arm alone was 0.536, suggesting a better fit than that observed for both upper limbs. Therefore, we calculated the threshold for muscle stiffness for each upper extremity rigidity score in the MDS-UPDRS using muscle stiffness on SWE in

the dominant arm. Through ROC analysis of the dominant arm only, we calculated the threshold for muscle stiffness using the MDS-UPDRS in the dominant arm as 93.55 kPa for rigidity scores 1 and 2 (Fig. 3) and 170.53 kPa for rigidity scores 2 and 3 (Fig. 4). Based on these results, it is considered possible to distinguish between rigidity scores 1, 2, and 3 using the threshold for muscle stiffness using SWE in the dominant arm: < 93.55 kPa for rigidity score 1, 93.55–170.53 kPa for rigidity score 2, and > 170.53 kPa for rigidity score 3.

Table 1 shows the criteria for upper extremity rigidity scores in the MDS-UPDRS [4]. A score of 0 indicates "Normal," while a score of 4 indicates "Rigidity detected without the activation maneuver, and full range of motion not achieved" (Table 1) [4]. In other words, it is generally assumed that the examiner can assess accurately when the score is 0 or 4. In contrast, scores 1–3 are subjectively evaluated by the examiner, suggesting potential variability in scoring compared with scores of 0 and 4 (Table 1) [3, 4]. However, the results of this study suggest the possibility of objectively distinguishing each rigidity score using the threshold for muscle stiffness obtained using SWE. To determine an appropriate treatment approach and assess the therapeutic effects of medications, it is essential to evaluate the rigidity score (severity) using the MDS-UPDRS with objective and quantifiable indicators. Furthermore, it is crucial to ensure standardized evaluation across all medical facilities. Based on the results of this study, SWE is considered an effective method for quantifying muscle stiffness in the biceps brachii of patients with PD.

5. Limitations

The authors acknowledge the limitations of this study as a single-center investigation. In previous studies on muscle stiffness measurement, no reports have compared muscle stiffness using SWE on ultrasound devices from different manufacturers. Therefore, a future challenge is to conduct collaborative, multicenter studies, including assessments of muscle stiffness using SWE, considering the differences between manufacturers.

6. Conclusion

Upper extremity rigidity scores of 2 and 3 on the MDS-UPDRS were factors affecting muscle stiffness measured using SWE. Furthermore, the use of threshold values for muscle stiffness using SWE in the dominant arm suggests the potential to distinguish between rigidity scores of 1, 2, and 3 in the upper extremities.

Acknowledgments

We express our heartfelt gratitude for the guidance and cooperation of the many people who participated in this study. We would like to thank Editage (www.editage.jp) for the English language editing.

Conflict of Interest

The authors declare no conflicts of interest regarding this study.

References

1) Jankovic J: Parkinson's disease: clinical features and diagnosis. J Neurol Neurosurg Psychiatry, Apr, 79(4), 368-376, 2008.
2) Djaldetti R, et al.: The mystery of motor asymmetry in Parkinson's disease. Lancet Neurol, Sep, 5(9), 796-802, 2006.
3) Fahn S, et al.: Members of the UPDRS Development Committee: Unified Parkinson's Disease Rating Scale. in Recent Developments in Parkinson's Disease, Vol.2 (ed. by Fahn S, et al.):. Macmillan Health Care Information, Florham Park, NJ, 153-163, 293-304, 1987.
4) Goetz CG, et al.: Movement Disorder Society-sponsored revision of the Unified Parkinson's Disease Rating Scale (MDS-UPDRS): scale presentation and clinimetric testing results. Mov Disord, Nov, 23(15), 2129-2170, 2008.
5) Creze M, et al.: Shear wave sonoelastography of skeletal muscle: basic principles, biomechanical concepts, clinical applications, and future perspectives. Skeletal Radiol, Apr, 47(4), 457-471, 2018.

6) Brandenburg JE, et al.: Ultrasound elastography: the new frontier in direct measurement of muscle stiffness. Arch Phys Med Rehabil, Nov, 95(11), 2207-2219, 2014.
7) Shinohara M, et al.: Real-time visualization of muscle stiffness distribution with ultrasound shear wave imaging during muscle contraction. Muscle Nerve, Sep, 42(3), 438-441, 2010.
8) Maïsetti O, et al.: Characterization of passive elastic properties of the human medial gastrocnemius muscle belly using supersonic shear imaging. J Biomech, Apr, 45(6), 978-984, 2012.
9) Chino K, et al.: Measurement of gastrocnemius muscle elasticity by shear wave elastography: association with passive ankle joint stiffness and sex differences. Eur J Appl Physiol, Apr, 116(4), 823-830, 2016.
10) Gennisson JL, et al.: Viscoelastic and anisotropic mechanical properties of in vivo muscle tissue assessed by supersonic shear imaging. Ultrasound Med Biol, May, 36(5), 789-801, 2010.
11) Eby SF, et al.: Shear wave elastography of passive skeletal muscle stiffness: influences of sex and age throughout adulthood. Clin Biomech (Bristol, Avon), Jan, 30(1), 22-27, 2015.
12) Nordez A, et al.: Muscle shear elastic modulus measured using supersonic shear imaging is highly related to muscle activity level. J Appl Physiol, May, 108(5), 1389-1394, 2010.
13) Chen J, et al.: Ultrasound shear wave elastography in the assessment of passive biceps brachii muscle stiffness: influences of sex and elbow position. Clin Imaging, Sep-Oct, 45, 26-29, 2017.
14) Du LJ, et al.: Ultrasound shear wave elastography in assessment of muscle stiffness in patients with Parkinson's disease: a primary observation. Clin Imaging, Nov-Dec, 40(6), 1075-1080, 2016.
15) Postuma RB, et al.: MDS clinical diagnostic criteria for Parkinson's disease. Mov Disord, Oct, 30(12), 1591-601, 2015.
16) Gennisson JL, et al.: Transient elastography in anisotropic medium: application to the measurement of slow and fast shear wave speeds in muscles. J Acoust Soc Am, Jul, 114(1), 536-541, 2003.
17) Gennisson JL, et al.: Human muscle hardness assessment during incremental isometric contraction using transient elastography. J Biomech, Jul, 38(7), 1543-1550, 2005.
18) Eby SF, et al.: Validation of shear wave elastography in skeletal muscle. J Biomech, Sep, 46(14), 2381-2387, 2013.
19) Murayama M, et al.: Changes in biceps brachii muscle hardness assessed by a push-in meter and strain elastography after eccentric versus concentric contractions. Sci Rep, Jun 2;12(1), 9214, 2022.
20) Gao J, et al.: Quantitative ultrasound Imaging to assess the biceps brachii muscle in chronic post-stroke spasticity: Preliminary observation. Ultrasound Med Biol, Sep, 44(9), 1931-1940, 2018.
21) Phan A, et al.: Ultrasound shear wave elastography in assessment of skeletal muscle stiffness in senior volunteers. Clin Imaging, Nov-Dec, 58, 22-26, 2019.
22) Lacourpaille L, et al.: Non-invasive assessment of muscle stiffness in patients with Duchenne muscular dystrophy. Muscle Nerve, Feb, 51(2), 284-286, 2015.
23) Akagi R, et al.: Acute effect of static stretching on hardness of the gastrocnemius muscle. Med Sci Sports Exerc, Jul, 45(7), 1348-1354, 2013.
24) Kanda Y: Investigation of the freely available easy-to-use software 'EZR' for medical statistics. Bone Marrow Transplant, Mar, 48(3), 452-458, 2013.

Received July 31, 2022; accepted January 3, 2023

Fundamental study for application of 3D phase-sensitive inversion recovery sequence to multiple sclerosis

ENOKI Takuya[1),2)], JOMOTO Wataru[2)], KIDA Katsuhiro[1)], GOTO Sachiko[1)], KOTOURA Noriko[2)]

1) Graduate School of Health Sciences, Okayama University
2) Department of Radiological Technology, Hyogo Medical University Hospital

Note: This paper is secondary publication, the first paper was published in the JART, vol. 70 no. 848: 20-27, 2023.

Key words: Phase sensitive inversion recovery, Inversion time, Magnetic resonance imaging, Brain

【Abstract】
This study clarified the relationship between imaging parameters and contrast during application of the 3D phase-sensitive inversion recovery (PSIR) method for detection of multiple sclerosis. In this phantom study, we investigated the effects of the turbo field echo (TFE) factor, shot interval, and inversion time (TI) on contrast. A TFE factor of 30 and shot interval of 1000 ms were employed. In the in vivo study, visual evaluations were performed to assess the brain tissue contrast when TI variations were noted. This in vivo study enrolled 10 healthy volunteers. 3D-PSIR images were acquired with six different inversion times (300, 400, 500, 600, 700, and 800 ms). A longer inversion time for 3D-PSIR increased the contrast of the brain tissue. To apply 3D-PSIR to multiple sclerosis lesions, a TI of 700 ms is suitable when the TFE factor is 30 and the shot interval is 1000 ms.

1 Introduction

Double inversion recovery (DIR) has been widely used to detect cortical lesions in patients diagnosed with multiple sclerosis (MS)[1–4]. However, DIR has been reported to have a low signal-to-noise ratio (SNR) and sensitivity for cortical lesions [4]. Phase-sensitive inversion recovery (PSIR) is a T_1-weighted sequence that uses the inversion recovery (IR) method, which has been reported to improve the detection of cortical lesions in patients with MS, compared to that of DIR, because of its excellent contrast between the white matter (WM), gray matter (GM), and cerebrospinal fluid (CSF) and higher SNR [5–11].

In a previous study, PSIR was obtained by reconstructing real images acquired using a 2D-IR turbo spin-echo (TSE) sequence [5–11]. In the present study, we investigated the contrast of 3D-PSIR based on a gradient echo sequence, in which two signals were acquired and phase correction was performed. Since 3D-PSIR can prevent IR-induced signal polarity reversal by phase correction, it is a well-known imaging sequence that enables visualization of the injured myocardium regardless of the inversion time (TI) to nullify the signal intensity of the normal myocardium in late gadolinium-enhanced cardiac imaging [12]. However, because PSIR uses the IR method, the contrast is expected to change depending on the timing of signal acquisition [7, 13]. In a previous study, a TI of approximately 400 ms was used in 2D-PSIR [5–11]; however, because the repetition time (TR) and echo time (TE) are different in each report, the contrast is expected to differ with the same TI. Furthermore, the optimal TI may differ when using 3D-PSIR, and the turbo field echo (TFE) factor and shot interval are also expected to affect the contrast.

The purpose of this study was to clarify the relationship between imaging parameters and

contrast when applying the 3D-PSIR method for detection of MS.

2 Materials and Methods

2.1 Theory

Magnetic resonance imaging (MRI) scans were acquired using a 3.0-T MRI system with a 32-channel phased-array head coil (Ingenia; Philips Healthcare, Best, Netherlands). In the PSIR of this study, after the nonselective inversion pulse, signal acquisition was performed with a fast gradient echo after each of the two TIs. The first TI (first acquisition) acquired the magnitude-T_1 contrast image, and the second TI (second acquisition) acquired the reference image. Since the T_1 contrast image has an inverted signal polarity depending on the TI setting, the following procedure was used to calculate the PSIR image with preserved signal polarity: A B1 field correction map was created from the phase information obtained in the second acquisition, and phase correction was performed on the signals obtained in the first and second acquisitions. The phase-corrected signal was divided into real and imaginary parts using quadrature phase-sensitive detection, and the real and imaginary images were calculated using a complex Fourier transform. Subsequently, a magnitude image was calculated from the first acquisition and a phase image was calculated from the second acquisition. The magnitude image was multiplied by the phase image to reconstruct the real image and obtain the PSIR image. The timing of the two acquisitions can be adjusted using shot intervals. Figure 1 presents an overview of the sequence.

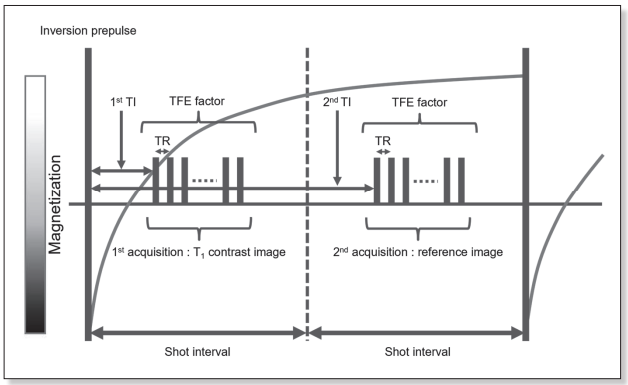

Fig. 1 Overview of PSIR sequence

After TI from the inversion pulse, the T_1 contrast image was acquired by a fast gradient echo. After a certain time, a fast gradient echo was used to acquire a reference image. The PSIR was reconstructed from the two images, and the timing of the two image acquisitions was adjusted by the shot interval.

2.2 Phantom study

To evaluate the image quality, we diluted manganese chloride tetrahydrate (MCT) and agar with saline to create phantoms for the WM model (MCT 16 w/v%, agar 0.2 w/v%), GM model (8 w/v%, agar 0.3 w/v%), and CSF model (saline). The three phantoms were stored in a polypropylene case, which was filled with agar diluted with saline (0.1 w/v%). Figure 2 shows an overview of the phantom. T_1 and T_2 values of these materials are listed in Table 1. Image quality was evaluated by the contrast-to-noise ratio (CNR) using a region of interest (ROI) for each phantom (Fig. 3). The signal intensity was measured on the console and the CNR was calculated using the following formula:

$$CNR = |SI_a - SI_b| / SD_{BG}, \quad (1)$$

where SI_a and SI_b are the mean signal intensities in phantoms a and b, respectively; SD_{BG} is the standard deviation of the background signal intensity. The background ROI was elliptical and large to reduce variation with measurement location. Preliminary experiments confirmed that the phantom created in this study provided a contrast similar to that of the in vivo phantom. Although it is desirable to create a phantom that simulates an MS lesion, the relaxation time of the lesion has not been clarified; therefore, it was difficult to create a phantom. In previous studies,

Table 1 T_1 and T_2 values of materials

Material	T_1 relaxation time (ms)	T_2 relaxation time (ms)
WM model	824.0	67.6
GM model	1329.0	114.1
CSF model	2906.2	2047.0

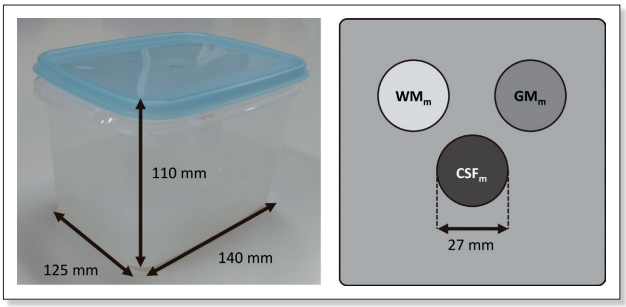

Fig. 2 Overview of the phantom

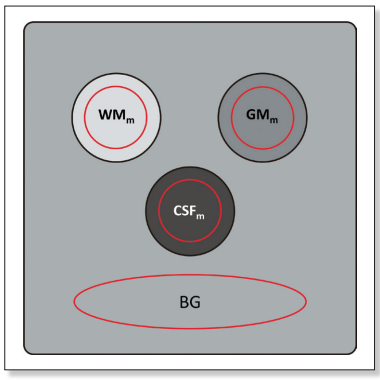

Fig. 3 Example of region of interest setting

MS lesions were more hypointense than GM lesions on 2D-PSIR [5–11] and were expected to have a signal intensity between those of GM and CSF.

3D-PSIR was performed using a 3D TFE sequence. 3D-PSIR images with three different TFE factors (20, 30, and 40), four different shot intervals (800, 1000, 1200, and 1400 ms), and nine different TIs (160, 200, 300, 400, 500, 600, 700, 800, and 840 ms) were acquired to investigate the CNR. Other parameters were as follows: field of view, 250 mm; slice orientation, coronal; pixel size, 0.98 × 0.96 mm; slice thickness, 4 mm; number of slices, 6; number of excitations, 1; sensitivity encoding factor, 1; profile order, linear; TR, 10 ms; TE, 4.6 ms; flip angle (FA), 20°; PSIR FA, 5°; bandwidth (BW), 540 Hz/pixel; and scan time, 29 s–1 min 38 s.

2.2.1 Investigation of TFE factor

The shot interval and TI were fixed at 1000 ms and 600 ms, respectively, and the TFE factor varied between 20, 30, and 40. We measured the CNR between the WM model and GM models (WM_m-GM_m), WM model and CSF models (WM_m-CSF_m), and GM model and CSF models (GM_m-CSF_m) and evaluated the change in CNR with changes in the TFE factor.

2.2.2 Investigation of shot interval

The TFE factor and TI were fixed at 30 and 600 ms, respectively, and the shot interval varied between 800, 1000, 1200, and 1400 ms. We measured the CNR between WM_m-GM_m, WM_m-CSF_m, and GM_m-CSF_m and evaluated the change in CNR with the changes in the shot interval.

2.2.3 Investigation of TI

The TFE factor and shot interval were fixed at 30 and 1000 ms, respectively, and TI varied between 160, 200, 300, 400, 500, 600, 700, 800, and 840 ms. We measured the CNR between WM_m-GM_m, WM_m-CSF_m, and GM_m-CSF_m and evaluated the change in CNR with the changes in TI. We evaluated the changes in the mean signal intensities of each phantom associated with TI change.

2.3 In vivo study

Ten healthy volunteers (five males and five females; age range, 23–57 years; median [interquartile range] age, 39.5 [12.5] years) were enrolled in this study. The Institutional Review Board of Hyogo Medical University approved this study, and informed consent was obtained from all participants in accordance with the Declaration of Helsinki (approval number 202104-521).

3D-PSIR was performed using a 3D TFE sequence. 3D-PSIR images with six different

TIs (300, 400, 500, 600, 700, and 800 ms) were acquired to investigate the brain tissue contrast. Other parameters were as follows: field of view, 230 mm; slice orientation, transverse; pixel size, 0.85 × 0.85 mm; slice thickness, 3 mm; number of slices, 35; number of excitations, 1; sensitivity encoding factor, 2; profile order, linear; TFE factor, 30; shot interval, 1000 ms; TR, 10 ms; TE, 4.6 ms; FA, 20°; PSIR FA, 5°; BW, 540 Hz/pixel; and scan time, 2 min 17 s. The imaging slab was parallel to the anterior commissure-posterior commissure line, and the center of the imaging slab was set at the level of the insular cortex.

2.3.1 Visual evaluation

Five radiologists (10–26 years of reading experience) performed the visual evaluation using the normalized ranking method [14]. WM-GM, WM-CSF, and GM-CSF contrasts at the insular cortex level were evaluated. The medical imaging display monitor was set to a six-split display, and the six TI images were randomly placed for each evaluation item and for each volunteer, and ranked accordingly. Since 3D-PSIR has a different background signal, the image was magnified to the furthest extent, so that the background signal was not observed.

2.3.2 Statistical analysis

Kendall's coefficient of concordance (W) was calculated from the ranked results obtained from the visual evaluation. W ranges from 0 to 1, where 0 indicates no agreement among raters and 1 indicates complete agreement. The ranked results were normalized, and a one-way analysis of variance was performed on the means of the normalized scores. The modified least significant difference (MLSD) of the Fisher–Hayter procedure was used to determine significant differences among the ranks [15].

Statistical analysis was performed using the JMP Pro ver.15.2.0 software (SAS Institute, Cary, NC, USA). Statistical significance was set at $p < 0.05$.

3 Results

3.1 Phantom study

Figures 4 and 5a show MR images and CNR results for the different TFE factors. The CNR decreased as the TFE factor increased. When the TFE factor was 40, strong blurring occurred. The CNR increased as the shot interval and TI increased (Fig. 5b and c). The signal intensities of WM_m, GM_m, and CSF_m increased as TI increased. The signal intensities of each phantom increased as TI increased,

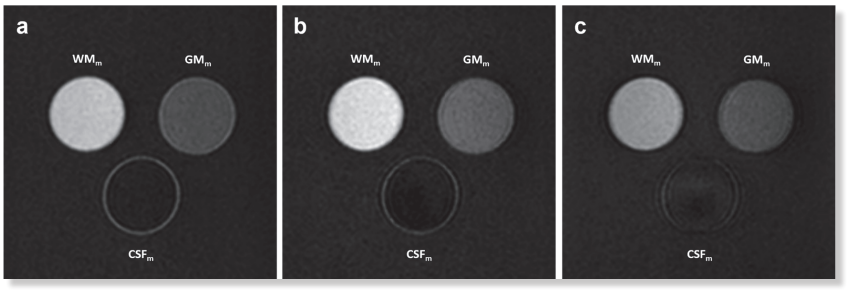

Fig. 4 MR images for different TFE factor
(a) TFE factor=20. (b) TFE factor=30. (c) TFE factor=40.

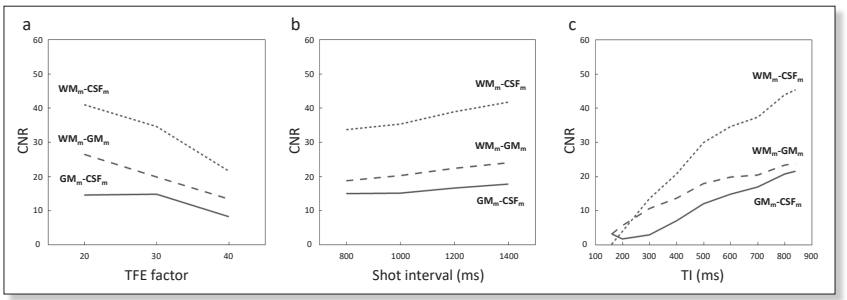

Fig. 5 Relationship between CNR of the phantom and each parameter
(a) CNR of WM_m-CSF_m, WM_m-GM_m, and GM_m-CSF_m for different TFE factors.
(b) CNR of WM_m-CSF_m, WM_m-GM_m, and GM_m-CSF_m for different shot intervals.
(c) CNR of WM_m-CSF_m, WM_m-GM_m, and GM_m-CSF_m for different TIs.

and the difference in the signal intensities of each phantom became larger (Fig. 6).

3.2 In vivo study

Figure 7 shows MR images of a volunteer. The tissue contrast varied for each TI. The signal intensities of WM, GM, and CSF increased as TI increased.

The rank order of the visual evaluation of the WM-GM contrast was 600 > 700 > 500 > 800 > 400 > 300 (Table 2). The differences in the normal scores among these ranks were 0.323, 0.212, 0.350, 0.359, and 0.628, respectively, and there were no significant differences between 500 and 700 (W = 0.55, p < 0.001, MLSD = 0.306). The rank order of the visual evaluation for WM-CSF contrast was 700 > 800 > 600 > 500 > 400 > 300 (Table 3). The differences in the normal scores among these ranks were 0.057, 0.264, 0.687, 0.456, and 0.630, respectively, and there were no significant differences between 700 and 800 (W = 0.89, p < 0.001, MLSD = 0.168). The rank order of visual evaluation for GM-CSF contrast was 700 > 800 > 600 > 500

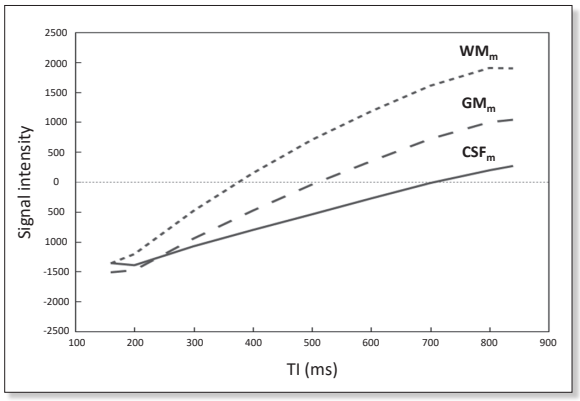

Fig. 6 Relationship between signal intensity of the phantom and each TI

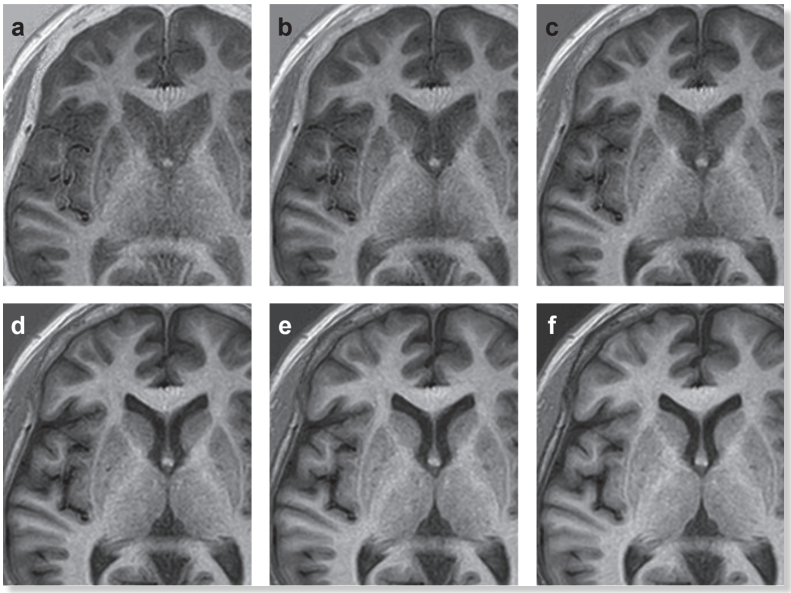

Fig. 7 Example of a PSIR image with the TI varying from 300 ms to 800 ms

(a) TI=300 ms. (b) TI=400 ms. (c) TI=500 ms. (d) TI=600 ms. (e) TI=700 ms. (f) TI=800 ms.

Table 2 Results of visual evaluation in WM-GM and significant differences in normal scores between each rank using Fisher–Hayter procedure (MLSD = 0.306)

		TI (ms)											
Rank	TI (ms)	600		700		500		800		400		300	
1	600	0		0.323	*	0.535	*	0.885	*	1.245	*	1.873	*
2	700			0		0.212	*n.s.*	0.562	*	0.921	*	1.550	*
3	500					0		0.350	*	0.709	*	1.338	*
4	800							0		0.359	*	0.987	*
5	400									0		0.628	*
6	300											0	

Significant difference: the difference between each rank is larger than that of the MLSD (α = 0.05) and indicated with *. MLSD, modified least significant difference; n.s., not significant; TI, inversion time

Table 3 Results of visual evaluation in WM-CSF and significant differences in normal scores between each rank using Fisher–Hayter procedure (MLSD = 0.168)

		TI (ms)											
Rank	TI (ms)	700		800		600		500		400		300	
1	700	0		0.057	*n.s.*	0.321	*	1.008	*	1.464	*	2.094	*
2	800			0		0.264	*	0.951	*	1.407	*	2.037	*
3	600					0		0.687	*	1.143	*	1.773	*
4	500							0		0.456	*	1.086	*
5	400									0		0.630	*
6	300											0	

Significant difference: the difference between each rank is larger than that of the MLSD (α = 0.05) and indicated with *. MLSD, modified least significant difference; n.s., not significant; TI, inversion time

Table 4 Results of visual evaluation in GM-CSF and significant differences in normal scores between each rank using Fisher–Hayter procedure (MLSD = 0.183)

		TI (ms)											
Rank	TI (ms)	700		800		600		500		400		300	
1	700	0		0.148	*n.s.*	0.229	*	0.977	*	1.458	*	2.071	*
2	800			0		0.081	*n.s.*	0.829	*	1.310	*	1.923	*
3	600					0		0.748	*	1.228	*	1.842	*
4	500							0		0.480	*	1.094	*
5	400									0		0.614	*
6	300											0	

Significant difference: the difference between each rank is larger than that of the MLSD (α = 0.05) and indicated with *. MLSD, modified least significant difference; n.s., not significant; TI, inversion time

> 400 > 300 (Table 4). The differences in the normal scores among these ranks were 0.148, 0.081, 0.748, 0.480, and 0.614, respectively. There were no significant differences between 700 and 800 or 800 and 600 (W = 0.87, $p < 0.001$, MLSD = 0.183).

4 Discussion

We conducted a fundamental study of imaging parameters for the application of 3D-PSIR in the detection of MS. The contrast between GM and CSF was important because MS lesions were expected to have a signal intensity between those of GM and CSF [5–11]. However, because MS lesions are located not only at the WM but also at the GM, evaluation of WM-GM and WM-CSF contrasts was necessary. Our study clarified the relationship between WM, GM, and CSF contrasts and varying TFE factors, shot intervals, and TIs in 3D-PSIR.

The phantom study showed that the CNR increased with a lower TFE factor, longer shot interval, and longer TI. A high TFE factor caused blurring and a decrease in CNR owing to the large number of echoes to be recorded and the inclusion of echoes with low signal intensities. A longer shot interval and TI accelerated the recovery of the longitudinal magnetization; therefore, the CNR of each phantom increased. The TFE factor and shot interval significantly affected the scan time. Since the phantom study showed that the CNR of GM_m-CSF_m was maintained up to a TFE factor of 30 and that the shot interval did not contribute significantly to CNR improvement, a TFE factor of 30 and shot interval of 1000 ms were employed. In the in vivo study, visual evaluations were performed to assess the contrast when TI variations were noted.

In the visual evaluation, considering the

results of the phantom study, the WM-CSF and GM-CSF contrasts were expected to be the highest among the images with a TI of 800 ms; however, this was not the case. As TI increased, the signal intensity and contrast of each tissue increased. Nevertheless, we assumed that it was impossible to visually distinguish the contrast above a specific value. W values in the visual evaluation of WM-GM (0.55) were lower than those of WM-CSF and GM-CSF (0.89 and 0.87, respectively). Since the CNR of WM_m-GM_m was almost constant at a TI of 500–700 ms in the phantom study, we assumed that the inter-rater variance was increased in the visual evaluation of WM-GM. Based on the changes in the signal intensities of GM_m and CSF_m in the phantom study, a longer TI is expected to improve the contrast with the MS lesion. However, considering the results of the phantom study and visual evaluations, we assumed that a TI of 700 ms was appropriate.

A TI of approximately 400 ms was used in previous studies that utilized TSE [5–11] and was different from the optimal TI noted in this study, which utilized the gradient echo. Gradient echo-based 3D-PSIR imaging has been reported to improve the detection of spinal cord lesions in patients with MS with a TI of 350–400 ms [16, 17]. These reports also differ from our results, but this is owing to the differences in the target area. In the spinal cord, CSF is distributed around the WM, and the WM-CSF contrast is high, even with a relatively short TI. Therefore, we assumed that a TI of 350–400 ms is acceptable in the spinal cord region. These studies also used a TFE factor of 67–69, which was higher than our imaging parameters of 30. A high TFE factor reduces the scan time but also causes a decrease in contrast and blurring; therefore, it must be considered carefully.

This study had some limitations. First, the TI setting is limited to a TFE factor of 30 and shot interval of 1000 ms. If other parameters are changed, the TI setting must be modified again. Secondly, a slice thickness of 3 mm was used. In a 3D sequence, it is desirable to use a slice thickness of approximately 1 mm. However, thicker slices were used to reduce the effect of noise because we focused on evaluating contrast. Third, the imaging parameters obtained in this study have not been evaluated in clinical use. Therefore, it is necessary to apply the results of the present study to the diagnosis of MS.

5 Conclusion

In 3D-PSIR, a smaller TFE factor, longer shot interval, and longer TI improve tissue contrast. To apply 3D-PSIR to MS lesions, a TI of 700 ms is suitable when the TFE factor is 30 and the shot interval is 1000 ms.

Declarations

Conflicts of Interest:

The authors declare that they have no conflicts of interest.

Ethical approval:

All procedures performed in this study involving human participants were in accordance with the ethical standards of the Institutional Review Board (IRB) and with the 1964 Helsinki declaration and its later amendments or comparable ethical standards.

Informed consent:

Informed consent was obtained from all individual participants included in the study.

References

1) Geurts JJ, et al.: Intracortical lesions in multiple sclerosis: improved detection with 3D double inversion-recovery MR imaging. Radiology, 236: 254-60, 2005.
2) Calabrese M, et al.: Detection of cortical inflammatory lesions by double inversion recovery magnetic resonance imaging in patients with multiple sclerosis. Arch Neurol, 64: 1416-22, 2007.
3) Calabrese M, et al.: A 3-year magnetic resonance imaging study of cortical lesions in relapse-onset multiple sclerosis. Ann Neurol, 67: 376-83, 2010.
4) Seewann A, et al.: Postmortem verification of MS cortical lesion detection with 3D DIR. Neurology, 78: 302-8, 2012.
5) Sethi V, et al.: Improved detection of cortical MS lesions with phase-sensitive inversion recovery MRI. J Neurol Neurosurg Psychiatry, 83: 877-82, 2012.
6) Harel A, et al.: Phase-sensitive inversion-recovery MRI improves longitudinal cortical lesion detection in progressive MS. PLoS One, 11: e0152180, 2016.
7) Hou P, et al.: Phase-sensitive T1 inversion recovery imaging: a time-efficient interleaved technique for improved tissue contrast in neuroimaging. AJNR Am J Neuroradiol, 26: 1432-8, 2005.
8) Nelson F, et al.: Improved identification of intracortical lesions in multiple sclerosis with phasesensitive inversion recovery in combination with fast double inversion recovery MR imaging. AJNR Am J Neuroradiol, 28: 1645-9, 2007.
9) Nelson F, et al.: Intracortical lesions by 3T magnetic resonance imaging and correlation with cognitive impairment in multiple sclerosis. Mult Scler, 17: 1122-9, 2011.
10) Sethi V, et al.: MS cortical lesions on DIR: not quite what they seem? PLoS One, 8: e78879, 2013.
11) Favaretto A, et al.: The parallel analysis of phase sensitive inversion recovery (PSIR) and double inversion recovery (DIR) images significantly improves the detection of cortical lesions in multiple sclerosis (MS) since clinical onset. PLoS One, 10: e0127805, 2015.
12) Kellman P, et al.: Phase-sensitive inversion recovery for detecting myocardial infarction using gadolinium-delayed hyperenhancement. Magn Reson Med, 47: 372-83, 2002.
13) Ishimori T, et al.: Preoperative identification of subthalamic nucleus for deep brain stimulation using three-dimensional phase sensitive inversion recovery technique. Magn Reson Med Sci, 6: 225-9, 2007.
14) Harter HL: Expected values of normal order statistics. Biometrika, 48: 151-65, 1961.
15) Williams LJ, et al.: Fisher's least significant difference (LSD) test. Encyclopedia of Research Design, 218: 840-53, 2010.
16) Mirafzal S, et al.: 3D PSIR MRI at 3 Tesla improves detection of spinal cord lesions in multiple sclerosis. J Neurol, 267: 406-14, 2020.
17) Fechner A, et al.: A 3T phase-sensitive inversion recovery MRI sequence improves detection of cervical spinal cord lesions and shows active lesions in patients with multiple sclerosis. AJNR Am J Neuroradiol, 40: 370-5, 2019.

Received September 23, 2021; accepted April 18, 2023

Creation of work skill items in the field of radiotherapy

TSUDA Shintaro[1)], SATO Kiyokazu[2)], HIGUCHI Hiromitsu[3)], ONO Yasushi[4)], NISHIMURA Tomonori[5)], AOYAMA Hideki[6)], KATAYAMA Hiroki[7)], HONDA Hirofumi[8)], KUMAMOTO Kengo[8)], OKU Yoshifumi[9)], GIBO Seiyo[10)], NAKASHIMA Takeo[1)], KIGUCHI Masao[11)]

1) Division of Radiation Therapy, Department of Medical Support, Hiroshima University Hospital
2) Division of Radiation, Department of Medical Technology, Tohoku University Hospital
3) Department of Radiation, Gunma University Hospital
4) Department of Radiation, Tottori University Hospital
5) Department of Radiation, Shimane University Hospital
6) Division of Radiological Technology, Okayama University Hospital
7) Department of Radiation, Kagawa University Hospital
8) Division of Radiation Technology, Department of Clinical Support, Ehime University Hospital
9) Division of Radiation, Department of Clinical Engineering, Kagoshima University Hospital
10) Department of Radiation, Ryukyu University Hospital
11) Department of Medical Support, Hiroshima University Hospital

Note: This paper is secondary publication, the first paper was published in the JART, vol. 70 no. 853: 26-33, 2023.

Key words: Work skill items, Radiation Therapy, Radiotherapy Technologist, Objective skill evaluation, Human resources development

【Abstract】
This study aimed to create knowledge and skills in the field of radiotherapy as work skill items through a multi-institutional collaboration. We created work skill items that cover the work forms of each institution, and considering the user's burden, we devised the order, number of items, and category classification that allows efficient input and evaluation. Work skill items consist of levels, items, tasks, and action goals and are divided into four levels, six items, seven tasks, and 123 action goals. Since the percentage of treatment generalists at the "level" was over 50% of the total items, it is considered to be of high importance for the development of newcomers and young staff. In addition, it is important to incorporate the contents of work skill items into the operation of each institution at the time of system introduction and to maintain the items due to periodic changes in work operations. It is hoped that the results of this study will serve as a reference for the development of human resources at facilities that perform radiation therapy and that the development of educational programs will proceed.

Introduction

In recent years, the situation surrounding radiotherapy has changed significantly because of high-precision radiotherapy techniques, such as stereotactic radiotherapy (SRT) and intensity-modulated radiation therapy (IMRT), as well as the increasing number of facilities offering particle beam therapy. Moreover, radiological technologists are responsible for radiation therapy [1)]. Technical skills related to radiation therapy are acquired through on-the-job training (OJT) at employment facilities. However, due to the absence of a unified index or system for skill acquisition, the quality and technical level of technology depends on the work environment.

In the field of information technology (IT), IT skill standards [2)] have been established by the Ministry of Economy, Trade, and Industry and the Information-Technology Promotion Agency, and intellectual property human resource skill standards [3)] by the Ministry of Economy, Trade, and Industry and the Patent Office. The importance of using these unified indicators based on skill standards for human resource development has been reported [4)]. In the medical field, the Japanese Nursing Association has released the "Nurse Clinical Ladder (Japanese Nursing Association Version)" for na-

tional standard indicators [5]. The goal of nursing education is to define job capabilities common to all nurses in stages or criteria to foster personnel who can provide diverse and high-quality nursing practices. The Clinical Ladder is a system for skill development and evaluation applied in nursing theory [6, 7].

The Japan Association of Radiological Technologists has outlined a new lifelong education system that incorporates the Clinical Ladder approach introduced by the Academic Education Committee. In the field of radiation therapy, levels 3 and 4 (specialists) have been established as the Clinical Ladder for radiation therapy professionals [8, 9]. Furthermore, in response to a request from the Ministry of Education, Culture, Sports, Science, and Technology (MEXT) to create standardized evaluation criteria for postgraduate education and its assessment for radiological technologists, the Association of Radiological Technologists at the National University has been planning and supervising the Skill Moral Cloud System (hereinafter referred to as the Skill Moral System) since 2016 and has been operating it under contract with BeNest Corporation [10]. The system, developed by the Association of Radiological Technologists at the National University, was created by the Skill Moral Evaluation Working Group and serves as a personnel management system for assessing job duties by multiple evaluators. It evaluates professional and moral (non-technical) skills in various fields, including general radiography, computed tomography (CT), magnetic resonance imaging (MRI), nuclear medicine, angiography, radiation therapy, and fluoroscopy. Using a cloud-based system, self-assessment and evaluator assessment results can be disseminated, enabling facilities to ensure consistent evaluations based on the same standards across organizational structures.

When considering the development of radiological technicians, it is important to utilize unified indicators and systems for skill acquisition to organize and categorize the knowledge and skills necessary for job duties. The conversion of tacit to explicit knowledge is crucial. Nonaka et al. described tacit knowledge as knowledge based on personal experience, thoughts, or know-how that is difficult to express in language or writing and as subjective knowledge that individuals unconsciously understand and use [11, 12]. Furthermore, formal knowledge is visualized through symbols, such as words or formulas, and can be expressed in language, manuals, or other written forms as objective knowledge. Defining job skill items that categorize skills in the workplace helps clarify job responsibilities, making it easier for new hires or transferees to understand the overview of the knowledge and skills required for their assigned tasks. It also promotes transparency of job responsibilities to other departments. For supervisors, this contributes to reassessing the knowledge and skills that they implicitly understand when developing their subordinates. By utilizing these factors, the required level of skill acquisition in salary increases, promotions, and other selection processes are reflected and foster expectations for OJT. Considering these points, it is believed that creating job skills is highly significant in constructing an educational system for radiological technologists involved in radiation therapy and can be effectively utilized for personnel development.

Matsuo et al [13]. categorized the abilities of radiological technologists into technical skills and human skills, dividing their career stages into early (1-10 years) and late (11 years and beyond), based on an analysis of questionnaire survey data. They emphasized the importance of training responsibilities and interactions with other professions. Within this context, they advocated the necessity of creating checklists to identify the abilities that should be acquired at each career stage, developing training plans, and establishing an OJT system to facilitate the smooth transfer of knowledge and

skills when transitioning modalities.

Based on the research findings on the development of radiological technologists, it is important to conduct studies aimed at creating specific work skill items. Furthermore, in national university hospitals where the skill moral system is implemented, operational practices vary among facilities owing to factors such as staff numbers, equipment usage, and work rotations, and the initial configuration of the skill moral system does not necessarily encompass the operational forms of each facility. In this study, we aimed to collaborate with radiological technologists at national university hospitals in the field of radiation therapy to objectively assess skills based on evaluation items of the skill moral system and examine work skill items. Our goal was to develop content that could be implemented in facilities nationwide, including comprehensive hospitals performing radiation therapy, by focusing on creating work skills in the field of radiation therapy.

Materials and Methods

We examined work skill items in the field of radiation therapy at 15 facilities in national university hospitals. The linear accelerator numbers at the 15 facilities were as follows: one facilities had five units, six facilities had three units, eight facilities had two units, and two facilities had separate particle-beam devices. In the initial setting of the skill moral system evaluation items for the 15 facilities, the operational forms for each facility were not fully covered. Therefore, we ensured comprehensive coverage and considered the sequence, number of items, and categorization for efficient input and evaluation based on improvement requests from users of the skill moral system at the 15 facilities.

The evaluation criteria for the skill moral system are divided into "levels" based on the proficiency and years of experience of radiological technologists, and into "items," "tasks," and "behavioral objectives" based on the nature of their duties. In the initial setup for radiation therapy, the "levels" are hierarchically structured into three stages: radiotherapy generalist, radiotherapy clinical coach, and radiotherapy department leader, which correspond to the career ladder. In this context, the consideration of which stage to set based on years of experience, qualifications, and positions is examined, considering the purpose of utilizing work skill items. Furthermore, the nature of the duties was hierarchically structured into "items," "tasks," and "behavioral objectives," where "items" were categorized into equipment management, treatment planning, safety management, simulation, and irradiation techniques. "Tasks" were classified into knowledge, skills/practice, and management, and "behavioral objectives" specified the concrete content of work skill items for radiation therapy duties. Here, "simulation" refers to the workflow for conducting radiation therapy, including immobilization device fabrication, CT imaging, surface marking, and breath management. Additionally, due to variations in naming and operational methods among manufacturers for patient information systems, a uniform representation using the general term "record and verify (R&V)" was adopted in the work skill items. Regarding content related to total body irradiation (TBI), facilities may also perform other specialized irradiation techniques such as half body irradiation (HBI) and total skin electron irradiation (TSEI), so the term "TBI, etc." was uniformly used. In this context, considering the workflow of radiation therapy duties, staff rotation, and effort involved in user input for items, opinions were aggregated to explore and encompass the various operational modes of each facility as much as possible.

Results

1. "Levels"

The levels were set in four stages: ① radio-

therapy generalist (1st year), ② radiotherapy generalist (2nd year and beyond), ③ radiotherapy clinical coaches, and ④ radiotherapy department leaders. For each, the years of practical experience, professional qualifications, and guidance based on managerial positions were recorded. Professional qualifications explicitly included radiotherapy technologists (RTT) (Table 1). radiotherapy generalists were divided into the first-year, second-year, and beyond categories.

Table 1 We have established four "levels" and categorized Radiotherapy generalists into ①first year and ②second year and beyond. Guidelines and reference information have been added for each level.

Levels	Guidelines	Supplementary Information
① Radiotherapy generalists	1st year	Newcomer - Until obtaining RTT certification
② Radiotherapy Generalist	2nd to 5th year	
③ Radiotherapy Clinical Coach	6th year onwards	RTT Qualified, Chief
④ Radiotherapy Department Leader	Managerial position	Deputy Chief Engineer, Department Head or above

2. "Items" and "Tasks"

Based on staff rotation as a criterion, six "items" were set: irradiation, simulation, treatment planning, brachytherapy, quality management, and management. Seven "tasks" were designated for "Tasks," including patient care, irradiation, equipment management, simulation, treatment planning, data transfer, and management (Table 2).

Table 2 "Items" are categorized by work unit and divided into several "Tasks". "Items" are further divided into six categories, and "Tasks" into seven categories.

Items	Tasks
Irradiation	Patient Care
	Irradiation
	Equipment Management
Simulation	Patient Care
	Simulation
	Equipment Management
Treatment Planning	Treatment Planning
	Data Transfer
Brachytherapy	Simulation
	Treatment Planning
	Irradiation
	Equipment Management
	Management
Quality Management	Equipment Management
Management	Management

3. Work Skill Items (Levels, Items, Tasks, and Behavioral Objectives)

The work skills items are presented in Tables 3-5. For ① radiotherapy generalist (1st year),

Table 3 The work skill items for Radiotherapy Generalists (①). Fifteen behavioral objectives are set for first year Radiotherapy Generalists.

Levels	Items	Tasks	Behavioral Objectives
① Radiotherapy Generalist	Irradiation	Patient Care	Capable of providing appropriate explanations of procedures to patients or families
			Able to establish good rapport with patients and their families
			Able to effectively explain the side effects of radiation therapy to patients or their families
		Irradiation	Able to safely perform irradiation tasks in the head region
			Able to safely perform irradiation tasks in the head and neck region
			Able to safely perform irradiation tasks in the chest region
			Able to safely perform irradiation tasks in the abdominal region
			Able to safely perform irradiation tasks in the pelvic region
			Able to safely perform irradiation tasks in the extremity region
			Able to safely perform irradiation tasks in electron beam therapy
		Equipment Management	Able to collect patient information necessary for irradiation tasks using HIS, RIS, R&V, etc
			Able to understand and implement the recording and storage methods for irradiation and positioning verification
			Able to understand the medical fee schedule and perform or verify irradiation accounting
			Able to understand the structure and operation of the accelerator, and operate it safely
			Able to understand and perform the start-up and shutdown checks of the accelerator

all were under irradiation with 15 behavioral objectives (Table 3). For ② radiotherapy generalist (2nd year and beyond), there were items such as irradiation, simulation, treatment planning, brachytherapy, and quality management, comprising 57 behavioral objectives (Table 4). Similarly, ③ radiotherapy clinical coach included items such as irradiation, simulation, treatment planning, brachytherapy, and quality management, with 35 behavioral objectives. ④ radiotherapy department leader's items were all under management, with 16 behavioral objectives (Table 5). Work skill items were classified into 123 behavioral objectives.

Table 4 The work skill items for Radiotherapy Generalists (②). Fifty-seven behavioral objectives are set for Radiotherapy Generalists in their second year and beyond.

Levels	Items	Tasks	Behavioral Objectives
② Radiotherapy Generalist	Irradiation	Patient Care	Able to understand the purpose and methods of infection control, and implement them appropriately
			Able to respond appropriately during disasters or emergencies
		Irradiation	Able to understand the irradiation procedures of Intensity Modulated Radiation Therapy (IMRT/VMAT) and perform them safely
			Able to understand the irradiation procedures of Stereotactic Radiotherapy (SRS/SRT/SBRT) and perform them safely
			Able to understand the irradiation procedures involving respiratory motion management and perform them safely
			Able to understand the irradiation procedures for special treatments such as whole-body irradiation and perform them safely
			Able to perform particle beam irradiation
			Able to perform intraoperative irradiation
		Equipment Management	Able to respond appropriately to incidents
			Able to handle interlock issues and perform recovery operations on the accelerator
			Able to perform emergency shutdown and normal startup of the accelerator
			Able to understand and perform standard measurements of water absorbed dose
	Simulation	Patient Care	Able to provide appropriate explanations of procedures to patients or their families
		Simulation	Able to perform simulation tasks in the head region
			Able to perform simulation tasks in the head and neck region
			Able to perform simulation tasks in the chest region
			Able to perform simulation tasks in the abdominal region
			Able to perform simulation tasks in the pelvic region
			Able to perform simulation tasks in the extremity region
			Able to perform simulation tasks in electron beam therapy
			Able to understand and perform the simulation procedures for IMRT/VMAT appropriately
			Able to understand and perform the simulation procedures for SRS/SRT/SBRT appropriately
			Able to understand and perform the simulation procedures for irradiation involving respiratory motion management appropriately
			Able to understand and perform the simulation procedures for special treatments such as whole-body irradiation appropriately
			Able to create electron beam field shaping blocks
			Able to perform CT simulation using contrast agents safely
			Able to perform simulation tasks for particle beam irradiation
			Able to perform simulation tasks for intraoperative irradiation
		Equipment Management	Able to appropriately collect patient information necessary for simulation tasks using HIS, RIS, etc
			Able to understand the medical fee schedule and perform or verify simulation accounting
			Able to understand the structure and operation of simulation equipment, and operate it safely
			Able to perform emergency shutdown and normal startup of simulation equipment
			Able to understand and perform the start-up and shutdown checks of simulation equipment

Levels	Items	Tasks	Behavioral Objectives
② Radiotherapy Generalist	Treatment Planning	Treatment Planning	Able to understand the usage of treatment planning equipment and use it safely
		Data Transfer	Able to perform data transfer and registration tasks of treatment plans created in the head region to the R&V system
			Able to perform data transfer and registration tasks of treatment plans created in the head and neck region to the R&V system
			Able to perform data transfer and registration tasks of treatment plans created in the chest region to the R&V system
			Able to perform data transfer and registration tasks of treatment plans created in the abdominal region to the R&V system
			Able to perform data transfer and registration tasks of treatment plans created in the pelvic region to the R&V system
			Able to perform data transfer and registration tasks of treatment plans created in the extremity region to the R&V system
			Able to perform data transfer and registration tasks of treatment plans created with SRS/SRT/SBRT to the R&V system
			Able to perform data transfer and registration tasks of treatment plans created for special treatments such as whole-body irradiation to the R&V system
			Able to perform data transfer and registration tasks of treatment plans created with electron beam therapy to the R&V system
			Able to perform treatment plan verification using independent verification devices
			Able to perform data transfer and registration tasks of treatment plans created with particle beam therapy to the R&V system
			Able to appropriately perform data transfer and registration tasks of treatment plans created with intraoperative irradiation to the R&V system
	Brachytherapy	Simulation	Able to perform simulation tasks for RALS
		Treatment Planning	Able to create treatment plans for RALS
		Irradiation	Able to safely perform irradiation tasks for RALS
		Equipment Management	Able to appropriately collect patient information necessary for RALS tasks using HIS, RIS, etc
			Able to understand the medical fee schedule and perform or verify accounting for RALS
			Able to understand the structure and operation of RALS, and operate it safely
			Able to understand the interlock system of RALS and respond appropriately
			Able to understand and perform the start-up and shutdown checks of RALS
			Able to understand and perform output measurements for RALS
			Able to perform emergency shutdown and normal startup for RALS
	Quality Management	Equipment Management	Able to perform measurements using dosimetry equipment for patient dose verification plans of IMRT/VMAT

Table 5 The work skill items for Radiotherapy Clinical Coaches and Radiotherapy Department Leaders (③, ④). Thirty-five behavioral objectives are set for Radiotherapy Clinical Coaches (③), and sixteen behavioral objectives are set for Radiotherapy Department Leaders (④).

Levels	Items	Tasks	Behavioral Objectives
③ Radiotherapy Clinical Coach	Irradiation	Equipment Management	Able to identify any inappropriate aspects in treatment plans or registration information
			Able to perform calibration of monitor ionization chamber
			Able to manage the schedule of the irradiation room
	Simulation	Equipment Management	Able to understand and implement geometric accuracy and image quality management in images from simulation equipment
			Able to understand and perform output measurements of simulation equipment

Levels	Items	Tasks	Behavioral Objectives
③ Radiotherapy Clinical Coach	Treatment Planning	Treatment Planning	Able to create treatment plans for the head region
			Able to create treatment plans for the head and neck region
			Able to create treatment plans for the chest region
			Able to create treatment plans for the abdominal region
			Able to create treatment plans for the pelvic region
			Able to create treatment plans for the extremity region
			Able to create treatment plans for whole-body irradiation
			Able to create treatment plans for electron beam therapy
			Able to create treatment plans for IMRT/VMAT
			Able to create treatment plans for SRS/SRT/SBRT
			Able to understand the indications and irradiation methods for particle beam therapy and create treatment plans
			Able to understand the indications and irradiation methods for intraoperative irradiation and create treatment plans
	Brachytherapy	Equipment Management	Able to understand and implement the accuracy control items of RALS
		Simulation	Able to perform simulation tasks for temporary insertion of sealed brachytherapy sources
		Treatment Planning	Able to create treatment plans for temporary insertion of sealed brachytherapy sources
		Irradiation	Able to perform irradiation tasks for temporary insertion of sealed brachytherapy sources
		Simulation	Able to perform simulation tasks for permanent insertion of sealed brachytherapy sources
		Treatment Planning	Able to create treatment plans for permanent insertion of sealed brachytherapy sources
		Irradiation	Able to perform irradiation tasks for permanent insertion of sealed brachytherapy sources
			Able to perform tasks related to unsealed brachytherapy treatment
		Management	Able to perform tasks related to source management
③ Radiotherapy Clinical Coach	Quality Management	Equipment Management	Able to create patient dose verification plans for IMRT/VMAT
			Able to understand and implement geometric accuracy management of the accelerator
			Able to understand and implement dosimetric accuracy management of the accelerator
			Able to understand and implement accuracy management of the positioning verification device
			Able to understand and implement accuracy management of dosimetry equipment
			Able to understand and implement data registration, management, and commissioning of treatment planning systems
			Able to understand and implement data registration and accuracy management of independent verification devices
			Able to understand and implement various factor evaluations and cross calibrations of dosimeters
			Able to understand the measurement points and methods for leakage dose measurements, and plan and conduct them
④ Radiotherapy Department Leader	Management	Management	Able to create specifications
			Able to create documentation for equipment updates
			Able to understand and explain maintenance contracts
			Able to develop equipment procurement plans
			Able to create financial plans for equipment upgrades
			Able to review treatment procedures in response to revisions in medical fee schedules
			Able to collaborate with medical departments to improve treatment methods
			Able to discuss examination content and operations with other professions
			Able to manage, record, and understand various aspects related to RI (Radioisotope) laws
			Able to develop risk management plans
			Able to respond to and address incidents
			Able to respond to and implement measures for infectious diseases
			Able to conduct inspections and respond to medical surveillance
			Able to manage overtime work
			Able to handle patient complaints and issues
			Able to respond to the Radiation Therapy Quality Management Committee, etc

Discussion

1. "Levels" Setting

In the skill moral system operated by national university hospitals, an appropriate level setting is crucial for clarifying the tasks for which users should aim. However, the roles and criteria of radiotherapy generalists, radiotherapy clinical coaches, and radiotherapy department leaders were perceived differently among the facilities. Therefore, by specifying guidelines such as practical experience and professional qualifications for each level, regardless of the actual practices of the facility, the system allows assessors to understand the skills and professional qualifications required for their current position. Since the proportion of radiotherapy generalists in the "level" exceeded 50% of the entire items, it is believed that there is a high demand for system usage among radiological technologists involved in radiotherapy through rotations from diagnostic departments or as recruits in the radiotherapy department. By setting radiotherapy generalists into ① radiotherapy generalist (1st year) and ② radiotherapy generalist (2nd year and beyond), the priority of skills to be acquired in the first year of employment and the skills to be mastered in the second to fifth years are clarified. This aims to organize the pathway to obtain RTT qualification, which requires more than five years of practical experience, and to encourage further growth towards the stage of radiotherapy clinical coach.

2. Setting of "Items," "Tasks," "Behavioral Objectives," and "Detailed Behavioral Objectives"

In the initial setting, tasks such as equipment management, safety management, and irradiation techniques were related to the irradiation tasks. In brachytherapy, tasks such as irradiation, simulation, and treatment planning were related, causing complexity in system usage during input and evaluation across multiple items. Based on the rotation of duties and operational forms in radiation therapy at each facility, the setting of "items" and "tasks" was adjusted to enable smooth input and evaluation, thereby reducing the burden and complexity for users. However, because the evaluation methods for each item's achievement level largely depended on the discretion of the evaluator, each facility needed to establish evaluation criteria to reduce differences among evaluators. Additionally, when comparing results between facilities, attention must be paid to the evaluation criteria for each facility.

3. Utilization for Personnel Development

When utilizing work skills for personnel development, the use of personnel management systems should be considered instead of Excel files to avoid the risk of inadvertent file loss or disposal. The introduction of such a system enables continuous data collection and analysis, allowing users to visually grasp their strengths and weaknesses using tools such as radar charts (Fig. 1). During the re-evaluation, the content of the unachieved items was indicated (Fig. 2). Furthermore, it served as a communication tool for superiors and subordinates to collectively consider clinical duties, thus serving not only as a tool for visualizing duties but also as a tool for personnel development and the smooth progress of clinical duties. An example of the operating mode is shown in the flowchart format (Fig. 3).

4. Usage, Modification, and Maintenance of Items

Through a multi-facility study conducted in 15 facilities, concerns were raised about differences in operational practices and personnel development philosophies owing to differences in operational practices and staff rotation policies between diagnostic areas. Therefore, it is necessary to establish the usage of personnel management systems and personnel development policies in each facility beforehand and adjust the contents of work skill items according to the facility's operation when introducing

the system. Even in small-scale facilities with only one accelerator, it is assumed that deployment is possible by similarly modifying the work skill items at the time of system introduction, such as by removing unnecessary items. Additionally, radiation therapy systems, including accelerators and peripheral equipment, have changed composition and functionality with technological advancements. Especially during equipment updates, there may be significant changes in operation owing to new functions or new treatment methods, such as particle therapy may be introduced. Because the items formulated at the time of system introduction may require reconsideration owing

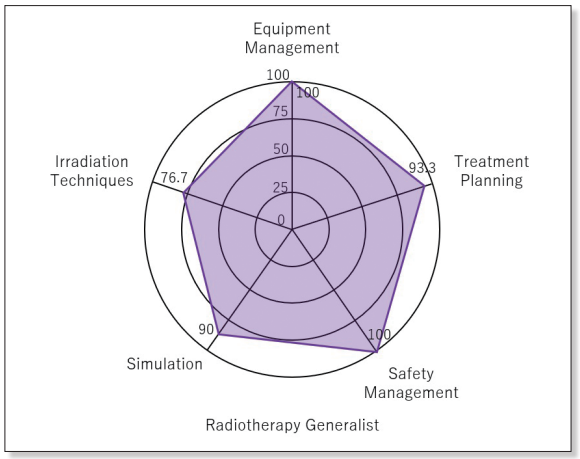

Fig. 1 An Example of Radar Chart Display: By indicating the achievement level of each item as a percentage, both the evaluator and the evaluated individual can visually grasp their strengths and weaknesses.

Levels	Items	Tasks	Behavioral Objectives	Two times ago	Last time	Self-assessment	Primary evaluation	Secondary evaluation	Comment (specific cases)
① Radiotherapy Generalist	Irradiation	Patient Care	Capable of providing appropriate explanations of procedures to patients or families	○	○	○			
			Able to establish good rapport with patients and their families	△	△	○			
			Able to effectively explain the side effects of radiation therapy to patients or their families	○	○	○			
		Irradiation	Able to safely perform irradiation tasks in the head region	○	○	○			
			Able to safely perform irradiation tasks in the head and neck region	×	×	△			
			Able to safely perform irradiation tasks in the chest region	×	×	×			
			Able to safely perform irradiation tasks in the abdominal region	△	△	○			
			Able to safely perform irradiation tasks in the pelvic region	△	△	△			
			Able to safely perform irradiation tasks in the extremity region	×	×	△			
			Able to safely perform irradiation tasks in electron beam therapy	×	×	×			
		Equipment Management	Able to collect patient information necessary for irradiation tasks using HIS, RIS, R&V, etc	○	○	○			
			Able to understand and implement the recording and storage methods for irradiation and positioning verification	△	△	△			
			Able to understand the medical fee schedule and perform or verify irradiation accounting	△	△	○			
			Able to understand the structure and operation of the accelerator, and operate it safely	×	△	△			
			Able to understand and perform the start-up and shutdown checks of the accelerator	△	△	○			

Fig. 2 An example of screen display of item contents. At the time of re-assesment, the contents of the items that have not been achieved are specified. It is possible to visually compare the progress of their achievement level with their previous results.

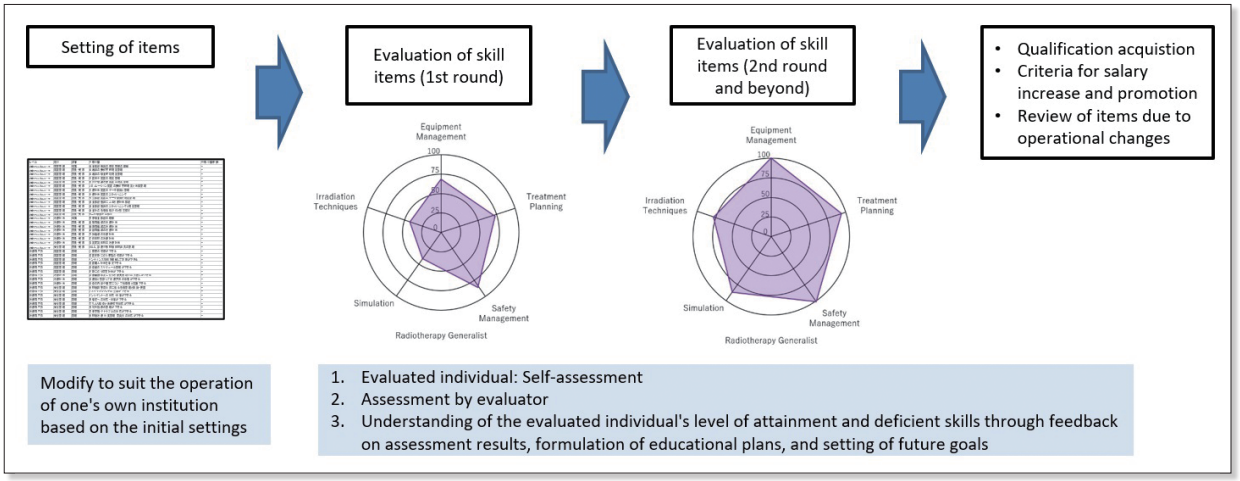

Fig. 3 An example of operational mode: By adapting the items to the operation of one's own institution and confirming one's level of attainment through regular assessment of skill items, communication between evaluators and those being evaluated is facilitated. The results can be applied to one's career path development and personnel evaluations.

to changes in operation over several years or decades, regular maintenance of items is crucial to prevent the system from becoming obsolete.

Conclusion

Through multi-facility deliberation, we created work skill items tailored to the realities and workflows of national university hospitals. These work-skill items feature common and general terms and names, allowing them to be reflected in the operations of each facility without being influenced by factors such as facility size or staffing levels. This enables an efficient and appropriate evaluation. Additionally, by visualizing the evaluations corresponding to each level, achievement status can be shared within the radiation therapy department. By utilizing the proposed work skill items, a personnel development system for radiological technologists involved in radiation therapy is expected to motivate radiological technologists and improve the quality of healthcare. Furthermore, it is anticipated to lead to the advancement and bottom-up development of radiological technologists.

Acknowledgments

We would like to express our sincere gratitude to Mr. Yamato Wakabayashi from the Department of Radiology, Medical Technology Division, Hokkaido University Hospital; Mr. Takahiro Fujimoto from the Department of Radiology, Kyoto University Hospital; Mr. Koya Fujimoto from the Graduate School of Medicine, Yamaguchi University; Mr. Tetsuya Kawashita from the Department of Radiological Technology, Medical Technology Division, Tokushima University Hospital; and Mr. Akira Tsuzuki from the Department of Radiology, Medical Technology Division, Faculty of Medicine, Kochi University (currently Kakogawa Central Citizens' Hospital Radiology Department) for their collaboration in developing the work skills and assistance in writing this manuscript.

We also wish to extend our heartfelt appreciation to Professor Yoshitada Masuda, Chairman of the Association of Radiological Technologists at National University, and former Chairman Katsuhiko Ueda for their guidance in writing this manuscript.

Some sections of this paper were presented at the 36th Japan Conference of Radiological Technologists (January 2021, held online).

Conflicts of Interest

The authors declare that they have no conflict of interest.

References

1) Okumura Masahiko, et al.: Standard Textbook of Radiation Therapy Techniques. Medical Science International, 2019.
2) Information-technology Promotion Agency, Japan, IT Skill Standards Center: IT Skill Standards V3 2011. https://www.ipa.go.jp/jinzai/itss/download_V3_2011.html (Accessed 2021.9.22)
3) Japan Patent Office: Intellectual Property Talent Skill Standards (version 2.0). https://www.jpo.go.jp/support/general/chizai_skill_ver_2_0.html (Accessed 2021.9.22)
4) Shigeyuki Ohara, et al.: Skill Standards and Human Resource Development in Information Technology. IPSJ Magazine, Vol.46, No.12, Dec 2005.
5) Japanese Nursing Association: Clinical Ladder for Nurses (Japanese Nursing Association Version). https://www.nurse.or.jp/nursing/education/jissen/index.html (Accessed 2021.9.22)
6) Hubert Dreyfus & Stuart Dreyfus, translated by Naoko Mukuta: What Computers Can't Do: The Limits of Artificial Intelligence. ASCII Corporation, 1987.
7) Patricia Benner: From novice to expert: Excellence and power in clinical nursing practice. Addison-Wesley Publishing, 1984.
8) Overview of Lifelong Education System by the Academic Education Committee of the Japan Association of Radiological Technologists, The Japan Association of Radiological Technologists, 67. 4: 80-93, 2020.
9) Overview of Lifelong Education System by the Academic Education Committee of the Japan Association of Radiological Technologists, The Japan Association of Radiological Technologists, 68. 4: 77-91, 2021.
10) Introduction to PE-net on Cloud: Support for Training Radiological Technologists. BeNest Co., Ltd. https://benest.co.jp/archives/products/79 (Accessed 2021.9.22)
11) Ikujiro Nonaka, et al.: The Knowledge−Creating Company.– published by Toyo Keizai Inc. 1995.
12) Ikujiro Nonaka: The Essence of Innovation - Leadership in Knowledge Creation.– in Trends in Academic Research, 12. 5: 60-69, 2007.
13) Makoto Matsuo, et al.: The Experiential Learning Process of Radiological Technologists, The Japan Association of Radiological Technologists, 61. 3: 13-20, 2014.

Received January 4, 2023; accepted May 16, 2023

Generation of standard time acquisition images from short time acquisition images of cerebral blood flow SPECT using deep learning

YAMAMOTO Yasushi[1)], SHIRAI Masato[2)], TAKAMURA Masahiro[3)], MATSUURA Kousuke[4)], HINO Yuuki[4)], FUKUDA Mitsuki[4)], YADA Nobuhiro[4)], MIYAHARA Yoshinori[4)], KURODA Hiroyuki[1)], KAJI Yasushi[1)]

1) Department of Radiology, Faculty of Medicine, Shimane University
2) Interdisciplinary Faculty of Science and Engineering, Shimane University
3) Department of Neurology, Shimane University Faculty of Medicine
4) Department of Radiology, Shimane University Hospital

Note: This paper is secondary publication, the first paper was published in the JART, vol. 70 no. 853: 34-39, 2023.

Key words: deep learning, pix2pix, GAN, 3D-SSP, Brain SPECT

【Summary】
We attempted image generation of cerebral blood flow SPECT from short time acquisition (10 minutes) to standard time acquisition (40 minutes) using artificial intelligence based image generation technique. The model was pix2pix and was constructed from training data of 19484 images both 10 min and 40 min. Using constructed model, 4878 images were generated and evaluated similarity to standard images.MSE, PSNR, SSIM, and DSC were used for physical evaluation, and 3D-SSP was used for visual evaluation. Although image quality improved in the physical evaluation, there were cases where the depiction of abnormal blood flow areas differed from standard time in 3D-SSP. In order to improve the accuracy, we consider it is necessary to reexamine this issue with training data using extended acquisition time.

Introduction

In image diagnosis of dementia, nuclear-medical Single Photon Emission Computed Tomography (SPECT) of brain perfusion has important roles. But the images are produced by a little gamma-ray information, so the inspection time is 40 minutes on routine of our facilities, which is long and painful for brain disease patients.

Therefore, there are some cases where we can't collect whole inspection data, and we produce images despite not collecting enough data, whose impact on image diagnosis is inevitable.

Furthermore, because of using isotope, the inspection cost is expensive, and from a viewpoint of cost, reexamination is difficult. If there is a way to improve the image quality which can be used for diagnosis even the collected data is insufficient, its value is great.

In these years, improvement of image quality is being achieved by the image generating task with deep learning, and the technology has possibility to enable us to use aforesaid SPECT images of brain perfusion from insufficient data.

There are various reports for reference. Regarding CT, there is a study to make image quality close to that at high-dose from collected data at low-dose [1)]. In terms of MRI, a study has reported that noise reduction and image quality improvement effects get possible [2, 3)].

In nuclear medical domain, there is a reference that when using PET, even if the dose of administrated isotope is lowered, image quality which is equivalent to normal dose can be ensured [4)].

Thus, we introduced deep learning, and examined if its method can improve the image quality of data collected in a short period of time and can generate images which is worthy

of diagnostic use.

1. Methods

1-1. Equipment and Collection Conditions

For SPECT data of brain perfusion that we prepared, 123I-isopropyl-p-iodoamphetamine (^{123}I-IMP), 167 MBq was used, Graph Plot Method [5, 6] was employed to collect data, and at the same time as drug was injected, 5 min/360°-collecting was carried out for 8 cycles on continuous-mode, and then 40-minute (normal examination time) -collecting-data was obtained. For image-reconstruction, Ordered Subset Expectation Maximization (OSEM) method was employed, and the setting were as follows. Iteration was 2, Subset was 24, Scattered light correction was Triple Energy Window (TEW), and Attenuation correction was CT-based Attenuation Correction (CTAC). Collecting equipment is GE Healthcare Discovery 670 pro, and reconstructing workstation is Xeleris 3.0. Computer which is used to generate images is server type Philips Intellispace Discovery (CPU: Intel Xeon Gold 5120, RAM: 192 GB, GPU: NVIDIA Tesla V100 16 GB, Operating system: Ubuntu 16.04 LTS 64-bit). Image generating program is Python 3.6.10, and PyTorch 1.8.0 is employed as Framework.

In addition, whole of this research, including the use of clinical data, was conducted after it was approved by the Shimane University Medical Research Ethics Committee (Research Management Number: 20211228-1).

1-1-1. Data used for image generation

To generate images, a series of training data for learning is needed to be prepared. In this research, the aim is generating normal-time-collecting-image by using short-time-collecting-image, so we treat SPECT image which is generated by 10-minute collecting data as short-time-collecting-image (10 min_S), and one which is done by 40-minute data as normal-time-collecting-image (40 min_S), and then both 10 min_S and 40 min_S in the same case were prepared. What is used as Train-data is samples of 400 patients who could take ^{123}I-IMP Graph Plot Method to the end for 40 minutes. That includes 191 females whose old mean is 73.6 (SD 13.4) and 209 males whose old mean is 73.6 (SD 13.4). As a result of diagnosis by radiologist, there are 152 samples of dementia, 109 cerebrovascular diseases, 47 the other disorders, and 92 no abnormal findings. A series of data which is used to evaluate the accuracy of generated model (Test_data) is needed to be prepared apart from Train_data, so we prepared 101 samples which were continuously surveyed from Jan 2020 to Jun 2020. That includes 43 females whose old mean is 72.6 (SD 13.3) and 58 males whose old mean is 72.4 (SD 11.6). there are 45 samples of dementia, 23 cerebrovascular diseases, 7 the other disorders, and 26 no abnormal findings. The number of images used in 10 min_S and 40 min_S for Train_data are 19484, and that for Test_data are 4878. From the parietal to the inferior cerebellar margin, 48 images per case were used as the basis for the composition. Recomposed 16 bit-Dicom data (matrix: 128×128, pixel size: 2.94 mm) was converted into 8 bit PNG file that can work with the image generative model. To include large area of brain parenchyma which is essential to generate images, we enlarged them 1.7 times when they are translated into PNG files to reduce the area outside of subject, and preserved them in 256×256 matrix so that blurring due to enlargement is taken into account.

1-2. Image generative model

To generate images, we used a model called pix2pix which was reported by Isora [7]. Pix2pix is a derivation model of Generative Adversarial Network (GAN). Generator in it generates images as close to the real thing as possible, and Discriminator identifies whether the images are real or fake, finally it generates images that Discriminator recognizes as real. In GAN, the

initial input to the Generator is a random noise vector from which image generation starts. In pix2pix, on the other hand, real images are used as input, allowing image generation based on real images. In this study, the same rules were used to train pairs of 10 min_S and 40 min_S images (same case, same coordinates), so that artificial intelligence (AI) can find detailed correspondence between the two images and the training data for the conditional adversarial generative network, which generates standard-time images from the short-time images, is completed. The AI can generate a 40-minute image (fake_S) that is close to the real one by inputting 10 min_S, which is the Test_data prepared separately from the training data, to the generator based on the relationships among the training data. Fig. 1 shows the architecture of pix2pix in this study, using U-net as the generator and PatchGAN [7] as the discriminator. L1 Loss [7] is used as the loss function, which enables us to identify the entire image and the so-called low-frequency component, and improves the agreement between the conditional image (10 min_S), the generated image (fake_S), and the correct image (40 min_S). The optimization algorithm is based on Adam [8]; please refer to the original paper [7] for details on the pix2pix architecture and hyperparameters. The source code was downloaded from the publicly available PyTorch implementation (https://github.com/junyanz/pytorch-CycleGAN-and-pix2pix).

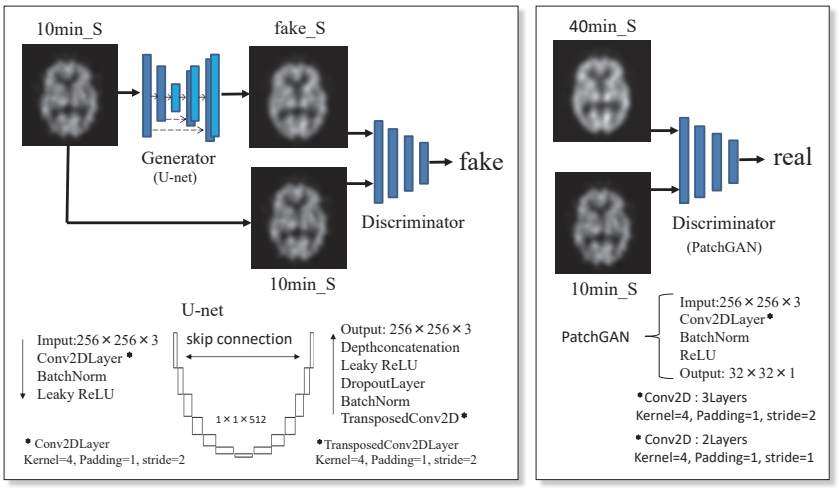

Fig. 1 Pix2pix architecture is shown. Generator generates fake_S from 10 min_S.
Discriminator is trained to judge 40 min_S as real and fake_S as fake. Generator uses U-net and Discriminator uses PatchGAN.

1-3. Physical evaluation of similar images

The physical evaluation of the generated images was performed using Mean squared error (MSE), Peak signal to noise ratio (PSNR), Structural similarity index (SSIM), and Dice similarity coefficient (DSC). MSE (Equation-1) is the sum of the squared difference between the corresponding pixel values of the generated image ($\hat{y}_i$) and the reference image (y_i) divided by the total number of pixels, where the smaller the value, the closer the pixel values are between the images. When the image to be handled is 8 bits, MSE takes a maximum value of 255 × 255, which is difficult to evaluate. In PSNR (Equation-2), a larger dB value can be easily judged as an approximate image by normalizing by R (255). MSE and PSNR evaluate pixel values by obtaining an approximation of the pixel values at the corresponding coordinates between images, but there may be cases where this does not correspond to the visual evaluation in diagnostic imaging. On the other hand, SSIM (Equation-3-1) can evaluate changes in pixel value, contrast, and structure in terms of variance, and is an index that is close to visual evaluation because it can be calculated for each small region while shifting its position within the image area, and finally evaluate structural differences across the entire image. In equation (3-1), μ_x and μ_y, σ_x and σ_y denote the local mean pixel values and standard deviations of the image, respectively, and σ_{xy} denotes the

covariance. C_1 and C_2 are the values C_1 = 0.01 × 2562 and C_2 = 0.03 × 2562 used in the 8-bit setting as reported by Fukui[9] et al. Mean SSIM (MSSIM) is the average of the calculated SSIM for each small area over the entire image and is calculated as Equation (3-2). DSC (Equation-4) evaluates the congruency of the shape of the binarized images. N_χ and N_y are the total number of pixels in the evaluation target region of the binarized image, and $N_{(\chi \cap y)}$ is the number of pixels where both images overlap on the same coordinate. In the above physical evaluation, the regions outside the brain parenchyma that are unnecessary for image generation should be excluded from the evaluation target and the Otsu binarization method[10] was used to determine the regions to be evaluated. This method determines the optimal threshold value (t) for each image so that the sum of the weighted intensity variance (σ_1^2, σ_2^2) of each region after segmentation (Equation-5) is minimized. Also, to visually evaluate SSIM, a unique SSIM map, which visualizes SSIM for each subregion, was added for visual evaluation.

$$MSE = \frac{1}{n}\sum_{i=0}^{n}(\hat{y}_i - y_i)^2 \cdots (1)$$

$$PSNR = 10\log_{10}\left(\frac{R^2}{MSE}\right) \cdots (2)$$

$$SSIM(x,y) = \frac{(2\mu_x\mu_y + C_1)(2\sigma_{xy} + C_2)}{(\mu_x^2 + \mu_y^2 + C_1)(\sigma_x^2 + \sigma_y^2 + C_2)} \cdots (3\text{-}1)$$

$$MSSIM = \frac{1}{n}\sum_{i=1}^{n} SSIM(x_i, y_i) \cdots (3\text{-}2)$$

$$DSC = \frac{2 \times N_{(x \cap y)}}{N_x + N_y} \cdots (4)$$

$$\sigma_w^2(t) = w_1(t)\sigma_1^2(t) + w_2(t)\sigma_2^2(t) \cdots (5)$$

1-4. Evaluation by Statistical Image

^{123}I-IMP SPECT data are generally used for diagnosis by performing three-dimensional stereotactic surface projection (3D-SSP)[11] analysis and Z-scoring the areas of hypoperfusion on brain surface images for healthy subjects. Therefore, 3D-SSP analysis was performed by converting the generated PNG data to Dicom format, and the Z-score maps from 40 min_S, 10 min_S, and fake_S were compared. When converting from PNG to Dicom format, each voxel value was multiplied by 128 times calculated from the ratio of the signal values of the original Dicom image and the PNG file to approximate the counts of the Dicom image, and the header information was added. Z-score map needs objective evaluation, so Stereotactic extraction estimation (SEE) analysis[12] was added. SEE uses the Talairach daemon to convert each pixel of the 3D-SSP Z-score map into the coordinate information that matches the Talairach brain coordinate map, enabling absolute evaluation according to the classification of Brodmann fields.

2. Result

The results of each index are shown in Fig. 2: MSE mean and standard deviation for 10 min_S and fake_S were 540.79 ± 458.02 and 333.35 ± 309.1, respectively, PSNR 22.00 ± 3.34 and 23.78 ± 2.56, MSSIM 0.68 ± 0.10 and 0.73 ± 0.09, DSC 0.92 ± 0.07 and 0.93 ± 0.06, and for each of the assessments, the fake_S was more similar to the 40 min_S than to the 10

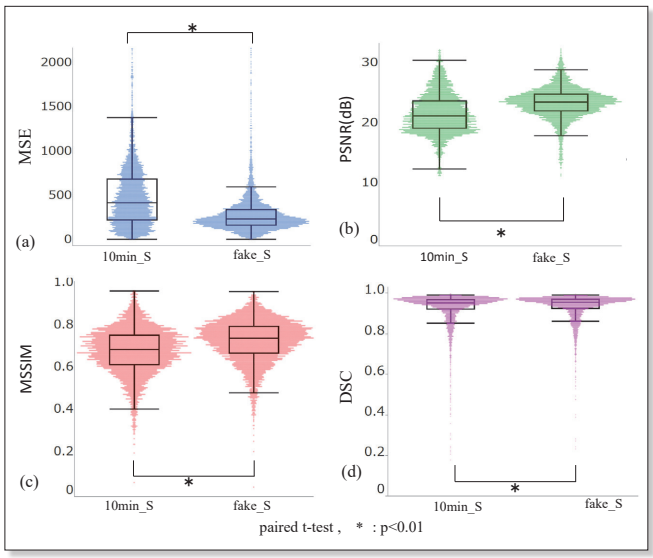

Fig. 2 The evaluation results of (a) MSE, (b) PSNR, (c) SSIM, and (d) DSC are shown in graphs.
By image generation, fake_S was rated higher than 10 min_S with a significant difference in all evaluations.

min_S with significant differences in the corresponding t-tests. Fig. 3 shows pix2pix analysis images from Test_data. There are examples of each condition: The upper panel shows No abnormality (N.A), the middle panel shows Alzheimer's dementia (AD), and the lower panel shows Right internal artery stenosis (R. IC).

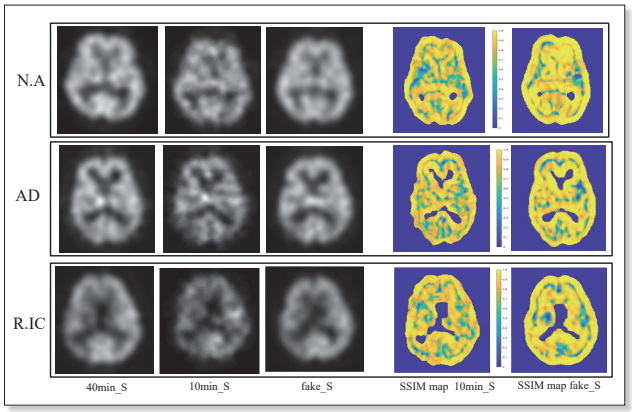

Fig. 3 The images show generated images and SSIM maps for three cases of no abnormality (Upper), Alzheimer's dementia (Middle), and right internal artery stenosis (Lower).

The SPECT images of each case shown in the figure are 40 min_S, 10 min_S, and fake_S in the same slice. The SSIM map shows 10 min_S and fake_S of the same slice as SPECT.

N.A is shown as Decrease, indicating areas of relative hypoperfusion, and Increase, indicating areas of relative hyperperfusion. AD and R.IC were displayed in comparison with Decrease. The selection criteria for cases were as follows: the patients with clear areas of hypoperfusion in dementia or cerebrovascular disease and higher than average MSSIM in the basal ganglia region were selected by referring only to the 3D-SSP at 40 min_S. The SSIM map shows low SSIM values for cold colors (blue) and high values for warm colors (yellow). In MSE, 10 min_S shows 647.76, fake_S shows 293.38. In PSNR, they show 20.02 and 23.46, respectively. MSE and PSNR for AD were from 914.17 to 395.17 and from 18.52 to 22.16, respectively, and for R.IC from MSE 749.42 to 237.19 and from PSNR 19.38 to 24.38, showing the same changes as for N.A. MSSIM changed to higher values in all cases, from 0.63 to 0.75 for N.A, 0.63 to 0.73 for AD, and 0.64 to 0.72 for R.IC. In DSC, the values were 0.96 to 0.97 for NA, 0.95 to 0.95 for AD, and 0.94 and 0.95 for R.IC.

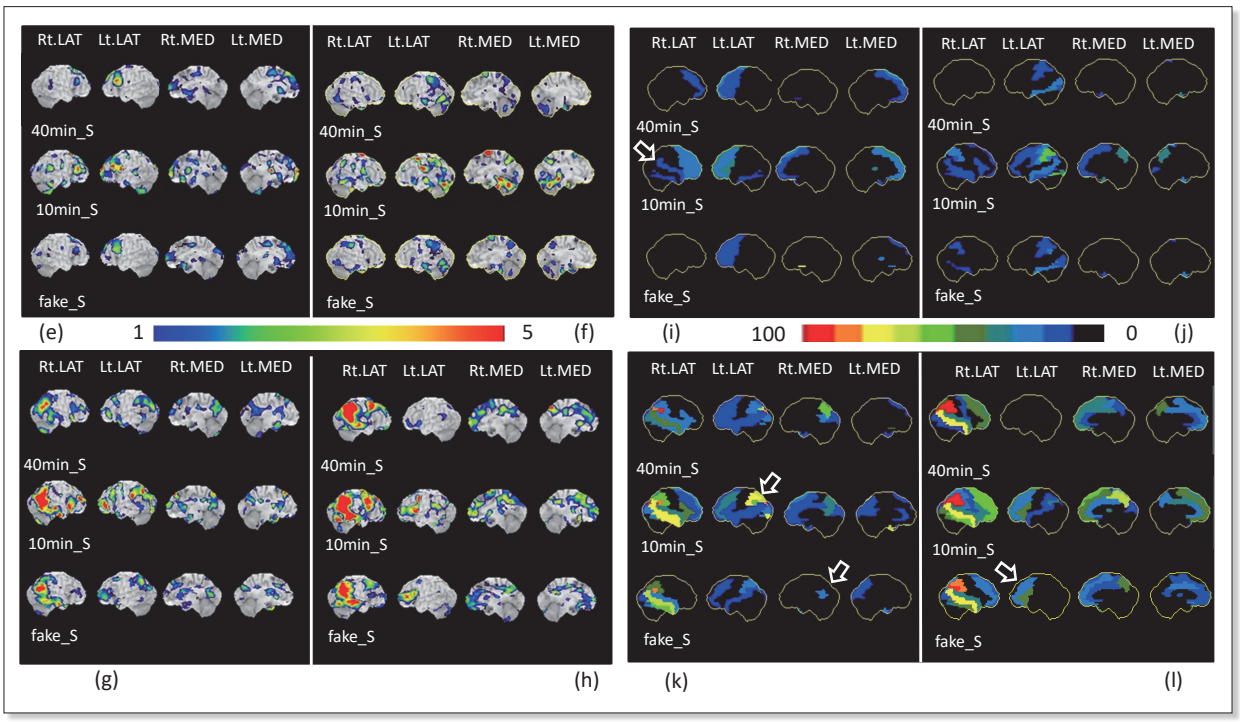

Fig. 4 Z-score map (e) (f) (g) (h) and SEE (i) (j) (k) (l) of the three cases in Fig. 3.

(e) (i): The indication of low blood flow for N.A, (f) (j) : The indication of increased blood flow for N.A,
(g) (k): The indication of low blood flow for AD, (h) (l) : The indication of low blood flow for R.IC.

Fig. 4 shows the results of 3D-SSP Z-score map and SEE analysis of the three cases in Fig. 3, which were analyzed using the normal database constructed at our institution. The Z-score map of the 3D-SSP is displayed with a lower limit of 1.0 and an upper limit of 5.0 as in the scale used for clinical diagnosis, and SEE is classified by Lobule (Level 3) and displayed as Extent ratio (%). In 10 min_S for N.A, the Z-score region was depicted with an extent ratio of 15% to 20% in the upper and lower temporal gyrus region in the Decrease and 15% to 55% in the right and left frontal and temporal lobe regions in the Increase, on the other hand, that in 40 min_S and fake_S was not depicted. In the AD patients, the Z-score regions were more extensive in the fake_S than in the 40 min_S, and furthermore, those in the 10 min_S were more extensive than in the others in all brain regions. In the fake_S, the precuneus, a specific area of hypoperfusion in AD, showed an Extent ratio of 50%, but not in the fake_S. In the R.IC, the left frontal region showed a Z-score with an Extent ratio of 20-50%, which was not seen in the 40 min_S (SEE⇨).

3. Consideration

In short-time collected SPECT image which includes much quantum noise, the effect of image quality improvement by deep learning is the most expected point, and the MSE and PSNR results show that the image quality is significantly improved in fake_S compared to 10 min_S, and is closer to 40 min_S. The case images in Fig. 3 also show noise reduction in fake_S compared to 10 min_S, which is consistent with the physical evaluation. The next issue is the similarity accuracy of signal information between corresponding voxels in the generated and reference images. In AI, it is common to evaluate similarity based on SSIM values, and Fukui [9] et al. refer to the index values in the guidelines [13] for image compression of digitized documents. The guideline evaluates the value of the text file when it is converted into an image. PSNR 30 to 40 [dB] and MSSIM 0.90 to 0.98 are considered to be "a level where degradation can be seen when enlarged," and PSNR less than 30 [dB] and MSSIM less than 0.90 are considered to be "clearly degraded." The results of FAKE_S were not satisfactory because the degradation was clearly visible. When we check the images with low MSSIM in Fig. 2, a proportion of skull base sections which has small parenchymal brain area that is depicted as radiopharmaceutical uptake is little is large, and the images with MSSIM 0.3 to 0.5 are majority, which is considered to be one of the reasons to degrade the evaluation value. These are predicted to have a significant effect on MSE and PSNR, and we believe that evaluation excluding skull base images is necessary in the future. Fig. 3 SSIM map shows that the MSSIM increased by 16% in N.A, 13% in AD, and 11% in R.IC at 40 min_S compared to 10 min_S. The map also shows that the number of cold regions decreased, and it is possible to partially visualize the similarity evaluation. Next, regarding the evaluation of the similarity of the Z-score map in all brain regions, the clinical diagnosis does not seem to differ significantly between the 40 min_S and fake_S Z-score maps in the validation case N.A. Decrease and Increase, but in AD, there is failure of depiction on Rt.LAT precuneus region, and that is a specific hypoperfusion region in AD, which influences the diagnosis. Also in R.IC, depiction of frontal brain region on Lt.LAT that is not depicted in 40 min_S is observed. The DSC is an image that evaluates the similarity between binarized images, and there is no significant difference between 40 min_S, 10 min_S, and fake_S. We believe that the threshold setting in the Otsu method was suitable for calculating each evaluation index. Finally, although pix-2pix image generation could improve the image quality of 10 min_S, it is difficult to generate a standard time distribution of cerebral perfusion for a short collection time. Therefore, it

is necessary to extend the collection time from 10min to find a collection time when the relative count ratio between each voxel in the brain parenchyma region is closer to 40 min, and then to train with the data.

4. Conclusion

Using pix2pix, an artificial intelligence-based image generation model, we attempted to generate a standard SPECT image with 40 minutes acquisition time from a 10 minutes acquisition time of the original cerebral perfusion SPECT image. The 3D-SSP analysis also showed that the generated images were more similar to the standard images than the original images. However, they were not at the level of clinical use as standard SPECT images.

Conflict of interest

There are no conflicts of interest to be disclosed by the first author or co-authors.

References

1) Nakamura Y, Narita K, Higashi T, et al.: Diagnostic value of deep learning reconstruction for radiation dose reduction at abdominal ultra-high-resolution CT. Eur Radiol, 31(7): 4700-9, 2021.
2) Njeh I, Mzoughi H, Ben Slima M, et al.: Deep Convolutional Encoder-Decoder algorithm for MRI brain reconstruction. Med Biol Eng Comput, 59(1): 85-106, 2021.
3) Kim M, Kim HS, Kim HJ, et al.: Thin-Slice Pituitary MRI with Deep Learning-based Reconstruction: Diagnostic Performance in a Postoperative Setting. Radiology, 298(1): 114-22, 2021.
4) Park CJ, Chen W, Pirasteh A, et al.: Initial Experience With Low-Dose 18F-Fluorodeoxyglucose Positron Emission Tomography/Magnetic Resonance Imaging With Deep Learning Enhancement. J Comput Assist Tomogr, 45(4): 637-42, 2021.
5) Okamoto K, Ushijima Y, Okamura C, et al.: Measurement of cerebral blood flow using graph plot analysis and I-123 iodoamphetamine. Clin Nucl Med, 27(3): 191-196, 2002.
6) Yamamoto Y, Onoguchi M, Wada A, et al.: Evaluation of Shortened Protocol of Graph Plot Method with ^{123}I-IMP. Jpan J.Radiol.Technol, 67(5): 524-33, 2011.
7) Phillip Isola, Jun-Yan Zhu, Tinghui Zhou, et al.: Image-to-Image Translation with Conditional Adversarial Networks. Proceedings of the IEEE Conference on Computer Vision and Pattern Recognition (CVPR), 1125-1134, 2017.
8) Diederik P. Kingma, Jimmy Ba: Adam: A Method for Stochastic Optimization. Published as a conference paper at ICLR, 2015.
9) Fukui R, Fujii S, Ninomiya H, et al.: Generation of the Pseudo CT Image Based on the Deep Learning Technique Aimed for the Attenuation Correction of the PET Image. Jpan J.Radiol.Technol, 76(11): 1152-62, 2020.
10) Nobuyuki Otsu: A Threshold Selection Method from Gray-Level Histograms. IEEE Transactions on Systems, Man, and Cybernetics, 9(1): 62-66, 1979.
11) Minoshima S, Frey KA, Koeppe RA, et al.: A diagnostic approach in Alzheimer's disease using three-dimensional stereotactic surface projections of fluorine-18-FDG PET. J Nucl Med, 36(7): 1238-48, 1995.
12) Mizumura S, Kumita S, Cho K, et al.: Development of quantitative analysis method for stereotactic brain image: assessment of reduced accumulation in extent and severity using anatomical segmentation. Ann Nucl Med, 17(4): 289-95 2003.
13) Kobako Masahiko: Process to Standardization, A Report by Committee of Standardization (3), Guidelines of Image Compression for Digitized Documents, Journal of image & information management, 50(5): 21-24, 2011.

Received August 29, 2022; accepted May 24, 2023

MiSDO:The Open-source Radiation Dose Management System

SUGIMOTO Kohei[1)], MATSUMOTO Masaki[2)], OITA Masataka[3)], FUJIWARA Yuta[4)], NAGASAKI Ryota[5)], SHODA Takashi[6)], KURODA Masahiro[7)]

1) Graduate School of Interdisciplinary Science and Engineering in Health Systems, Okayama University/ Division of Imaging Technology, Okayama Diagnostic Imaging Center
2) Graduate School of Interdisciplinary Science and Engineering in Health Systems, Okayama University/ Department of Radiological Technology, Ehime University Hospital
3) Faculty of Interdisciplinary Science and Engineering in Health Systems, Okayama University
4) Division of Clinical Radiology Service, Okayama Central Hospital
5) Department of Radiology Diagnosis, Aoki Internist and Pediatrics Clinic
6) Department of Radiology, Kawasaki Medical School General Medical Center
7) Department of Radiological Technology, Faculty of Health Sciences, Okayama University

Note: This paper is secondary publication, the first paper was published in the JART, vol. 70 no. 854: 29-35, 2023.

Key words: dose management system, open-source, digital imaging and communications in medicine, radiation dose structured report

【Abstract】
All medical facilities with diagnostic imaging equipment in Japan must recently record and manage radiation doses. Accordingly, a radiation dose management system (DMS) is essential for recording and managing radiation doses, and it is difficult to introduce in all medical facilities because of its high cost. In this study, we developed an open-source DMS called "MiSDO" and verified its capability through simulations. The results showed that it could record and manage radiation doses quickly and accurately. "MiSDO" is promising as free software to record and manage radiation doses that anyone can use.

1. Introduction

The International Commission on Radiological Protection recommends establishing diagnostic reference levels (DRLs) to optimize radiation dose for imaging procedure[1)]. Over the past decade, radiation dose optimization with DRLs has been implemented worldwide[2-8)]. Moreover, several reports suggest DRLs have contributed to reducing radiation dose in clinical practices[9, 10)]. The first step of radiation dose optimization is to obtain representative dose index values for each radiological examination in medical facilities. There are two principal approaches for collecting data: manual and automatic methods. Although manual data collection is simple, it has the problem of inaccurate data collection[11)]. Therefore, in recent years, a method that considers the value calculated from a dose management system (DMS)[12)], which can collectively manage radiation doses from radiological examinations, as the representative value of the medical facility and comparing the value with DRLs would be suitable for optimizing radiation doses[13)].

However, because commercially available DMSs are often expensive, there are problems with accelerating their introduction in all medical facilities. Under these circumstances, Japanese Enforcement Regulations on the Medical Care Act were revised in April 2020, making the recording and managing radiation doses mandatory for all medical facilities. Radiation dose recording is usually implemented by referring to the secondary capture output from the X-ray imaging modalities to the picture archiving and communications system (PACS). On the other hand, radiation dose management could be necessary to compare the representative dose index values of the facility with

DRLs, and consider what to do if the representative values exceed one. As mentioned above, considering that manual recording of radiation doses is inaccurate[11] and comparing values calculated from DMS with DRLs as representative values are suitable[13], all medical facilities in Japan would be better to install DMS.

To achieve a possible solution, we have developed an open-source DMS called "MiSDO" that can record and manage radiation doses for the X-ray imaging modalities such as computed tomography (CT), angiography, and nuclear medicine examinations (URL: https://github.com/dose-mmasaki/MiSDO_release). Although there are several reports of developing in-house DMS systems for CT[14-21] and fluoroscopically guided intervention[20, 22-24] for referring to radiation dose information in digital imaging and communications in medicine (DICOM) format data. There has been no free DMS, including all modalities under the revised Enforcement Regulations on the Medical Care Act[14-24]. In this study, we verified the operation of "MiSDO" using DICOM files retrieved from diagnostic imaging modalities of several manufacturers. Then, we simulated the recording and management of radiation dose using "MiSDO" and clarified its usefulness.

2. Materials and Methods

2.1 Development environment and devices

The development environments were used Visual Studio 2019 (Microsoft Corporation, WA, USA) as the integrated development environment, Python (version 3.7.8; Python Software Foundation, DE, USA), and Visual C# (version 7.3; Microsoft Corporation) as the programming language, and SQLite as the database. Pydicom, a Python library, was used to process DICOM files, including radiation dose structured report (RDSR). A computer with Windows 10 education operating system (Microsoft Corporation), which has a single Intel core i5-3470S CPU 2.9-GHz processor and 4 GB RAM, was used to verify the software's operation. CT systems used were SOMATOM Sensation 64 (VB42B; Siemens, Munich, Germany), Discovery CT 750HD (17BW50.7B; GE Healthcare, WI, USA), Aquilion NEW PRIME TSX-303A/MW (7.0; Canon Medical Systems, Tochigi, Japan), and Aquilion 64 (3.10; Canon Medical Systems). Infinity Celeve-i INFX-8000C (N9; Canon Medical Systems), Symbia Dual Head System (VB10B; Siemens), and Biograph Horizon (VJ21B; Siemens) were used as angiography, single photon emission CT (SPECT) and positron emission tomography (PET)/CT systems, respectively.

2.2 Development of "MiSDO"

Figure 1A shows an overview of the system configuration of "MiSDO." It consists of two main modules for recording and managing radiation doses. The recording module consists of "DoNuTS," which extracts dose information from DICOM headers and RDSRs, and "ChuRROs," which automatically extracts dose information from secondary captures (only Aquilion 64) with an optical character reader (OCR). This OCR algorithm adds the image pixels in the column direction to obtain the marginal distribution. Then, we performed the pattern matching classification between the marginal distribution and the previously registered information (Fig. 1B). The radiation dose information of CT and X-ray angiography are extracted almost equivalently to the DEN Dose software[13]. Radiopharmaceutical dose is also extracted in nuclear medicine examinations, such as SPECT and PET. The management module consists of programs for visualization and output functions using data stored in the database. "MiSDO" was developed as a program that worked with these modules and could operate through a graphical user interface.

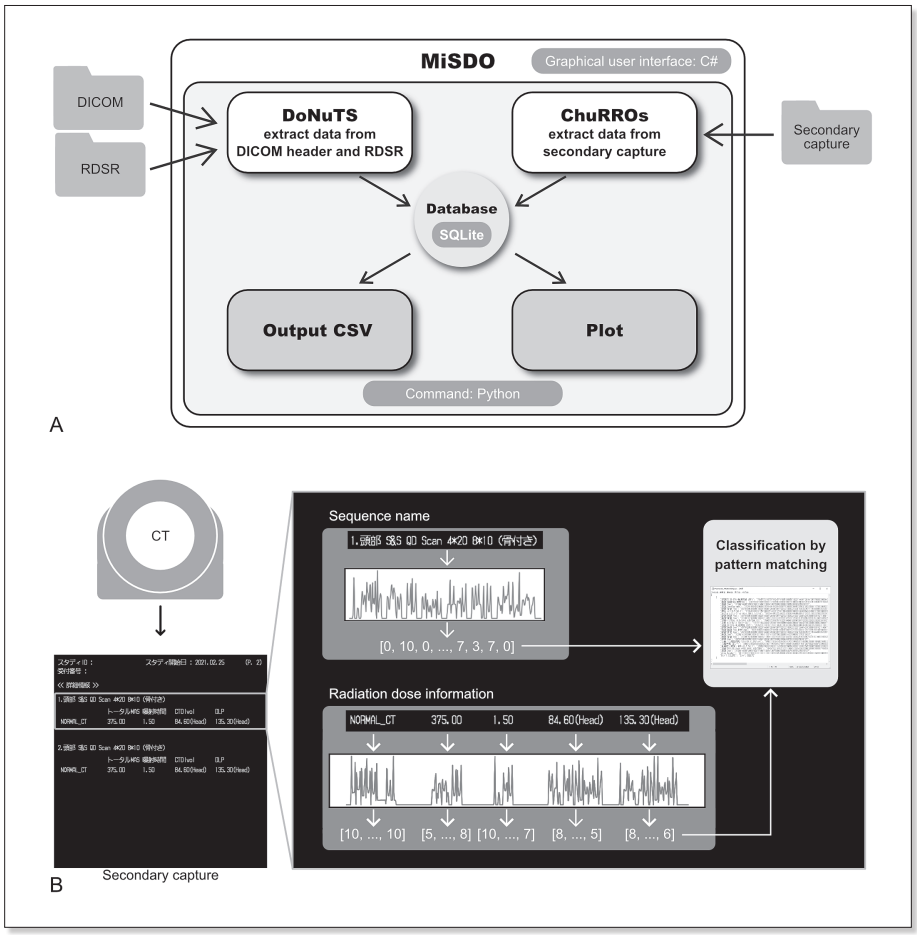

Fig. 1 Overview and details of the developed radiation dose management system.

(A) An overview of the system configuration of "MiSDO."
(B) Details of the algorithm for the optical character reader function of "MiSDO." Character strings of secondary capture output from CT are acquired row by row, and the marginal distribution added in the column direction is used for character classification by pattern matching.

2.3 Operation validation of the developed DMS

The recording and management modules of "MiSDO" were operationally validated. A water phantom was scanned using one of the protocols routinely used in each imaging modality. Then, the RDSRs and secondary captures were retrieved from the CT, X-ray angiography, SPECT, and PET/CT devices in DICOM format. To verify the accuracy of OCR, randomly selected ten protocols from the protocols list used in clinical practice and scanned the phantom using the Aquilion 64. These DICOM files were imported using "MiSDO" to confirm that they were working correctly. Also, we simulated the recording and management of radiation dose from CT examinations. Referring to the report by Ogawa[25], the number of CT examinations per day was assumed to be 25. Then, the RDSR file outputs from Aquilion NEW PRIME TSX-303A/MW were duplicated for one day, one week, one month, six months, and one year, respectively. The number of these data were 25, 175, 700, 4,375, and 8,750, respectively. The volume CT dose index ($CTDI_{vol}$) and the dose length product (DLP) of the duplicated data were replaced with simulated data computed from regression equations created using patients' height and weight. "MiSDO" was used to store these data and measured the time required for analysis. The median values of the replicated one-year data

were compared with the values of the routine chest CT scan for adults of the DRLs 2020 in Japan ($CTDI_{vol}$ = 13 mGy, DLP = 510 mGy·cm)[26].

3. Results

3.1 Operation validation

Figure 2 shows a screen capture of the developed DMS. All radiation dose information was extracted accurately without any errors from DICOM files of one scan for each of the six modalities (SOMATOM Sensation 64, Discovery CT 750HD, Aquilion NEW PRIME TSX-303A/MW, Infinity Celeve-i INFX-8000C, Symbia Dual Head System, and Biograph Horizon) and secondary captures of 10 scans for one modality (Aquilion 64).

3.2 Processing time

Figure 3 shows the time it took "MiSDO" to record the duplicated RDSR. The recording time increased as the number of data increased. The time required for 25 recordings for the number of daily examinations and 8,750 recordings for annual examinations was 14 seconds (0.23 min) and 10,243 seconds (170.7 min), respectively.

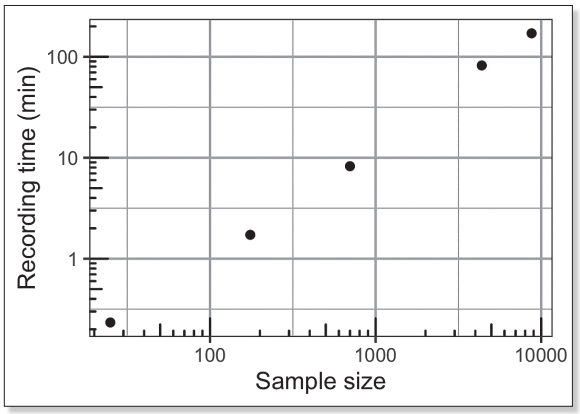

Fig. 3 Double logarithmic plot of recording time for extracting information from duplicated radiation dose structured reports.

The time required for the Data analysis of 25 records for assuming some daily examinations, 175 records for weekly, 700 records for monthly, 4,375 records for semi-annually, and 8,750 records for annually were 14 seconds (0.23 min), 103 seconds (1.72 min), 494 seconds (8.23 min), 4,923 seconds (82.1 min), and 10,243 seconds (170.7 min), respectively.

3.3 Simulation of dose management

Figure 4 shows that the median $CTDI_{vol}$ and DLP of the standard body weight extracted from the duplicate RDSRs were 12.5 mGy and 487.2 mGy·cm, respectively. These data assume a routine chest CT scan for adults, and the corresponding values DRLs 2020 in Japan[26] are 13 mGy and 510 mGy·cm, respectively. The median values of the data simulated in this study were lower than those in DRLs.

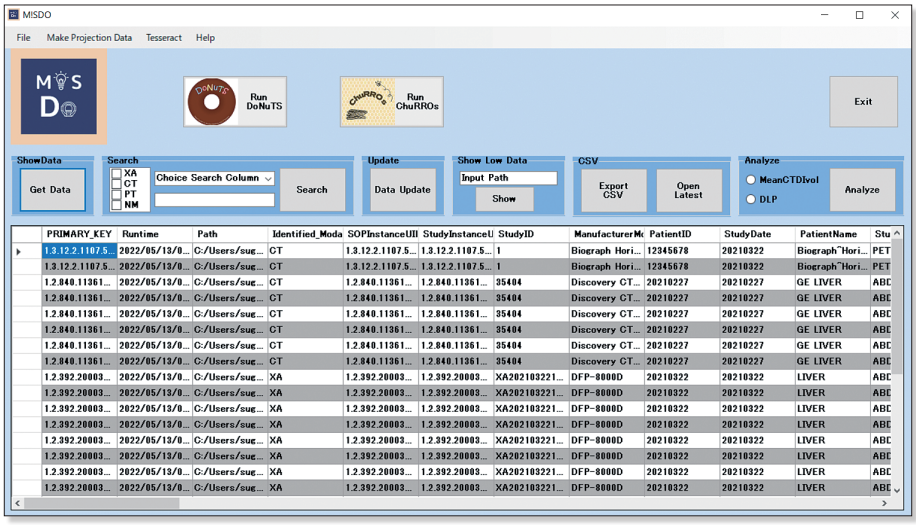

Fig. 2 Screen capture of the developed radiation dose management system after extracting radiation dose information from multiple modalities.

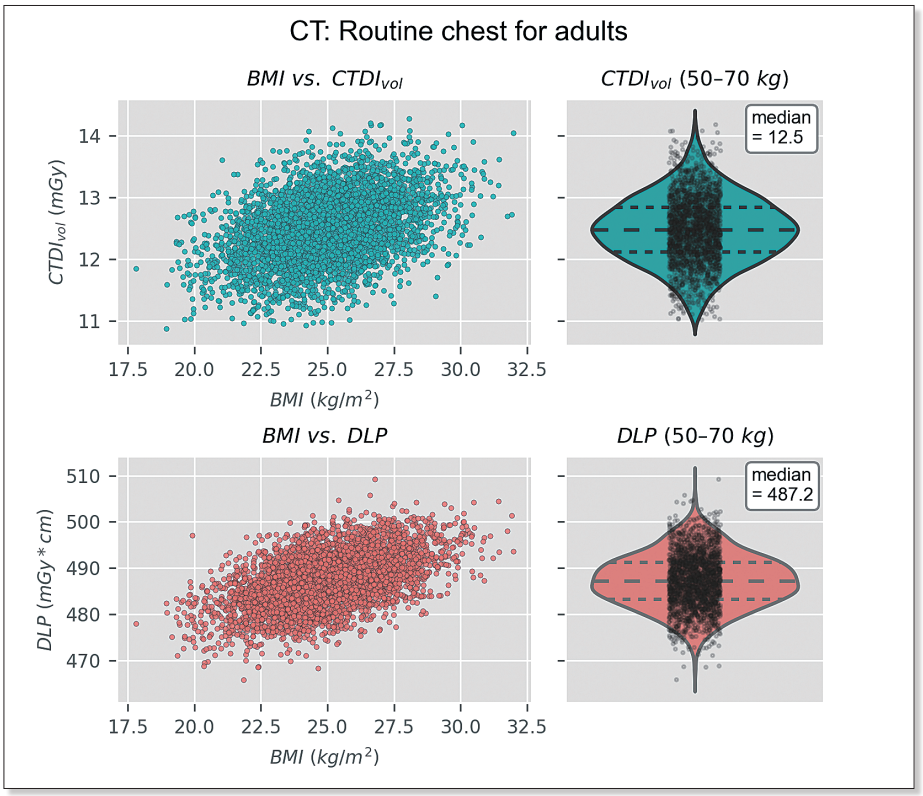

Fig. 4 Scatter plots and violin plots for $CTDI_{vol}$ and DLP simulated routine chest CT scan for adults.

The left column shows the scatter plots, where the horizontal axis represents body mass index (BMI) and the vertical axis represents $CTDI_{vol}$ (first row) and DLP (second row). The right column shows violin plots of $CTDI_{vol}$ (first row) and DLP (second row) for standard body weight (50-70 kg). Strip plots are shown within the violin plots. The dotted lines in the violin plots are quartiles, representing the 25th, 50th, and 75th percentiles from the top, respectively. The median values of these data (12.5 and 487.2 mGy, respectively) are displayed in the upper right corner.

4. Discussion

In this study, we verified that "MiSDO" could accurately extract data necessary for recording and managing radiation dose from multiple manufacturers' DICOM files retrieved from each modality. Furthermore, the extracted data were duplicated to simulate radiation dose management. "MiSDO" has been able to extract data quickly, revealing that it can accurately process large amounts of data generated in clinical practice. "MiSDO" can easily calculate representative dose index values and compare them with DRLs, suggesting that the system can be used as a tool to optimize radiation doses.

The developed DMS could extract information on one year of CT examination data (8,750 records) in less than three hours. The program that reads the data necessary for dose management only retrieves text data from the DICOM file so that the data can be extracted at high speed. The commercial DMS is designed to perform a DICOM query/retrieve on the PACS at night time to get the data into the DMS. "MiSDO" has been able to achieve short-time processing even on the local PC used for this simulation. Thus, we considered "MiSDO" acceptable enough for use in a clinical practice where data is expected to be extracted at night-time, similar to commercially available DMSs. Because there are many CT scanners in Japan[28], manual storage of radiation dose data is more time-consuming than in other countries. This issue may lead to prolonged work for radiological technologists. "MiSDO" could be an effective solution to this problem since

the mechanical recording of radiation dose data can increase work efficiency and prevent human error.

"MiSDO" has the following two strengths compared to the previously reported in-house developed DMSs. The First is that all "MiSDO" source code is publicly available. Commercially available DMSs are guaranteed to work and are regularly inspected by the manufacturer. However, it is not possible with a free DMS. If the source code of the DMS is disclosed, the program errors can be addressed by reading the source code. RADIANCE[14] was a visionary open-source DMS; however, as of 2022, it is closed to the public. DEN Dose[20] is also a free DMS; however, the source code is not publicly available. Although there are several reports of other privately developed DMSs, the systems are private[19], or even if the source code is publicly available, only a limited number of systems[21] are available in the supported modalities. In other words, "MiSDO" is the only open-source DMS that supports many modalities.

The second is the ability to achieve accurate OCR for the Japanese. Compared to English, Japanese is more challenging to apply for OCR accurately due to the lack of spaces between words and the fact that it has more than 3,000 character types. Interestingly, "MiSDO" could read Japanese in secondary captured CT images with high accuracy. Since the secondary captured image is digital data, the marginal distribution of characters and phrases is uniquely determined. Therefore, it could be achieved with high accuracy by using a pattern-matching algorithm. To the best of our knowledge, the only language supported by the OCR functions of the free DMSs reported is English[14, 15, 17, 21], and this capability is an advantage when considering use in Japan.

A limitation of "MiSDO" is that it cannot connect with PACS. When using "MiSDO" to record dose information, it is necessary to read a DICOM file from the PACS system or to connect a workstation to the PACS and then process the data with "MiSDO". It is a significant drawback for fluoroscopically guided intervention, where the maximum skin dose needs to be calculated immediately; however, almost free DMSs also do not support this[27].

5. Conclusion

"MiSDO" is a DMS that can realize free and accurate recording and management of exposure doses. It is also the only free DMS compliant with the revised Japanese laws. "MiSDO" is expected to solve problems when manually recording and managing radiation doses.

Acknowledgments

We thank Mr. Eiji Ohnishi (Okayama Saiseikai General Hospital, Okayama, Japan) for his cooperation in obtaining image data.

Conflict of interest

The authors declare that they have no conflict of interest.

References

1) Vañó E, et al.: ICRP publication 135: Diagnostic reference levels in medical imaging. Ann ICRP, 46(1), 1-144, 2017.
2) Foley SJ, et al.: Establishment of CT diagnostic reference levels in Ireland. Br J Radiol, 85(1018), 1390-1397, 2012.
3) Fukushima Y, et al.: Diagnostic reference level of computed tomography (CT) in Japan. Radiat Prot Dosimetry, 151(1), 51-57, 2012.
4) Roch P, et al.: French diagnostic reference levels in diagnostic radiology, computed tomography and nuclear medicine: 2004-2008 review. Radiat Prot Dosimetry, 154(1), 52-75, 2012.
5) van der Molen AJ, et al.: A national survey on radiation dose in CT in The Netherlands. Insights Imaging, 4(3), 383-390, 2013.
6) Saeed MK, et al.: Regional survey of image quality and radiation dose in computed tomography examinations in Saudi Arabia. Australas Phys Eng Sci Med, 37(2), 279-283, 2014.
7) Sulieman A: Establishment of diagnostic reference levels in computed tomography for paediatric patients in Sudan: a pilot study. Radiat Prot Dosimetry, 165(1-4), 91-94, 2015.

8) Kanal KM, et al.: U.S. diagnostic reference levels and achievable doses for 10 adult CT examinations. Radiology, 284(1), 120-133, 2017.
9) Matsunaga Y, et al.: Diagnostic reference levels and achievable doses for common computed tomography examinations: Results from the Japanese nationwide dose survey. Br J Radiol, 92(1094), 20180290, 2019.
10) Katsari K, et al.: Implementation of a computed tomography dose management program across a multinational healthcare organization. Eur Radiol, 31(12), 9188-9197, 2021.
11) Dickinson N, et al.: A comparison of manually populated radiology information system digital radiographic data with electronic dose management systems. Br J Radiol, 93(1111), 20200055, 2020.
12) Gress DA, et al.: AAPM medical physics practice guideline 6.a.: Performance characteristics of radiation dose index monitoring systems. J Appl Clin Med Phys, 18(4), 12-22, 2017.
13) Osman ND, et al.: Radiation dose management in CT imaging: Initial experience with commercial dose watch software. J Phys Conf Ser, 1497(1), 012020, 2020.
14) Cook TS, et al.: Informatics in radiology: RADIANCE: An automated, enterprise-wide solution for archiving and reporting CT radiation dose estimates. Radiographics, 31(7), 1833-1846, 2011.
15) Shih G, et al.: Automated framework for digital radiation dose index reporting from CT dose reports. AJR Am J Roentgenol, 197(5). 1170-1174, 2011.
16) Christianson O, et al.: Automated size-specific CT dose monitoring program: Assessing variability in CT dose. Med Phys, 39(11), 7131-7139, 2012.
17) Sodickson A, et al.: Exposing exposure: Automated anatomy-specific CT radiation exposure extraction for quality assurance and radiation monitoring. Radiology, 264(2), 397-405, 2012.
18) Dave JK, et al.: Extraction of CT dose information from DICOM metadata: Automated Matlab-based approach. AJR Am J Roentgenol, 200(1), 142-145, 2013.
19) Nitrosi A, et al.: Patient dose management solution directly integrated in the RIS: "Gray Detector" software. J Digit Imaging, 27(6), 786-793, 2014.
20) Dendo Y, et al.: Development of computer code for dose management using DICOM radiation dose structured report in X-ray computed tomography. Medical Imaging and Information Sciences, 33(2), 43-47, 2016.
21) Weisenthal SJ, et al.: Open-source radiation exposure extraction engine (RE3) with patient-specific outlier detection. J Digit Imaging, 29(4), 406-419, 2016.
22) Johnson PB, et al.: Skin dose mapping for fluoroscopically guided interventions. Med Phys, 38(10), 5490-5499, 2011.
23) Borrego D, et al.: A hybrid phantom system for patient skin and organ dosimetry in fluoroscopically guided interventions. Med Phys, 44(9), 4928-4942, 2017.
24) Borrego D, et al.: Physical validation of UF-RIPSA: A rapid in-clinic peak skin dose mapping algorithm for fluoroscopically guided interventions. J Appl Clin Med Phys, 19(3), 343-350, 2018.
25) Ogawa K: Study on the running condition and the operation of CT in Saitama prefecture. Journal of JART, 60(8), 904-909, 2013.
26) Japan Network for Research and Information on Medical Exposure (J-RIME), et al. National diagnostic reference levels in Japan (2020) -Japan DRLs 2020-. [Accessed 21 May 2021] http://www.radher.jp/J-RIME/report/DRL2020_Engver.pdf
27) Malchair F, et al.: Review of skin dose calculation software in interventional cardiology. Phys Med, 80, 75-83, 2020.
28) OECD: Computed tomography (CT) scanners (indicator). [Accessed 26 December 2022]

Received September 2, 2022; accepted June 23, 2023

Effects of radioprotective equipment on radiation exposure to the operator's eye lens during computed tomography fluoroscopy-guided procedure

HASEGAWA Takaaki, M.D., Ph.D.[1)], SHIMIZU Hidetoshi, R.T., Ph.D.[2)], CHATANI Shohei, M.D.[1)], MURATA Shinichi, M.D.[1)], HATTORI Hisashi, R.T.[1)], INABA Yoshitaka, M.D., Ph.D.[1)]

1) Department of Diagnostic and Interventional Radiology, Aichi Cancer Center Hospital
2) Department of Radiation Oncology, Aichi Cancer Center Hospital

Note: This paper is secondary publication, the first paper was published in the JART, vol. 70 no. 854: 44-49, 2023.

Key words: radiation exposure, CT fluoroscopy, radioprotective equipment, eye lens

【Abstract】
Purpose: To evaluate whether radiation exposure to the operator's eye lens is reduced by radioprotective equipment of shield and lead drape during computed tomography (CT) fluoroscopy-guided procedures.
Materials and Methods: Radiation doses were measured using small optically stimulated luminescence dosimeters outside and inside radioprotective glasses of the operator during 16 lung nodule localizations. Measurements were performed under four settings: A) with radioprotective shield and lead drape; B) with radioprotective shield, without lead drape; C) without radioprotective shield, with lead drape; and D) without radioprotective shield or lead drape. The fluoroscopy duration was compared between settings, with and without a shield, using Welch's t-test. Radiation doses per procedure were compared among the four settings of radioprotective equipment using the one-way analysis of variance.
Results: Mean duration of fluoroscopy was significantly longer in settings with shield (53.8 ± 5.5s for settings of A and B) than in those without shield (45.6 ± 2.6s for settings of C and D) ($p=0.005$). Mean radiation doses were 26.0 ± 4.9 μGy, 43.1 ± 3.5 μGy, 66.4 ± 3.5 μGy, and 79.1 ± 7.0 μGy outside the glasses, for settings A, B, C, and D, respectively, and 11.9 ± 4.2 μGy, 20.9 ± 3.4 μGy, 30.9 ± 2.7 μGy, and 34.2 ± 3.6 μGy inside the glasses, for settings A, B, C, and D, respectively. Significant differences were detected among the four settings for the radiation dose both outside ($p<0.001$) and inside ($p<0.001$).
Conclusion: Radioprotective equipment reduces radiation doses to the operator's eye lens during CT fluoroscopy-guided procedures.

INTRODUCTION

The importance of reducing radiation exposure in medical staff has recently increased. The International Commission on Radiological Protection has recommended an annual dose limit to the eye lens of 20 mSv averaged over a defined period of five years, with doses not exceeding 50 mSv in any single year[1)]. The International Atomic Energy Agency has adopted this new dose limit[2)]. Thus, we must consider radiation exposure to the eye lens during interventional radiology procedures.

Computed tomography (CT) fluoroscopy is one of imaging modality used during interventional radiology. It offers the advantage of rapid and objective visualization of the puncture target[3, 4)] and is widely used in performing procedures such as biopsy, ablation, and preoperative lung nodule localization[5-11)]. However, this procedure has the strong drawback of radiation exposure to both patients and medical staff[3, 9-12)]. In particular, the eye lens of operators are exposed to relatively high radiation doses[11, 12)].

Several methods to reduce operator radiation exposure during CT fluoroscopy-guided procedures have been reported. For example, the installation of a radioprotective shield in front of the scan plane has been reported to reduce

the radiation exposure to the operator[13, 14]. Placement of a lead drape over the patient to block scattered radiation reaching the operator has been shown to be an effective option[15-17]. However, such results have been derived from experimental studies using phantoms; therefore, the extent to which radiation exposure could be reduced by these methods has not been evaluated in clinical settings. In this study, we measured doses to the eye lens received by the operator during CT fluoroscopy-guided procedures and evaluated the clinical reduction in radiation doses to the operator using shields and lead drapes as radioprotective equipment.

METHODS

Study design

Radiation doses were measured during preoperative localization of the lung nodules. This procedure was chosen for the analysis because the fluoroscopy time was relatively short and did not vary between sessions.

This study was approved by our institutional review board as a survey for operator radiation exposure. Written informed consent was obtained from the operator performing the procedure before measuring the radiation dose. Informed consent to perform lung nodule localization under CT fluoroscopy, which provides medical exposure, was obtained from each patient.

Measurement of radiation doses

Radiation doses were measured during 16 sessions of lung nodule localization between November 2020 and January 2021. The procedure was performed percutaneously using real-time CT fluoroscopy (Aquilion LB; Canon Medical Systems Corp., Otawara, Japan). Local anesthesia was performed with 1% lidocaine (Xilocaine Injection Polyamp 1%; Aspen Japan K.K., Tokyo, Japan) using a 6 cm 23-G needle (Terumo Cattelan Needle; Terumo Corp., Tokyo, Japan). Subsequently, the needle was advanced to the target nodule and a mixture of indigo carmine (Indigo Carmine; Daiichi Sankyo Co. Ltd., Tokyo, Japan) and lipiodol (Lipiodol; Fuji Pharma Co. Ltd., Tokyo, Japan) was injected into the lung parenchyma while withdrawing the needle until lipiodol accumulation reached the pleural surface on CT fluoroscopy images. A real-time 3 slices CT image was displayed by treading on the foot panel of the operator. The fluoroscopic images were obtained with a tube voltage of 120 kV and a tube current of 10 mA, and the duration of fluoroscopy was recorded. The procedures were performed by an interventional radiologist (T.H., with approximately 10 years of experience in interventional radiology). Measurements were performed with four settings of radioprotective equipment using a 0.5-mm lead shield (KYOWAGLAS XA; KURARAY Trading Co., Tokyo, Japan) and a 0.25-mm lead drape (Smart light; HOSHINA Co., Tokyo, Japan): A) with shield and lead drape; B) with shield, without lead drape; C) without shield, with lead drape; and D) without shield or lead drape. No significant differences on body weight and body mass index of patients ($p=0.58$) and tumor size ($p=0.90$) were detected by the one-way analysis of variance (ANOVA) between settings.

Fig. 1 A radioprotective shield (asterisk) was set in front of the scan plane at settings A and B, and a lead drape (arrow) was placed on the patient outside the computed tomography gantry at settings A and C.

Table 1 Detail and result of the procedure of each radiation dose measurement setting

Case	Age	Sex	Body weight (kg)	BMI	Tumor location	Tumor size (mm)	Body position	Duration of CT fluoroscopy (sec)	Radiation dose outside the glasses (μGy)	Radiation dose inside the glasses (μGy)
Setting A										
1	76	M	56.3	21.1	Right lower	8	Prone	54.4	25.6	11.9
2	75	M	62.7	22.9	Right upper	5	Prone	57.0	27.3	11.9
3	73	F	57.4	24.5	Right upper	8	Prone	55.7	32.4	17.9
4	71	F	52.5	22.5	Right lower	6	Left decubitus	50.8	18.8	6.0
Setting B										
1	69	M	51.8	20.2	Right upper	3	Left decubitus	58.4	43.5	25.6
2	64	M	63.7	21.5	Right upper	18	Prone	42.5	40.1	19.6
3	30	F	72.6	29.2	Left lower	6	Right decubitus	50.3	48.6	22.2
4	65	F	69.8	25.4	Right lower	7	Prone	61.4	40.1	16.2
Setting C										
1	48	F	59.8	19.8	Right lower	3	Prone	47.9	70.8	33.3
2	65	F	49.3	22.8	Right upper	13	Left decubitus	41.9	63.1	28.1
3	61	F	55.6	23.2	Left upper	4	Supine	44.3	69.1	34.1
4	71	F	42.8	19.4	Right upper	10	Prone	48.0	62.8	28.3
Setting D										
1	65	M	62.4	22.1	Left upper	9	Prone	44.3	78.4	30.7
2	71	F	42.8	19.4	Right upper	8	Prone	47.9	80.1	36.7
3	68	F	61.0	26.3	Right lower	11	Left decubitus	42.3	69.1	30.7
4	66	F	54.6	21.5	Right lower	7	Prone	48.6	88.7	38.9

BMI: body mass index

The radioprotective shield was set in front of the scan plane, and a lead drape was placed on the patient outside the CT gantry. Each setting comprised four sessions of localization procedure.

The radiation dose was measured using small optically stimulated luminescence dosimeters (OSLDs) (NanoDot; Nagase Landauer, Tsukuba, Japan). These small OSLDs were taped outside and inside the left surface of the radioprotective glasses, with the plane of the dosimeters facing the CT scan plane (Panoramashield; TORAY Industries, Tokyo, Japan). Taped OSLDs were removed from the radioprotective glasses and the data were read using a microSTAR reader (Nagase Landauer) immediately after each session.

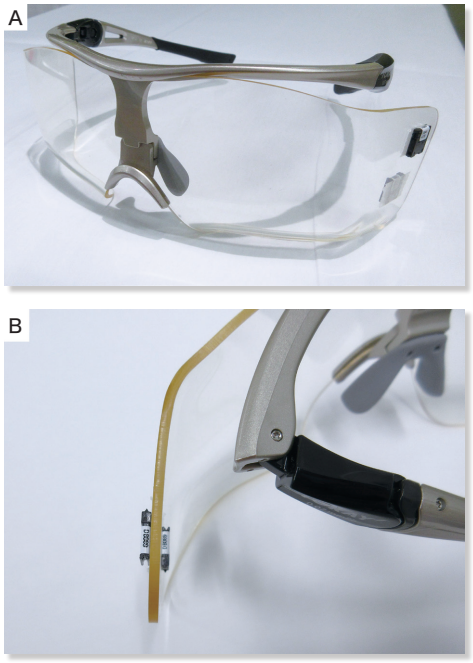

Fig. 2 A) Locations of small optically stimulated luminescence dosimeters (OSLDs) on the radioprotective glasses.
B) Small OSLDs were taped outside and inside the left surface of the radioprotective glasses.

Assessment

The duration of fluoroscopy and the radiation dose of CT fluoroscopy outside and inside

the radioprotective glasses were measured. Data are expressed as mean ± standard deviation. To evaluate the influence of the usage of radioprotective shield on the fluoroscopy duration, the duration was compared between settings with and without a shield using Welch's t-test. The radiation doses per procedure among the four radioprotective equipment settings were evaluated using the one-way ANOVA, and the difference between each setting was compared using Tukey's multiple comparison test. Statistical significance was set at $p<0.05$. Statistical analyses were performed using a commercially available software (SPSS for Windows, version 24; IBM, Armonk, NY, USA).

RESULTS

Duration of fluoroscopy

Durations of fluoroscopy were 54.5 ± 2.3 s, 53.1 ± 7.4 s, 45.5 ± 2.6 s, and 45.8 ± 2.6 s for settings A, B, C, and D, respectively. Mean duration of fluoroscopy was significantly longer in settings with shield (53.8 ± 5.5 s at settings A and B) than in those without shield (45.6 ± 2.6 s at settings C and D) ($p=0.005$).

Radiation dose

Radiation doses were 26.0 ± 4.9 μGy, 43.1 ± 3.5 μGy, 66.4 ± 3.5 μGy, and 79.1 ± 7.0 μGy, outside the radioprotective glasses, for settings A, B, C, and D, respectively, and 11.9 ± 4.2 μGy, 20.9 ± 3.4 μGy, 30.9 ± 2.7 μGy, and 34.2 ± 3.6 μGy, inside the radioprotective glasses, for settings A, B, C, and D, respectively. Significant differences were detected among the four settings for the radiation dose both outside ($p<0.001$) and inside ($p<0.001$) the radioprotective glasses by one-way ANOVA. In the following Tukey's multiple comparison test, significant differences were seen between all settings at outside the glasses (A vs B: $p=0.005$, A vs C: $p<0.001$, A vs D: $p<0.001$, B vs C: $p<0.001$, B vs D: $p<0.001$, C vs D: $p=0.04$) and all settings except between Settings C and D at inside (A vs B: $p=0.04$, A vs C: $p<0.001$, A vs D: $p<0.001$, B vs C: $p=0.02$, B vs D: $p=0.003$, C vs D: $p=0.68$).

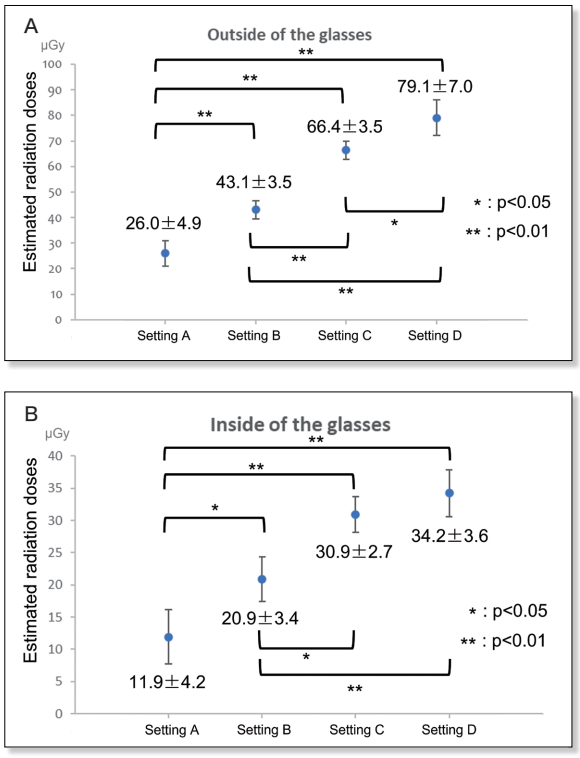

Fig. 3 A) Estimated radiation doses outside the radioprotective glasses. Radiation doses were: A) 26.0 ± 4.9 μGy; B) 43.1 ± 3.5 μGy; C) 66.4 ± 3.5 μGy; and D) 79.1 ± 7.0 μGy. The one-way analysis of variance revealed significant differences among settings ($P<0.001$).
B) Estimated radiation dose inside the radioprotective glasses. Radiation doses were: A) 11.9 ± 4.2 μGy; B) 20.9 ± 3.4 μGy; C) 30.9 ± 2.7 μGy; and D) 34.2 ± 3.6 μGy. The one-way analysis of variance revealed significant differences among settings ($P<0.001$).

DISCUSSION

This study showed that radioprotective equipment comprising a shield and a lead drape was effective in reducing radiation exposure to the eye lens of the operator during clinical CT fluoroscopy-guided procedures. These results support the concept that radioprotective equipment should be used during CT fluoroscopy-guided procedures, as suggested in previously reported experimental

studies[13-17].

It has been reported that the occupational radiation dose could be reduced by 71–97% with a radioprotective shield or lead drape[14-17] in a phantom study. However, radiation dose was reduced up to 67% (1-26.0 μGy/79.1 μGy) in this study, even though both shield and lead drape were used. This suggests that the theoretical maximum dose reduction could not be achieved in a clinical setting. The reason for this is unclear; however, the measurement point might be one explanation. The measurement points close to the scan plane are associated with more scattered radiation[16]. If the measurement point of the phantom study is closer to the scan plane than the eye position in clinical settings, the reduction in radiation dose by radioprotective equipment might be overestimated. The reduced sensitivity of OSLDs to the higher X-ray energy may be another explanation[18]. Nonetheless, we must pay attention to reducing the occupational dose as much as possible by using radioprotective equipment during CT fluoroscopy-guided procedures.

The fluoroscopy duration was significantly longer when a radioprotective shield was used. The movement of the operator's arm was interfered with by the shield set in front of the scan plane, which might have prolonged the fluoroscopy time. Despite the longer fluoroscopy time, the radiation dose was reduced using a shield. However, shortening the duration of fluoroscopy is important to reduce occupational exposure doses to medical staff and exposure to patients[19, 20]. The use of curtain-type radioprotective equipment might also be effective as a less obstructive option[17]; however, comparisons of whether and how such equipment might shorten the duration of fluoroscopy and reduce radiation doses have yet to be performed. Further investigations are required to determine which type of equipment is better.

This study has several limitations. First, radiation doses measured using small OSLDs were environmental radiation doses; therefore, the results did not entirely match the dose to the eye lens. However, the OSLDs were placed near the eye, and the results were thought to represent doses close to the actual dose to the eye lens. Second, the sample size was small. Third, tumor location was not matched between the groups. This may affect fluoroscopy duration and the distances between the scan plane and the operator. Further investigation to evaluate the relation of them may help to validate the result of this study.

Conclusion

We measured the radiation doses to the operator's eye lens during CT fluoroscopy guided procedures and showed that radioprotective equipment of glasses, shield, and lead drape reduces the radiation doses to the operator's eye lens during CT fluoroscopy-guided procedures. In particular, using both a shield and lead drape might be effective in maximizing the full benefit of all equipment.

Statement and Declarations

This work was supported by the Aichi Cancer Research Foundation.

The authors declare that they have no conflict of interest.

References

1) International Commission on Radiological Protection (ICRP): ICRP Statement on Tissue Reactions/Early and Late Effects of Radiation in Normal Tissues and Organs—Threshold Doses for Tissue Reactions in a Radiation Protection Context. ICRP Publication 118, 2012. Available online: https://journals.sagepub.com/doi/pdf/10.1177/ANIB_41_1-2 (accessed on 30 April 2022).
2) International Atomic Energy Agency (IAEA): Radiation Protection and Safety of Radiation Sources: International Basic Safety Standards; General Safety Requirements Part 3. Available online: https://www-pub.iaea.org/MTCD/Publications/PDF/Pub1578_web-57265295.pdf (accessed on 30 April 2022).
3) Silverman SG, Tuncali K, Adams DF, Nawfel RD, Zou KH, Judy PF: CT fluoroscopy-guided abdominal interventions: Techniques, results, and radiation exposure. Radiology, 212, 673-681, 1999.
4) Fu YF, Li GC, Cao W, Wang T, Shi YB: Computed Tomography Fluoroscopy-Guided Versus Conventional Computed Tomography-Guided Lung Biopsy: A Systematic Review and Meta-analysis. J Comput Assist Tomogr, 44(4): 571-577, 2020.
5) Shibamoto K, Mimura H, Fukuhara Y, Nishino K, Kawamoto H, Kato K: Feasibility, safety, and efficacy of artificial carbon dioxide pneumothorax for computed tomography fluoroscopy-guided percutaneous radiofrequency ablation of hepatocellular carcinoma. Jpn J Radiol, 39(11): 1119-1126, 2021.
6) Hasegawa T, Kuroda H, Sato Y, et al.: The Utility of Indigo Carmine and Lipiodol Mixture for Preoperative Pulmonary Nodule Localization before Video-Assisted Thoracic Surgery. J Vasc Interv Radiol, 30(3): 446-452, 2019.
7) Tomita K, Iguchi T, Hiraki T, et al.: Computed Tomography Fluoroscopy-guided Core Needle Biopsy of Abdominal Para-aortic Lesions: A Retrospective Evaluation of the Diagnostic Yield and Safety. Interventional Radiology, 5(3): 128-133, 2020.
8) Iguchi T, Matsui Y, Tomita K, et al.: Computed Tomography-guided Core Needle Biopsy for Renal Tumors: A Review. Interventional Radiology, 2021. doi: 10.22575/interventionalradiology.2020-0019.
9) Kim GR, Hur J, Lee SM, et al.: CT fluoroscopy-guided lung biopsy versus conventional CT-guided lung biopsy: a prospective controlled study to assess radiation doses and diagnostic performance. Eur Radiol, 21(2): 232-239, 2011.
10) Knott EA, Rose SD, Wagner MG, et al.: CT Fluoroscopy for Image-Guided Procedures: Physician Radiation Dose During Full-Rotation and Partial-Angle CT Scanning. J Vasc Interv Radiol, 32(3): 439-446, 2021.
11) Inaba Y, Hitachi S, Watanuki M, Chida K: Occupational radiation dose to eye lenses in CT-guided interventions using MDCT-fluoroscopy. Diagnostics 11(4): 646, 2021.
12) Kaartinen S, Husso M, Matikka H: Operator's eye lens dose in computed tomography-guided interventions. Eur Radiol, 31(6): 4377-4385, 2021.
13) Mahnken AH, Sedlmair M, Ritter C, Banckwitz R, Flohr T: Efficacy of lower-body shielding in computed tomography fluoroscopy-guided interventions. Cardiovasc Intervent Radiol, 35(6): 1475-1479, 2012.
14) Haipt F, Kirsch M, Hosten N: Evaluation of a leaden radiation protection barrier for dose reduction for the physician during CT fluoroscopy-guided interventions. Rofo, 182(6): 512-517, 2010.
15) Stoeckelhuber BM, Leibecke T, Schulz E, et al.: Radiation dose to the radiologist's hand during continuous CT fluoroscopy-guided interventions. Cardiovasc Intervent Radiol, 28(5): 589-594, 2005.
16) Nawfel RD, Judy PF, Silverman SG, Hooton S, Tuncali K, Adams DF: Patient and personnel exposure during CT fluoroscopy-guided interventional procedures. Radiology, 216(1): 180-184, 2000.
17) Neeman Z, Dromi SA, Sarin S, Wood BJ: CT fluoroscopy shielding: decreases in scattered radiation for the patient and operator. J Vasc Interv Radiol, 17(12): 1999-2004, 2006.
18) Al-Senan RM, Hatab MR: Characteristics of an OSLD in the diagnostic energy range. Med Phys, 38(7): 4396-4405, 2011.
19) Li J, Udayasankar UK, Carew J, Small WC: CT-guided liver biopsy: correlation of procedure time and radiation dose with patient size, weight, and lesion volume and depth. Clin Imaging, 34(4): 263-268, 2010.
20) Pradella M, Trumm C, Stieltjes B, Boll DT, Zech CJ, Huegli RW: Impact factors for safety, success, duration and radiation exposure in CT-guided interventions. Br J Radiol, 92(1099): 20180937, 2019.

Received May 17, 2023; accepted September 4, 2023

Exploring the Significance of Subject Color Absorption and Indoor Lighting Interference in Three-Dimensional Surface Scanner Applications

SUZUKI Hidekazu, MSc.[1)], SAITO Masahide, Ph.D.[2)], UEDA Koji, RTT.[3)], KOIDE Tomoki, RTT.[3)], SANO Naoki, Ph.D.[4)], AIKAWA Yoshihito, Ph.D.[4)], ONISHI Hiroshi, Ph.D.[5)]

1) Department of Radiology, University of Yamanashi Hospital
2) Medical Physicist, Department of Radiology, University of Yamanashi
3) Department of Radiology, University of Yamanashi Hospital
4) Department of Radiology, University of Yamanashi Hospital
5) Doctor, Department of Radiology, University of Yamanashi

Note: This paper is secondary publication, the first paper was published in the JART, vol. 70 no. 855: 25-31, 2023.

Key words: SGRT, Radiation Therapy, 3D surface scanner, Ambient light factor

【Abstract】
There is a three-dimensional surface scanner that utilizes the reflection of red laser light as a device for surface-guided radiation therapy. However, depending on the color of the object, sufficient reflected light might not be obtained, and accurate surface recognition could be hindered by the contamination of ambient light similar to the reflected light, originating from indoor illumination. Therefore, this system aimed to elucidate how the recognition capability is affected by the color of the target object and the ambient light.

Various hues, grayscale variations, and skin colors were employed to investigate whether recognition could be achieved by altering the color temperature and illuminance of the surrounding light. It was found that recognition was not possible for colors that absorb red laser light, such as blue, green, black, and darker colors with insufficient reflection. Furthermore, while the impact of ambient illuminance was substantial, the influence of color temperature was minimal.

1. INTRODUCTION

In radiotherapy, precise irradiation position matching holds paramount importance, serving as a fundamental technique for achieving high-precision radiotherapy outcomes [1)]. Currently, Image-guided radiation therapy (IGRT) encompasses various methods, including the 2D-2D matching technique employing electronic portal imaging devices (EPID) and linac graphs (LG), the 3D matching approach utilizing cone beam computed tomography (CBCT) with kV X-rays for three-dimensional positioning. There is also a technique for the prostate and similar areas that uses an ultrasound probe transrectally for localization [2)]. However, these methodologies entail invasive procedures involving patient exposure to radiation.

Nevertheless, a recent advancement known as surface guided radiation therapy (SGRT) has emerged, enabling the acquisition of three-dimensional positional data of an object's surface by externally irradiating light and analyzing the resulting information. Within SGRT, body surface recognition primarily relies on three-dimensional scanner technology, employing methods such as patterned light projection, where a fixed shape pattern like a triangle is projected onto the object, capturing and analyzing its deformation via an optical camera to ascertain three-dimensional shape and measure alterations. Notably, there are two primary types: patterned light projection [3)] and triangulation [4)], each with distinct operational principles. While the laser-based method can depict three-dimensional images over time by continuously irradiating a monochromatic laser beam across a wide area and analyzing the re-

flected light, it is susceptible to environmental factors within the treatment room and the hue of the object being scanned. Specifically, ambient room illumination and the object's color may influence the collected data. Therefore, the aim of this study is to elucidate the impact of treatment room conditions and object hue on the body surface position data acquired by a non-contact laser-based 3D body surface scanner (VOXELAN® HEV-600M/RMS, Electronics Research & Development Corporation, Okayama, Japan; hereinafter referred to as VOXELAN).

2. METHOD

2-1 Equipment used:

The VOXELAN employed in this study is suspended from the ceiling and equipped with two laser beams and a camera to capture reflected light. A red laser beam is emitted near the isocenter (Fig. 1), with a distance of 1.6 meters to the isocenter and an elevation angle of 45 degrees. Continuously irradiating the red laser, the system collects data to depict profiles of three-dimensional changes over time.

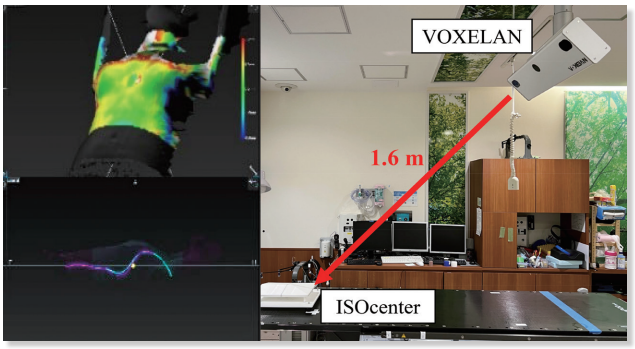

Fig. 1 Overview of VOXELAN.

VOXELAN can grasp the three-dimensional shape by irradiating the object with a red laser (two places on the left and right) from the ceiling suspended main body and continuously shooting the reflected light with the camera (center part) of the main unit. The position displacement amount with the reference data can be displayed in a color map (upper left figure) or in a profile (lower left figure).

2-2 Recognition ability of an object (subject or patient) in different hues and lightness

We created the color sample sheets shown below using a color printer (ColorMultiWriter 9100C: NEC, Japan), and evaluated their discriminative ability. To examine the influence of hue, we selected 24 colors based on the RGB color code (Fig. 2), and to investigate the effect of brightness, we classified 51 shades from white (#FFFFFF) to black (#000000), from which 25 shades were extracted (Fig. 3). Additionally, to consider the impact of skin color, we created 11 colors ranging from No. 25 to

Number	C1	C2	C3	C4	C5	C6	C7	C8
Color								
RGB code	#F20C0C	#F2460C	#F27F0C	#F2B80C	#F2F20C	#B8F20C	#7FF20C	#46F20C
Number	C9	C10	C11	C12	C13	C14	C15	C16
Color								
RGB code	#0CF20C	#0CF246	#0CF27F	#0CF2B8	#0CF2F2	#0CB8F2	#0C7FF2	#0C46F2
Number	C17	C18	C19	C20	C21	C22	C23	C24
Color								
RGB code	#0C0CF2	#460CF2	#7F0CF2	#B80CF2	#F20CF2	#F20CB8	#F20C7F	#F20C46

Fig. 2 24-Color RGB Color Code for hue evaluation.

Number	(G0)	G40	G45	G50	G55	G60	G65	G70	G75
Color									
RGB code	(#000000)	#282828	#2D2D2D	#323232	#373737	#3C3C3C	#414141	#464646	#4B4B4B
Number	G80	G85	G90	G95	G100	G105	G110	G115	G120
Color									
RGB code	#505050	#555555	#5A5A5A	#5F5F5F	#646464	#696969	#6E6E6E	#737373	#787878
Number	G125	G130	G135	G140	G145	G150	G155	G160	(G255)
Color									
RGB code	#7D7D7D	#828282	#878787	#8C8C8C	#919191	#969696	#9B9B9B	#A0A0A0	(#FFFFFF)

Fig. 3 25 Grayscale Codes for color brightness evaluation (including white and black additions).

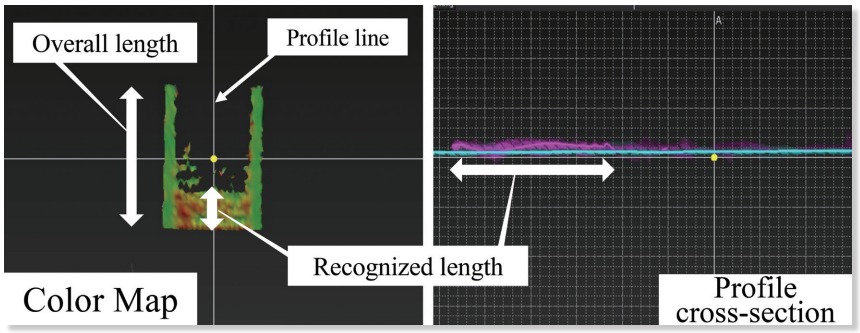

Fig. 4 How to find the recognition rate.
The recognition rate was measured using the VOXELAN profile function. The blue line in the right figure indicates the reference position, while the red line indicates the position of the recognized object.

No. 35, which are the darkest on the skin chart based on Von Luschan's chromatic scale [5].

VOXELAN measures the distance to the object by emitting a laser beam from the main unit mounted on the ceiling at an elevation angle of 45 degrees, and recognizes the three-dimensional object using the triangulation method. Therefore, even if an object on a horizontal bed reflects the laser beam uniformly, if the object is large or located far away from the isocenter, the distance from the object to the detector will increase, and the amount of light reflected and delivered to the detector will change slightly, resulting in a change in recognition performance. Using this phenomenon, the total length of the colored paper as the object was measured from the profile display, which is a function of the 3D body surface scanner used in this study, and the recognition rate was calculated using Equation (1) (Fig. 4).

Recognition rate (%) = Recognized length (cm) / Total length of object (cm) ×100(%), ····· (1)

2-3 Difference in recognition ability due to difference in ambient light illuminance:

VOXELAN measures distances based on reflected red laser light emitted by objects, capturing their three-dimensional shapes over time. In radiotherapy rooms, patient positioning often utilizes in-room lasers, and dimmed lighting is common to mitigate patient discomfort. Hence, ambient brightness might affect VOXELAN's recognition ability. Ambient brightness was measured using an illuminance meter (LightSpectrum Pro Ver. 4.3.0, iPhone 14.3: AM Power Software, Italy), and illuminance varied for each color temperature at the isocenter surface as shown in Table 1. Recognition rates were calculated using Equation (1) for the 25 grayscale shades used in Method 2-2.

Table 1 Combination table for investigating the impact of differences in illuminance on recognition accuracy.

Color temperature	Illuminance 1	Illuminance 2	Illuminance 3	Illuminance 4
2800 K		728 lx	1478 lx	4158 lx
3600 K	34 lx	931 lx	1290 lx	4317 lx
5600 K		695 lx	1787 lx	4639 lx

Table 2 Combination table for investigating the impact of differences in color temperature on recognition accuracy.

Illuminance	Color temperature 1	Color temperature 2	Color temperature 3
700 lx	2876 K	3356 K	5643 K
1700 lx	2752 K	3481 K	5559 K
4200 lx	2745 K	3639 K	5730 K

2-4 Difference in Recognition Ability due to Difference in Ambient Light Color Temperature:

As VOXELAN captures reflected light from a red laser,

we examined the impact of incident red light other than that emitted by the red laser from the main unit by varying the color temperature of ambient light. Ambient light's color temperature was adjusted using a smart LED bulb (SwitchBot, Shenzhen, China), with variation for each illuminance at the isocenter plane as shown in Table 2. Recognition rates were determined from Equation (1), and the color temperature component at the isocenter surface was measured using a spectroradiometer (LightSpectrum Pro Ver. 4.3.0, iPhone 14.3: AM Power Software).

3. RESULT

3-1 Effects of differences in hue and lightness of the object (subject or patient):

Regarding hue variances, red (C1), yellow (C5), and peach (C21) demonstrated a 100% recognition rate. However, green (C8) and purple (C18) exhibited an 80% recognition rate, while dark green (C9), light blue (C13), and blue (C16) were not recognized (Fig. 5).

Grayscale lightness exhibited a 100% recognition ability for white, with sufficiently high lightness, while black, with low lightness, remained unrecognized. The recognition bound-

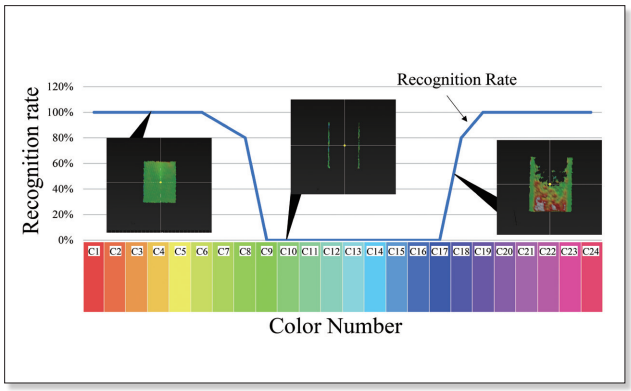

Fig. 5 Differences in recognition due to differences in hue.
It could not be recognized by the hues of C9 to C17.

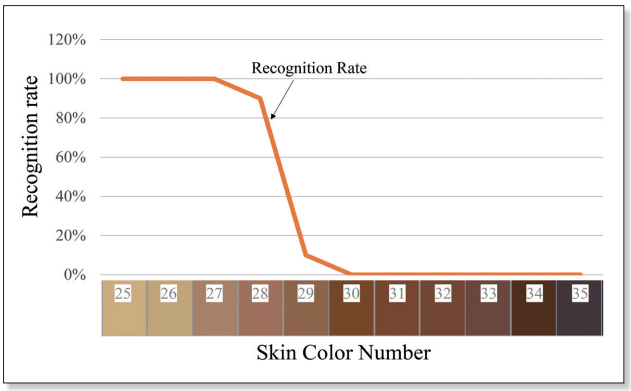

Fig. 6 Differences in recognition due to differences in skin color.
Colors darker than skin color number 29 are not recognized.

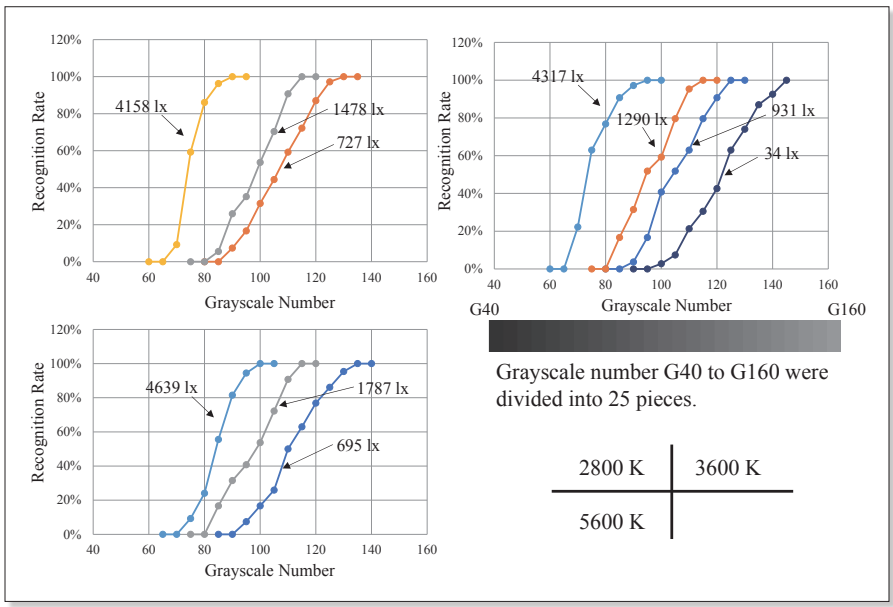

Fig. 7 The effect of differences in illuminance due to variations in the color temperature of ambient light on recognition rates.

ary ranged from G120 to G60 on the grayscale spectrum in Figure 3. Concerning skin color, Von Luschan's chromatic scale No. 28 served as the threshold, with darker skin tones remaining unrecognized. No. 28 on Von Luschan's chromatic scale corresponds to Type V on the Fitzpatrick Skin Type (Fig. 6).

3-2 Effect of ambient light illuminance:

Under ambient light with a color temperature of 3600 K and an illuminance of 34 lx, the recognition rate decreased from No. G140 and became unable to recognize at No. G95. As ambient light illuminance increased, image brightness decreased, reaching the recognition limit at No. G65 with an illuminance of 4317 lx. Moreover, image brightness decreased with ambient light illuminance at 2800 K and 5600 K (Fig. 7).

3-3 Effect of ambient light color temperature:

Maintaining constant ambient illuminance while changing the color temperature did not alter the recognition rate, with threshold values remaining nearly consistent (Fig. 8). However, lower color temperatures (2700 K) resulted in the object's edge displaying a higher position than the reference, indicating increased light entering the detector at that location (Fig. 9).

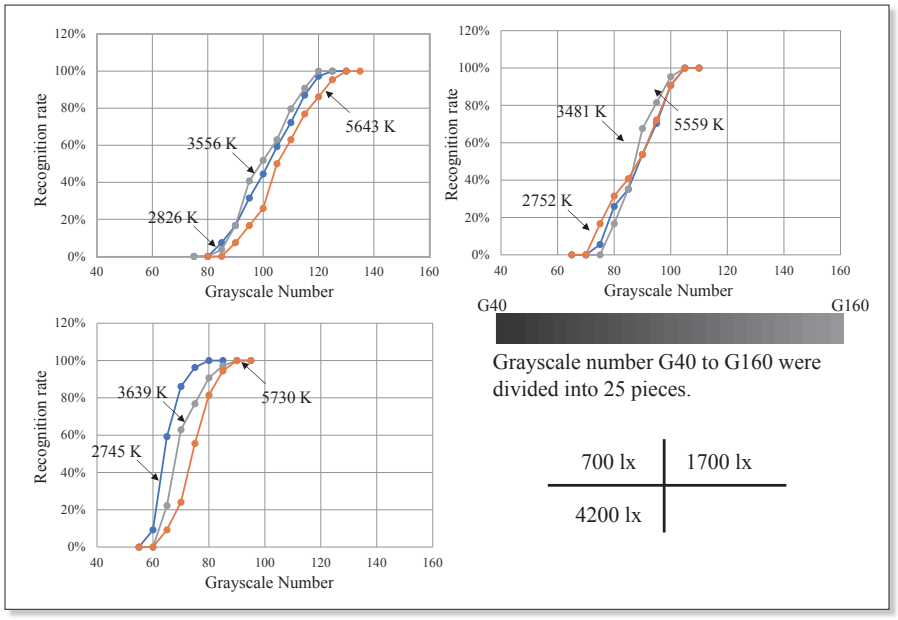

Fig. 8 The effect of color temperature differences due to variations in ambient light irradiance on recognition rates.

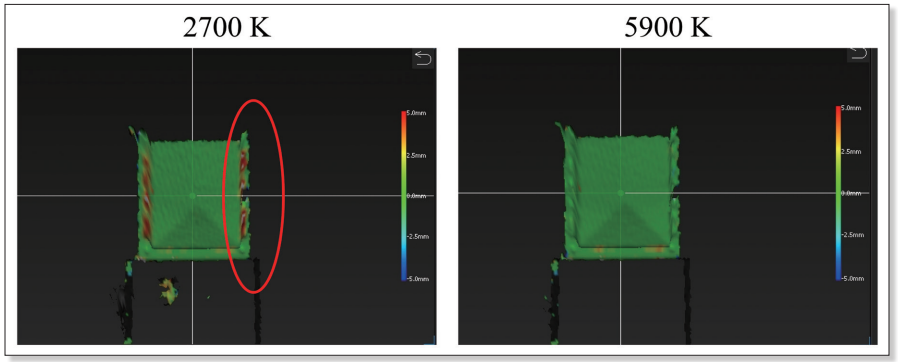

Fig. 9 An example of how the color temperature of ambient light affected recognition.
Differences in ambient light color temperature caused image distortion at the edges of the reference object. The red areas on the image indicate higher values compared to the reference position.

4. DISCUSSION

4-1 Effects of hue and lightness:

VOXELAN identifies objects by emitting a red laser from the main unit installed on the ceiling and capturing laser reflections with a camera. Consequently, objects not reflecting the red laser cannot be recognized. When the reflected light's color component reaches the eyes, it's perceived as the object's color. Objects absorbing red light, such as green, blue, and indigo, remain unrecognized.

Regarding color lightness, a scale from white to black was utilized in this study. White reflects all colors of light, while black absorbs all colors, making white recognizable but black not. Colors between white and black absorb red light to varying degrees, leading to a recognition threshold at a certain lightness, as shown in Result 3-1. As the object-detector distance increases, reflected light decreases, potentially lowering the recognition threshold. Skin color lacks a quantifiable threshold due to hue and lightness variations. Nevertheless, using Von Luschan's chromatic scale and the Fitzpatrick Skin Type, a threshold allowing 80% recognition based on these patterns was established.

SGRT has demonstrated efficacy in irradiating breast cancer [4]. however, concerns have been raised regarding diminished recognition capability due to skin discoloration during irradiation. Yet, understanding the skin color recognition threshold elucidated in this study enables the assessment of SGRT continuity in scenarios involving temporal skin discoloration, such as whole breast irradiation. Through comparison of discoloration severity with color samples from Von Luschan's chromatic scale and the Fitzpatrick Skin Type, SGRT viability can be pre-assessed, even in an international medical context where patients exhibit diverse skin tones.

4-2 Effect of ambient light illuminance:

From Result 3-2, VOXELAN's red laser, emitting at 680 nm, matches the detector's measurement wavelength. Consequently, ambient light of the same wavelength reaching the detector as reflected laser light is also captured, influencing data collection. As ambient light increases, reflected light from the object and the recognition threshold decrease due to the presence of fluorescent lamps emitting light at 680 nm.

4-3 Effect of ambient light color temperature:

The study confirmed that ambient light, including the 680 nm red laser component, affects recognition ability when mixed from sources other than the emitting laser. Changes in room light color for patient psychological effects did not affect the red laser [6]. Fluorescent lamps commonly used in treatment rooms typically emit neutral light (5000 K). Results 3-3 indicated no recognition performance differences at various color temperatures. The examination of the wavelength components of light at the color temperatures used in this study revealed that at around 3000 K, which corresponds to warm white lighting, the yellow to red components are predominant, with few blue and green components (Fig. 10). Additionally, for neutral light color at 5000 K and daylight color at 6000 K, the blue, green, and red components are distributed almost evenly. From these results, it's inferred that contamination aside from the red laser component is unaffected by ambient light color temperature but depends on light intensity.

Moreover, observed ambient noise appears caused by excessive red component entering the detector, leading to misrecognition. Lower color temperatures contain relatively more red components, even at the same illumination level, potentially mixing the 680 nm wavelength into the detector. Implementing filters attenuating the 680 nm wavelength or reducing room illumination could mitigate misrecognition effects.

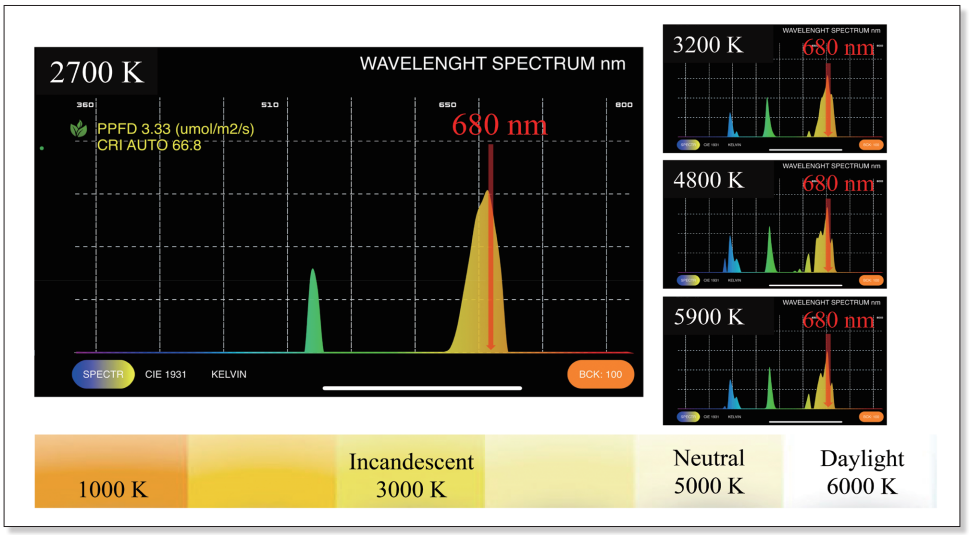

Fig. 10 Wavelength components of LED lighting.

The laser wavelength used by VOXELAN is 680 nm, so there is a high possibility of misrecognition in the surrounding light with a color temperature of 2700 K, where components of that wavelength are relatively prominent.

5. CONCLUSION

The VOXELAN HEV-600M 3D body surface scanner utilized in this study demonstrated compatibility with the lighting conditions typical of daily clinical practice. Nonetheless, given its reliance on red light, consideration of both the object's color and ambient lighting hue is imperative. Additionally, the determination of Von Luschan's chromatic scale No. 28 as the skin color recognition threshold for VOXELAN signifies a critical criterion for its future application.

6. CONFLICT OF INTEREST

The VOXELAN used in this study was borrowed from Hamano Engineering Co., Ltd. as part of a commissioned research project.

ACKNOWLEDGMENTS

This study is the result of research funded by the Japan Association of Radiological Technologists' academic research grant. Additionally, I presented part of the abstract of this study at the 38th Annual Meeting of the Japan Association of Radiological Technologists held on September 17, 2022.

References

1) Dawson LA, et al.: Advances in Image-Guided Radiation Therapy. J. Clin. Oncol. 25(8), 938-946, 2007.
2) Lachaine M, et al.: Intrafractional prostate motion management with the Clarity Autoscan system. Med. Phys. Int. 1(1), 72-80. 2013.
3) Bert C, et al.: A phantom evaluation of a stereo-vision surface imaging system for radiotherapy patient setup. Med. Phys. 32(9), 2753-2762, 2005.
4) Freislederer P, et al.: Recent advances in Surface Guided Radiation Therapy. Radiat. Oncol. 15(1), 187, 2020.
5) Gupta V, et al.: Skin typing: Fitzpatrick grading and others. Clin. Dermatol. 37(5), 430-436, 2019.
6) Dalke H, et al.: Colour and lighting in hospital design. Opt. Laser Technol. 38(4-6), 343-365, 2006.

Received July 21, 2021; accepted November 17, 2022

Consideration of the optimum dose rate in intensity-modulated radiation therapy for patients with prostate cancer

SAITO Hitoshi, Ph.D., MIURA Shuta, SASAKI Hiroshi, SUZUKI Keiko

Department of Radiology, Akita Kousei Medical Center

Note: This paper is secondary publication, the first paper was published in the JART, vol. 70 no. 848: 28-38, 2023.

Key words: MLC, Gamma pass rate, IMRT, Dose rate, Radiochromic film

【Abstract】

This study aimed to determine the optimum dose rate (DR) of intensity-modulated radiation therapy (IMRT) for patients with prostate cancer in relation to the multileaf collimator (MLC) position errors based on the DR and gamma pass rate (GPR). A gamma evaluation was performed using a 3% dose difference and 2 mm distance-to-agreement criteria with a dose threshold of 10%. The MLC position error was measured using DynaLog files. The GPR was measured using MapCHECK2 and EBT3. The delivery time decreased from 97 sec to 83 sec when the DR increased from 500 to 600 monitor units per minute (MU/min). However, the difference between DR 500 and 600 MU/min was not significant ($p > 0.05$). The MLC position errors increased with increasing DR but no significant difference was observed in the maximum root mean square errors between the DRs of 300 and 400 MU/min, 400 and 500 MU/min, and 500 and 600 MU/min ($p > 0.05$). The mean percentage GPRs of 97.6%, 96.2%, 97.0%, and 95.7% were observed for the DRs of 300, 400, 500, and 600 MU/min, respectively, in EBT3. However, no significant difference was observed in the GPRs of DRs 300, 400, 500, and 600 MU/min ($p > 0.05$). The GPR of a DR 600 MU/min using EBT3 were at the very limit of 95% criteria. Therefore, we suggested that a DR of 500 MU/min was the most acceptable rate considering clinical safety.

Introduction

The intensity-modulated radiation therapy (IMRT) technique uses a multileaf collimator (MLC) to modify the beam fluence in the same treatment field in order to improve the conformity of the prescribed dose distribution around the tumor region[1-5]. This modulation using MLC can be achieved using the sliding window (dynamic MLC [DMLC]) technique. DMLC is a treatment technique in which both the dose rate (DR) and leaf velocity (LV) are continually adjusted by MLC shapes when the beam is on. An increase in the DR greatly reduced the delivery time[6, 7], thus decreasing the burden on the patient; in particular, a longer delivery time causes result in patient repositioning or movement during a therapeutic session. However, increasing DR cause the faster LV, and a DR of 300 monitor units per minute (MU/min) or 400 MU/min is routinely applied in DMLC-IMRT because higher LV affects the MLC position accuracy[8-10]. Vorwerk et al.[9] recommended that the DR for sliding window IMRT should be 300 MU/min or 400 MU/min for patients with prostate cancer according to the dose volume histograms of the organs at risk. Kaviarasu et al.[10] examined the effect of DR on treatment accuracy using portal dosimetry gamma evaluation (GE) and created a workflow for pretreatment IMRT quality assurance (QA) using portal dosimetry with a default DR of 400 MU/min for the approved treatment plan. Thus, a higher DR of 500 or 600 MU/min was not applicable.

On the contrary, Ghasroddashti et al.[6] conducted a survey of the relationship between DR and the number of MUs; however, they did not explicitly indicate which DR was

acceptable, and a higher DR will possibly allow sufficient time to increase the number of patients treated in a day. Furthermore, Slosarek et al.[7] suggested that the difference between DRs of 100 MU/min and 600 MU/min, measured using the radiation planning index, was minor, and a low DR of 100 MU/min did not have a significant impact on the differences in treatment accuracy even if larger MLC position errors occurred in DR 600 MU/min than that in DR 100 MU/min. These studies can potentially apply a higher DR of 500 or 600 MU/min.

Although these studies evaluated dose distribution using GE, few studies have evaluated proportion of MLC position errors in detail based on DR changes in the clinical radiation plan. Furthermore, the optimal DR has not been determined such as previous studies[6-10]. This study aimed to determine the optimal DR in DMLC-IMRT for patients with prostate cancer in terms of relationship with the MLC position errors according to the DR and the influence of DR on dose distribution.

Materials and Methods

Patient data

Data of 15 patients with prostate cancer treated using DMLC-IMRT in our institution between June 2019 and January 2020 were retrospectively obtained. Their median age was 71 years (range, 56–81 years). According to the Comprehensive Cancer Network Risk classification for Prostate cancer (ver. 4, 2018), four patients had low-grade prostate cancer and 11 had intermediate-grade prostate cancer[11]. All patients were treated for prostate cancer with a dose of 76 Gy (2 Gy per fraction) using a 7 field IMRT with 10 MV photon beams energy.

Computed tomography simulation and delineation

Computed tomography (CT) axial scans with a slice thickness of 2.5 mm were performed for all patients using a 16 slice CT scanner (Bright Speed Elite Pro Vision; GE Healthcare, USA). The CT images were then transferred to a treatment planning system (TPS; Varian Medical Systems, Palo Alto, CA, USA) for treatment planning. The target volumes were contoured by a physician. The clinical target volumes (CTVs) were the prostate, the proximal 1 cm of the seminal vesicle for intermediate-risk patients, and the prostate for low-risk patients. The planning target volumes (PTVs) consisted of the CTV with a posterior 5 mm margin and a 7 mm margin for other directions (superior, inferior, anterior, right lateral, and left lateral). The prescribed dose was planned to be 95% of the PTV.

Linear accelerator and treatment planning system

The treatment plans were calculated using a Clinac iX (Varian Medical Systems) linear accelerator equipped with a Millennium 120-leaf MLC (central: 20 cm of field, 5 mm leaf width; outer: 20 cm field, 10 mm leaf width) capable of IMRT delivery for different DRs (300, 400, 500, and 600 MU/min). All plans were created using Varian's Eclipse TPS incorporating the Anisotropic Analytical Algorithm version 13.6, and the associated

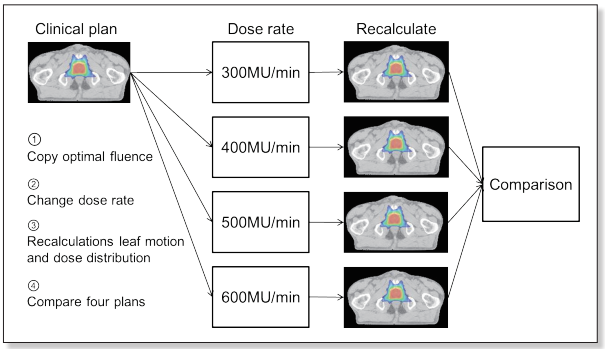

Fig. 1 Flow of copied clinical plans for four DRs: 300, 400, 500, and 600 MU/min.

First, the clinical plan was copied, and optimization process was not modified; second, the clinical plan was changed based on the four DRs: 300, 400, 500, and 600 MU/min; and third, the leaf motion calculator was rerun for each field, and the dose distribution was recalculated in four copied plans.

Table1 Dosevolumehistgramparametersofthecopiedfourplans.

Structure	Constrainttype	Doserate (MU/min)			
		300	400	500	600
PTV	Max (Gy)	80.33	80.34	80.34	80.35
	Mean (Gy)	77.84	77.84	77.83	77.81
	D99% (%)	97.46	97.49	97.52	97.53
Rectum	V76Gy (%)	2.39	2.43	2.47	2.49
	V70Gy (%)	8.43	8.45	8.47	8.49
	V65Gy (%)	11.06	11.08	11.10	11.12
	V60Gy (%)	13.36	13.39	13.40	13.42
	V50Gy (%)	17.99	18.03	18.05	18.08
	V40Gy (%)	24.05	24.10	24.14	24.19
Bladder	V75Gy (%)	8.80	8.80	8.76	8.76
	V65Gy (%)	16.41	16.42	16.41	16.41
	V40Gy (%)	34.89	34.91	34.92	34.96

Dataarepresentedasmeanvalues.
PTV,planningtargetvolume

leaf motion calculator version 13.6 (Varian Medical Systems). The linear accelerator was equipped with a maximum LV of 2.5 cm/sec. In addition, the number of segment settings for DMLC-IMRT was automatically calculated in the TPS. Clinical plans (DR 600 MU/min) were copied for four DRs: 300, 400, 500, and 600 MU/min. Figure 1 shows the flow of the four copied plans. The optimal fluence patterns determined during the initial optimization process were not modified, and the only DRs were changed for all plans. Table 1 lists the dose volume histogram parameters for four copied plans. These parameters were much the same values in spite of the different DRs.

MLC position error

The positional accuracy of the DMLC was evaluated from a DMLC log (DynaLog) file containing MLC details[12-14]. These log files contained DMLC delivery details recorded every 50 ms to analyze the inaccuracy in MLC motion for banks A and B. We analyzed the log files of all IMRT copied plans while changing only the DRs using the DoseLab v.6.8 FractionLab software (Mobius Medical Systems, TX, USA). We assessed the following factors: delivery time, number of MU, number of segments, and proportion of MLC position errors (0–0.05, 0.05–0.5, 0.5–1.0, and 1.0–1.5 mm). The MLC position errors represent the differences in the MLC positions between the planned and actual delivery positions. The analysis value of DynaLog files was expressed as the root mean square (RMS). The RMS errors are used to condense a set of errors into a single representative value[15]. The RMS errors are always greater than or equal to the mean of the absolute value of the errors. FractionLab software is used to calculate the RMS errors for individual leaves in files, ranges of gantry angles in files, and entire leaf banks in a collection of files. For a set of n errors (differences between the set and delivered positions), the RMS errors were calculated using the following formula:

$$\text{RMS error} = \sqrt{\frac{\Sigma(\text{Error})^2}{n}}$$

Gamma evaluation (two-dimensional diode array detector)

To evaluate the influence of DRs on the dose distribution, all IMRT copied plans were measured using MapCHECK2 (Sun Nuclear Corporation, Melbourne, FL, USA) to compare the dose distributions between the calculated and measured doses; a GE was performed using a 3% dose difference and 2 mm distance-to-agreement criteria with a dose threshold (TH) of 10% (3%/2 mm) to remove the noise, as recommended by the American Association of Physicists in Medicine Task Group (AAPM TG) 21[16, 17]. MapCHECK2 has a measuring area of 26 cm × 32 cm that consists of 1,527 solid-state SunPoint diode detectors with a resolution of 0.8 mm × 0.8 mm, diagonal detector spacing of 7.07 mm, and parallel

detector spacing of 10 mm. MapCHECK2 was set up under an 8 cm water-equivalent phantom (Solid Water HE; GAMMEX-RMI, Middleton, WI, USA) and placed in a plane with an isocenter. All treatment parameters in the copied plans were the same as those in the clinical plan, excluding the gantry and collimator angles set to 0° for all fields. Before the GE, MapCHECK2 was calibrated according to the manufacturer's guidelines. A GE was performed at an absolute dose. The calculated and measured dose distributions were compared using the SNC Patients™ v. 6.7.4 (Sun Nuclear Corporation). In addition, Woon et al.[18] reported that the criterion of 3%/1 mm was the most sensitive gamma criterion for MapCHECK2 to detect systematic MLC errors. Therefore, we conducted a GE using the criterion of 3%/1 mm in the additional investigation.

Gamma evaluation (Film)

The radiochromic film used in this study was a Gafchromic EBT3 (International Specialty Products, Wayne, NJ, USA) with sheet dimensions of 20.3 cm × 25.4 cm. The film was used according to the methods described in the AAPM TG-55 report[19]. To obtain the calibration curve, the EBT3 film was cut into smaller pieces measuring 6 cm × 6 cm in size, and 12 of the smaller films were selected. Each piece of film was placed under a 10 cm solid water phantom with a 10 cm space underneath to provide adequate backscatter, a field size of 10 cm × 10 cm, and a 90 cm source-to-surface distance. The films were then irradiated using the Clinac iX linear accelerator with a 10 MV photon beam energy in the range of 0 MU to 500 MU (0, 10, 25, 50, 100, 150, 200, 250, 300, 350, 400, and 500 MU). To evaluate the influence of DR on dose distributions, the EBT3 film was sandwiched between I' mRT phantoms (IBA Dosimetry, GmbH, Schwarzenbrunk, Germany) and placed in the sagittal plane at the center of the phantom

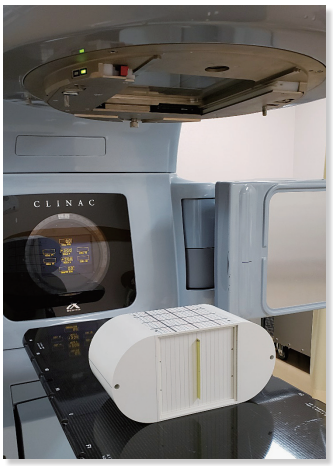

Fig. 2 Experimental set-up for film evaluation using I'mRT phantom.

To evaluate the influence of dose rate on the dose distribution, the EBT3 film was sandwiched between I'mRT phantoms and located in the sagittal plane at the center of the phantom. Because sagittal plane could draw the most rectum which was organ at risk, we verified the dose distribution using sagittal plane. We evaluated the dose distribution at the center of the PTV.

(Fig. 2). After irradiation, the films were kept in a box in order to protect them from fluorescent light for 24 h after irradiation exposure, and an unexposed film was scanned using a flatbed scanner (Epson Expression DS-G20000; Epson Tokyo, Japan) in 48-bit RGB mode (red, 16-bit color; green, 16-bit color; and blue, 16-bit color) with a resolution of 75 dots/inch. All treatment parameters in the copied plans were the same as those in the clinical plan, including the gantry and collimator angles. The calculated and measured dose distributions were compared using the DoseLab dose comparison software ver.6.8 (Mobius Medical Systems). A GE was performed with an absolute dose using criteria of 3%/2 mm, TH10%.

Dose rate dependence (preliminary experiment)

Actually delivered DRs of linear accelerator were measured using two-dimensional (2D) diode array detector (Profiler2 model1174; Sun Nuclear Corporation). The measurement were 20 cm × 20 cm open field size for 300 MU of 10 MV photon beams using DRs of 300, 400, 500, and 600 MU/min. In

addition, to verify the variations of radiation output with DR in Clinac iX, a cylindrical ion chamber (Farmer 30013; PTW GmbH, Freiburg, Germany) and an electrometer (RAMTEC Smart; TOYO Medic, Tokyo, Japan) were used. The measurements were made in water with a depth 10 cm and in an open filed size of 10 cm × 10 cm for 100 MU of 10 MV photon beams using the DRs of 300, 400, 500, and 600 MU/min. The measurement values for each DR were obtained from ten measurements. Furthermore, we confirmed the DR dependence of MapCHECK2 by measuring 100 MU in 10 cm × 10 cm open fields with 10 MV photon beams in the same setup (under an 8 cm solid water).

Statistical analysis

A comparison of Dynalog files for MLC position errors between the four copied plans was performed by repeated-measures ANOVA or the Friedman test and post hoc comparisons with Bonferroni/Dunn's test or Steel–Dwass test. Statistical significance was set at $P < 0.05$. All statistical analyses were performed using Excel 2015 software (Microsoft, Redmond, WA, USA) with the add-in software application Statcel4 (OMS Publishing Inc. Tokyo, Japan).

Results

In the preliminary experiment

Table 2 shows the results of actually delivered DRs. The actually delivered DR of 600 MU/min was slightly lower than that of nominal value. Delivery beams for other DRs (400, and 500 MU/min) measured by Profiler2 were the equivalent magnification values as nominal values normalized with a dose rate of 300 MU/min. Figure 3 shows the results of DR dependence for ion chamber and MapCHECK2 in the preliminary experiment. The output of the machine with a 10 MV photon beam energy measured by the ion chamber was quite constant for this range of DRs with a maximum variation of 0.04% for DR of 600 MU/min (normalized with a DR of 300 MU/min). The response of MapCHECK2 increased with increasing DR value, with a maximum variation of 0.4%, which is equivalent and comparable to the value of 0.21%–0.35% from previous studies[20, 21].

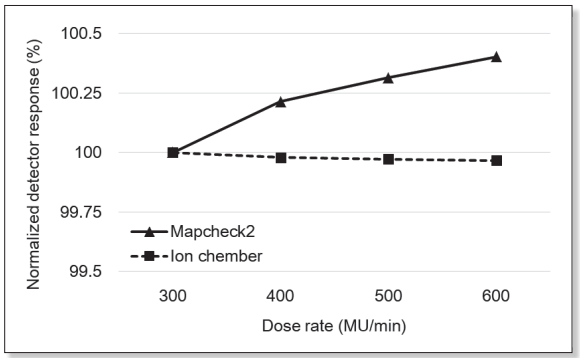

Fig. 3 Results of the dose rate (DR) dependence for ion chamber and MapCHECK2.

The output of the Clinac iX with 10 MV photon beams measured by the ion chamber was quite constant for this range of DRs with the maximum variation of 0.04% for the DR of 600 MU/min (normalized with the DR of 300 MU/min). The response of the MapCHECK2 increased with increasing DR value with a maximum variation of 0.4%.

MLC position error

Tables 3 and 4 show the differences in the DRs analyzed based on the MLC position errors in this study. Table 5 shows the results of the statistical analysis of MLC position errors. The delivery time decreased from 97 sec to 83 sec when the DR increased from 500 to 600 MU/min. However, the difference

Table 2 Results of actually delivered dose rates of linear accelerator

Dose rate (MU/min)	300	400 (×1.33)	500 (×1.67)	600 (×2.0)
Profiler2 (pulse/sec)	180	240 (×1.33)	300 (×1.67)	350 (×1.94)

The number in parentheses indicated the magnification values normalized with a dose rate of 300 MU/min.

between DR 500 and 600 MU/min was not significant ($p > 0.05$, Table 4). The MU values normalized with a DR of 300 MU/min were expressed as a percentage increase in increased DRs, and gains of 3.12% were achieved for 400 MU/min, 6.47% for 500 MU/min, and 9.80% for 600 MU/min; however, no significant difference was observed in the respective comparisons ($p > 0.05$, Table 4). No significant differences were also observed between the DRs of 300 and 400 MU/min, 400 and 500 MU/min, and 500 and 600 MU/min for the number of segments ($p > 0.05$, Table 3). Expressed in terms of percentage increased in MUs per 100 MU/min increase DR, we observed gains of approximately 3.3% which was approximately the same and comparable to the value of 4.1% from a previous study[6]. The number of MUs and segments increased with increasing DR but MU per segment was slightly lower with increasing DR (Table 3). Moreover, no significant difference was observed in the maximum RMS between the DRs of 400 and 500 MU/min, and 500 and 600 MU/min ($p > 0.05$, Table 4).

The proportion of MLC position errors in

Table 3 Results of MLC position errors based on the dose rates.

	300 MU/min	400 MU/min	500 MU/min	600 MU/min
Delivery time (sec)	151.85 ± 21.64	116.82 ± 15.89	97.22 ± 12.75	83.71 ± 10.66
Monitor unit (MU)	757.27 ± 108.49	780.87 ± 107.73	806.27 ± 106.41	831.47 ± 106.43
Segment	668.27 ± 51.10	696.87 ± 63.63	735.33 ± 65.83	770.07 ± 65.70
MU per segment	1.13	1.12	1.09	1.08
Leaf speed Minimum (cm/sec)	0.20 ± 0.06	0.24 ± 0.06	0.28 ± 0.07	0.33 ± 0.09
Leaf speed Maximum (cm/sec)	2.10 ± 0.08	2.20 ± 0.07	2.24 ± 0.08	2.26 ± 0.07
Mean RMS error (mm)	0.18 ± 0.03	0.23 ± 0.03	0.27 ± 0.03	0.30 ± 0.03
Max RMS error (mm)	0.47 ± 0.07	0.54 ± 0.07	0.59 ± 0.07	0.64 ± 0.08
MLC bank A				
0-0.05 mm (%)	41.53 ± 13.58	36.51 ± 13.45	33.16 ± 13.26	30.58 ± 13.01
0.05-0.5 mm (%)	54.74 ± 14.13	57.32 ± 13.14	57.99 ± 15.03	57.47 ± 16.35
0.5-1.0 mm (%)	3.47 ± 2.52	5.49 ± 3.73	7.96 ± 5.03	10.32 ± 5.68
1.0-1.5 mm (%)	0.24 ± 0.37	0.55 ± 0.57	0.89 ± 0.76	1.36 ± 0.94
MLC bank B				
0-0.05 mm (%)	42.39 ± 12.43	36.58 ± 12.97	33.02 ± 12.87	30.49 ± 12.15
0.05-0.5 mm (%)	54.25 ± 12.63	57.53 ± 13.13	58.72 ± 13.56	58.90 ± 13.44
0.5-1.0 mm (%)	3.13 ± 2.27	5.08 ± 3.22	7.23 ± 4.03	9.43 ± 4.89
1.0-1.5 mm (%)	0.22 ± 0.35	0.52 ± 0.56	0.83 ± 0.73	1.28 ± 0.98

Data are presented as mean ± standard deviation.
MLC, multi leaf collimator; RMS, root mean square.

Table 4 Results of DynaLog files based on the dose rates.

Analysis of variance						
Data		Delivery time	Monitor unit	Segment	Leaf speed	
					Minimum	Maximum
p-value		2.84E-33	4.12E-38	1.17E-65	3.22E-07	1.02E-06
Post hoc comparisons						
comparison		Delivery time	Monitor unit	Segment	Leaf speed	
Dose rate 1	Dose rate 2				Minimum	Maximum
300	400	**	n.s.	n.s.	n.s.	*
	500	**	n.s.	*	*	**
	600	**	n.s.	**	**	**
400	500	**	n.s.	n.s.	n.s.	n.s.
	600	**	n.s.	*	*	n.s.
500	600	n.s.	n.s.	n.s.	n.s.	n.s.

Analysis of variance was calculated using repeated measures of analysis of variance or the Friedman test. The Bonferroni/Dunn's test or Steel-Dwass test was used for post hoc comparisons. n.s., not significant; *, $p < 0.05$; **, $p < 0.01$.

Table 5 Results of the statistical analysis of MLC position errors.

Analysis of variance											
Leaf position		Mean RMS error	Max RMS error	0-0.05 mm		0.05-0.5 mm		0.5-1.0 mm		1.0-1.5 mm	
				bank A	bank B	bank A	bank B	bank A	bank B	bank A	bank B
p-value		7.66E-44	2.70E-32	6.91E-66	2.92E-104	2.33E-12	1.10E-17	5.46E-66	1.2E-65	4.4E-60	2.7E-60
Post hoc comparisons											
comparison		Mean RMS error	Max RMS error	0-0.05 mm		0.05-0.5 mm		0.5-1.0 mm		1.0-1.5 mm	
Dose rate 1	Dose rate 2			bank A	bank B	bank A	bank B	bank A	bank B	bank A	bank B
300	400	**	n.s.	**	**	n.s.	n.s.	**	**	**	**
	500	**	**	**	**	n.s.	*	**	**	**	**
	600	**	**	**	**	n.s.	*	**	**	**	**
400	500	**	n.s.	n.s.	n.s.	n.s.	n.s.	**	**	**	**
	600	**	**	**	**	n.s.	n.s.	**	**	**	**
500	600	*	n.s.	n.s.	n.s.	n.s.	n.s.	**	**	**	**

Analysis of variance was calculated using repeated measures of analysis of variance or the Friedman test. The Bonferroni/Dunn's test or Steel-Dwass test was used for post hoc comparisons. n.s., not significant; *, $p < 0.05$; **, $p < 0.01$. MLC, multi leaf collimator; RMS, root mean square.

approximately > 90% of the total errors in the DRs 300, 400, 500, and 600 MU/min in banks A and B were within 0–0.05 mm and 0.05–0.5 mm (Table 3). No significant difference was observed in the MLC position errors between the DRs of 300 and 400 MU/min, 400 and 500 MU/min, 400 and 600 MU/min, and 500 and 600 MU/min in banks A and B (range 0.05–0.5 mm) ($p > 0.05$, Table 5). In addition, no significant difference was observed in the MLC position errors between the DRs of 400 and 500 MU/min, 500 and 600 MU/min in banks A and B (range: 0 mm–0.05 mm) ($p > 0.05$, Table 4). Furthermore, no significant difference was observed in the Max RMS errors between 300 and 400 MU/min, 400 and 500 MU/min, and 500 and 600 MU/min ($p > 0.05$, Table 5). On the contrary, MLC position errors of the all comparisons in banks A and B (range: 0.5–1.0 mm and 1.0–1.5 mm) were statistically differences. ($p < 0.05$, Table 5).

Gamma evaluation

Figure 4 shows the mean values of gamma pass rates (GPRs) for MapCHECK2 and EBT3 according to DRs. The mean percentage GPRs of 99.6%, 99.5%, 99.4%, and 99.5% were observed for the DRs of 300, 400, 500, and 600 MU/min, respectively, in MapCHECK2. The mean percentage GPRs of 97.6%, 96.2%, 97.0%, and 95.7% were observed for the DRs of 300, 400, 500, and 600 MU/min, respectively, in EBT3. Based on the GE of EBT3 films, the GPR of a DR of 600 MU/min was lowest than that of other DRs. However, no significant difference was observed in the GPRs of DRs 300, 400, 500, and 600 MU/min ($p > 0.05$).

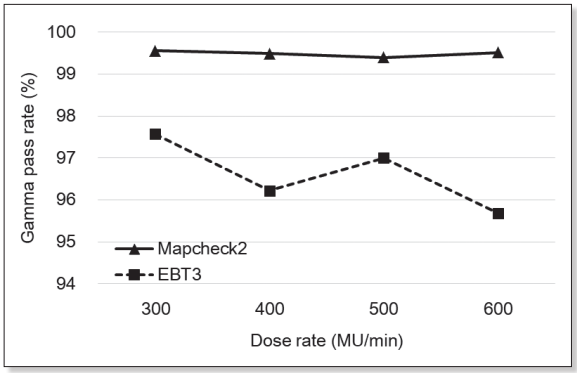

Fig. 4 Gamma pass rates (GPRs) for MapCHECK2 and EBT3 according to the varying dose rates (DRs).

The mean percentage GPRs of 99.6%, 99.5%, 99.4%, and 99.5% were observed for the DRs of 300, 400, 500, and 600 MU/min, respectively, with the gamma criteria of 3%/2 mm in MapCheck2. The mean percentage GPRs of 97.6%, 96.2%, 97.0%, and 95.7% were observed for the DRs of 300, 400, 500, and 600 MU/min, respectively, with the gamma criteria of 3%/2 mm in EBT3.

Figure 5 shows the mean values of GPRs with the most sensitive criterion 3%/1 mm for MapCHECK2 according to DRs. The mean percentage GPRs of 90.3%, 89.8%, 89.6%, and

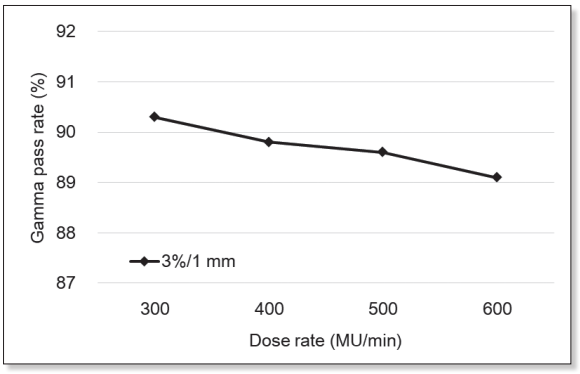

Fig. 5 Gamma pass rate (GPR) with the most sensitive criterion 3%/1 mm for MapCHECK2 [18].

The mean percentage GPRs of 90.3%, 89.8%, 89.6%, and 89.1% were observed for the DRs of 300, 400, 500, and 600 MU/min, respectively, with the gamma criteria of 3%/1 mm in MapCHECK2.

89.1% for DRs of 300, 400, 500, and 600 MU/min, respectively, were observed (Fig. 5). The GPRs decreased with increasing DR; the GPR of a DR of 600 MU/min was lowest value as well as in EBT3. However, no significant difference was observed in the GPRs of DRs 300, 400, 500, and 600 MU/min ($p > 0.05$).

Discussion

In this study, we evaluated the MLC position errors between the planned and actual delivery positions using DynaLog files. These log files of the delivered IMRT contain significant information used to assess the routine IMRT QA and are commonly used for patient-specific IMRT QA[22, 23]. Furthermore, these log files are a promising tool for IMRT QA automation that reduces the time spent on IMRT QA and can be used to analyze the entire IMRT day-to-day delivery[24]. In this study, DynaLog files were considered to reflect the accuracy of the MLC position, and our results were highly reliable.

The number of MUs increased with increasing DR (Table 3), suggesting a larger number of small MU segments. Previous studies demonstrated that a small MU segment may result in delivery inaccuracy in IMRT[25-27]. Huang et al.[28] reported that the presence of small MU segments has a strong impact on GPRs. However, these studies did not investigate a small MU segment with MUs fewer than 1. Therefore, small MU segments had a little effect on the GPRs in this study because the MU per segment value was much the same based on the DR (Table 3). In a comprehensive multicenter study, Kerns et al.[29] revealed that the parameters, including gantry angle, number of beam holdoffs, and number of segments, commonly thought to affect MLC performance were found to have no such effect. Therefore, we considered that increasing the number of small MU segments had no effect on the GPRs and MLC position errors.

A patient-specific QA for IMRT is extremely important for ensuring the quality of care for patients with cancer during radiotherapy. Various methods, including the use of an ion chamber, 2D array detectors, and an electronic portal imaging device (EPID), have been employed during pretreatment verification to detect possible errors between the calculated dose and the measured dose[30-32]. The MapCHECK2 used in this study has a detection accuracy and a stability of GPR equivalent to those of MatriXX (ion chamber 2D array) and EPID[33]. MapCHECK2 showed that a systematic MLC error of up to 0.5 mm was not detected with a gamma criterion of 3%/1 mm[18]; in this study, almost all MLC position errors in banks A and B were within 0–0.05 mm and 0.05–0.5 mm (Table 3). Therefore, MapCHECK2 with a GE of 3%/2 mm could not detect a slight difference in the dose distribution according to the difference in DRs (Fig. 4). However, the GPRs decreased with increasing DR using criteria of 3%/1 mm (Fig. 5). Previous studies were demonstrated that 1 mm MLC position error produced about 5% errors in dose delivery and decreased in average GPRs[34, 35]. We considered that decreasing GPRs were influenced by MLC position errors within 0.5–1.0 mm and 1.0–1.5

mm (Table 5) .

By contrast, Gafchromic films were designed for IMRT and QA because they have high resolution and can detect slight differences in the dose distribution[36, 37]. Furthermore, Marroquin et al.[38] evaluated the uncertainty in an EBT3 film dosimetry system, including the dynamic reproducibility, uniformity, and orientation. They noted that higher uncertainties were found because of the relative orientation of the film and the uniformity in the response of the scanner. However, they reported that one must strictly control the position and orientation of the film, so that the total uncertainties are considerably reduced. We considered that the GE using EBT3 had a little uncertainty because we performed the film analysis in the same position on the scanner and in the same orientation. In addition, Borca et al.[39] evaluated DR dependence in IMRT (6 MV and 15 MV) among various DRs (100, 300, and 600 MU/min). In another study by Ataei et al.[40], DR dependence (6 MV and Co-60 gamma rays) was observed between DRs of 200 and 400 cGy/min. These studies found that DR dependence was not significantly different between the EBT3 films. Therefore, results of the GE using the EBT3 films were not affected by the difference in DRs, and the decrease in the GPR with increasing DR in EBT3 was considered to mainly reflect the inaccuracy of MLC position errors according to the DRs.

Vorwerk et al.[9] recommended that mechanical and technical aspects limit for the LV of 2.5–3.0 cm/sec and for the DR of 300–400 MU/min should be respected for prostate patients. In addition, we considered that MLC position errors were less in the same DRs because maximum LV was 2.5 cm/sec in our study. Furthermore, Kaviarasu et al.[10] indicated that some fields of a DR 500 MU/min showed the worse gamma value than DR 400 MU/min. They discussed that increasing the DR increased the number of control points per min and increased the complexity of the MLC delivery, but they did not investigate the MLC. In addition, average gamma values were same values for 400 and 500 MU/min, and the maximum gamma value of a DR 400 MU/min was slightly better (0.08 point) than that of a DR 500 MU/min, and difference of point absolute dose using ion chamber showed that < 1% mean deviation for 400 and 500 MU/min. These results showed that there were few difference between the DR 400 and 500 MU/min same as our study. More importantly, we considered that intrafractional displacement of the prostate during IMRT had a greater effect on dose distribution than slightly difference of MLC position errors between the DR 400 and 500 MU/min. Previous studies demonstrated that the average 3D displacements of intrafraction prostate were approximately 2–3 mm according to the immobilization system and duration of radiotherapy[41, 42]. Furthermore, Kontaxis et al.[43] reported that the average drops in D99% coverage due to displacement of the intrafraction prostate for the PTV and CTV during radiation delivery were 11% and 2.1%, respectively, using combined 1.5T magnetic resonance imaging and a linear accelerator system. Therefore, we considered the influence for dose distribution, the delivery time should be as short as possible.

These results indicated that a DR of 500 or 600 MU/min was the acceptable rate when reducing the delivery time. However, no significant difference was observed between DR 500 and 600 MU/min for the delivery time (Table 4). Those causes were considered that actually delivered DR of 600 MU/min was slightly lower than that of nominal value. In addition, the GPRs of a DR 600 MU/min was larger decreased compared to DR 400 and 500 MU/min using MapCHECK2 with a gamma criterion 3%/1 mm (Fig. 5). Furthermore, the GPR of a DR 600 MU/min using EBT3 were at the very limit of 95% criteria deciding by TG

218[17] (Fig. 4). Therefore, we suggested that a DR of 500 MU/min was the most acceptable rate considering clinical safety.

With regard to the limitations, according to our analysis, the MU values in DMLC-IMRT increased with increasing DR. The usage of greater MUs results in an increase in scattered radiation and radiation leakage, causing secondary malignancies[44-46]. In addition, the transmitted radiation dose, which depends on the transmission through the leaves, is also higher[47] and consequently increases the integral dose to the organ at risk because of inter- and intraleaf transmission leakage and scatter. Decreasing these radiation doses is important for the protection of organs at risk and in normal tissues. However, we did not consider these influences in terms of radiation exposure in this study.

Conclusion

We considered the influence of DR on the MLC position errors and GPR and found that a DR of 500 MU/min was the most acceptable rate when reducing the delivery time while maintaining the MLC positional accuracy and GPR.

Conflict of interest

The authors declare that they have no conflict of interest.

Statement of human rights

This study was approved by the Ethics Committees of Akita Kousei Medical Center (approval No. 2020-155).

References

1) Ezzell GA, et al.: Guidance document on delivery, treatment planning, and clinical implementation of IMRT: Report of the IMRT Subcommittee of the AAPM Radiation Therapy committee. Med Phys, 30, 2089-2115, 2003.
2) Bortfeld T: IMRT: A review and preview. Phys Med Biol, 51(13), R363-379, 2006.
3) Staffurth J: A review of the clinical evidence for intensity-modulated radiotherapy. Clin Oncol, 22(8), 643-657.
4) Bortfeld TR, et al.: X-ray field compensation with multileaf collimators. Int J Radiat Oncol Biol Phys, 28(3), 723-730, 1994.
5) Mell LK, et al.: Intensity-Modulated Radiation Therapy Use in the U.S., 2004. Cancer, 104(6), 1296-1303, 2005.
6) Ghasroddashti E, et al.: Clinical consequences of changing the sliding window IMRT dose rate. J Appl Clin Med Phys, 13(4), 4-12, 2012.
7) Slosarek K, et al.: Beam rate influence on dose distribution and fluence map in IMRT dynamic technique. Reports of practical oncology and radiotherapy, 17, 97-103, 2012.
8) Intensity modulated radiation therapy collaborative working group: Intensity-modulated radiotherapy: current status and issues of interest. Int J Radiat Oncol Biol Phys, 51, 880-914, 2001.
9) Vorwerk H, et al.: Impact of different leaf velocities and dose rates on the number of monitor units and the dose-volume-histograms using intensity modulated radiotherapy with sliding-window technique. Radiat Oncol, 31(3), 2008.
10) Kaviarasu K, et al.: Impact of dose rate on accuracy of intensity modulated radiation therapy plan delivery using the pretreatment portal dosimetry quality assurance and setting up the workflow at hospital levels. J Med Phys, 40(4), 226-232, 2015.
11) National Comprehensive Cancer Network Website. https://www.nccn.org/professionals/physician_gls/pdf/prostate.pdf. Accessed 17 October 2022.
12) Calvo-Ortega JF, et al.: A Varian DynaLog file-based procedure for patient dose-volume histogram-based IMRT QA. J Appl Clin Med Phys, 15(2), 4665, 2014.
13) Osewski W, et al.: Clinical examples of 3D dose distribution reconstruction, based on the actual MLC leaves movement, for dynamic treatment techniques. Rep Pract Oncol Radiother J Gt Cancer Cent Poznan Pol Soc Radiat Oncol, 19(6), 420-427, 2014.
14) Kumar R, et al.: Quick, efficient and effective patient-specific intensity-modulated radiation therapy quality assurance using log file and electronic portal imaging device. J Can Res Ther, 13(2), 297-303, 2017.
15) Klein EE et al.: Quality assurance of medical accelerators: Recommendations of AAPM Task Group No. 142. Med. Phys, 36(9), 2009.
16) Low DA, et al.: Evaluation of the gamma dose distribution comparison method. Med phys, 30, 2455-2464, 2003.
17) Miften M, et al.: Tolerance limits and methodologies for IMRT measurement-based verification QA: Recommendations of AAPM Task Group No. 218. Med. Phys, 45(4) 2018.
18) Woon W, et al.: A study on the effect of detector resolution on gamma index passing rate for VMAT and IMRT QA. J Appl Clin Med Phys, 19, 2, 230-248, 2018.

19) Niroomand-Rad A, et al.: Radiochromic film dosimetry: recommendations of AAPM Radiation Therapy Committee Task Group 55. American Association of Physicists in Medicine. Med Phys, 25, 2093-115, 1998.
20) Létourneau D, et al.: Evaluation of a 2D diode array for IMRT quality assurance. Radiother Oncol, 70(2), 199-206, 2004.
21) Khamfongkhruea C, et al.: Dosimetric evaluation of radiation dose rate effect in respiratory gated intensity modulated radiation therapy. Biomed Imaging Interv J, 8(1), e5, 2012.
22) Litzenberg DW, et al.: Verification of dynamic and segmental IMRT delivery by dynamic log file analysis. J Apple Cline Med physics, 3, 63-72, 2002.
23) Defoor DL, et al.: Investigation of error detection capabilities of phantom, EPID and MLC log file based IMRT QA methods. J Appl Clin Med Phys, 18(4), 172-179, 2017.
24) Dinesh Kumar M, et al.: QA of intensity-modulated beams using dynamic MLC log files. J Med Phys, 31, 36-41, 2006.
25) Xia P, et al.: Communication and sampling rate limitations in IMRT delivery with a dynamic multileaf collimator system. Med Phys, 29(3), 412-423, 2002.
26) Xia P, et al.: Point/counterpoint. Segmental MLC is superior to dynamic MLC for IMRT delivery. Med Phys, 34(7), 2673-2675, 2007.
27) Rangel A, et al.: Tolerances on MLC leaf position accuracy for IMRT delivery with a dynamic MLC. Med Phys, 36(7), 3304-3309, 2009.
28) Huang L, et al.: Impact of small MU/segment and dose rate on delivery accuracy of volumetric-modulated arc therapy (VMAT). J Appl Clin Med Phys, 17(3), 203-210, 2016.
29) Kerns JR, et al.: A multi-institution evaluation of MLC log files and performance in IMRT delivery. Radiation Oncology, 9, 176, 2014.
30) Dong L, et al.: Patient-specific point dose measurement for IMRT monitor unit verification. Int J Radiat Oncol Biol Phys, 56, 867-877, 2003.
31) Howell RM, et al.: Establishing action levels for EPID-based QA for IMRT. J Appl Clin Med Phys, 9, 2721, 2008.
32) Agnew A, et al.: Monitoring daily MLC positional errors using trajectory log files and EPID measurements for IMRT and VMAT deliveries. Phys Med Biol, May 7, 59(9), N49-63, 2014.
33) Son J, et al.: A comparison of the quality assurance of four dosimetric tools for intensity modulated radiation therapy. Radiol Oncol, 49(3), 307-313, 2015.
34) LoSasso T, et al.: Physical and dosimetric aspects of a multileaf collimation system used in the dynamic mode for implementing intensity modulated radiotherapy. Med Phys, 25, 1919-1927, 1998.
35) Yan G, et al.: On the sensitivity of patient-specific IMRT QA to MLC positioning errors. J Appl Clin Med Phys, 10(1), 120-128, 2009.
36) Zeidan OA, et al.: Characterization and use of EBT radiochromic film for IMRT dose verification. Med. Phys, 33(11), 4064-72, 2006.
37) Shimohigashi Y, et al.: Evaluation of a single-scan protocol for radiochromic film dosimetry. J Appl Clin Med Phys, 16(2), 412-424, 2015.
38) Marroquin EYL, et al.: Evaluation of the uncertainty in an EBT3 film dosimetry system utilizing net optical density. J Appl Clin Med Phys, 17(5), 466-481, 2016.
39) Borca VC, et al.: Dosimetric characterization and use of GAFCHROMIC EBT3 film for IMRT dose verification. J Appl Clin Med Phys, 14(2), 158-171, 2013.
40) Ataei G, et al.: Evaluation of dose rate and photon energy dependence of Gafchromic EBT3 film irradiating with 6 MV and Co-60 photon beams. J Med Signals Sens, 9(3), 204-210, 2019.
41) Xie Y, et al.: Intrafractional motion of the prostate during hypofractionated radiotherapy. Int J Radiat Oncol Biol Phys, 72(1), 236-46, 2008.
42) Mostafaei F, et al.: Preliminary clinical evaluation of intrafraction prostate displacements for two immobilization systems. Cureus, 12(9), e10206, 2020.
43) Kontaxis C, et al.: Delivered dose quantification in prostate radiotherapy using online 3D cine imaging and treatment log files on a combined 1.5T magnetic resonance imaging and linear accelerator system. Phys Imaging Radiat Oncol, 15, 23-29, 2020.
44) Hall EJ: Intensity-modulated radiation therapy, protons, and the risk of second cancers. Int J Radiat Oncol Biol Phys, 65, 1-7, 2006.
45) Hall EJ, et al.: Radiation-induced second cancers: The impact of 3D-CRT and IMRT. Int J Radiat Oncol Biol Phys, 56, 83-88, 2003.
46) Purdy JA: Dose to normal tissues outside the radiation therapy patient's treated volume: A review of different radiation therapy techniques. Health Physics, 95, 666-676, 2008.
47) Schmidhalter D, et al.: Leaf transmission reduction using moving jaws for dynamic MLC IMRT. Med Phys, 34, 3674-3687, 2007.

Received June 26, 2022; accepted January 6, 2023

Effect of luminance non-uniformity caused by aged deterioration of a medical liquid-crystal display for low-contrast detectability

TAKARABE Shinya[1), 2)], TAKAHASHI Keita[1)], AKAMINE Hiroshi[1)], AWAMOTO Shinichi[1)], OGAWA Kazuhisa[1)], KATO Toyoyuki[1)]

1) Division of Radiology, Department of Medical Technology, Kyushu University Hospital
2) Department of Oral and Maxillofacial Radiology, Faculty of Dental Science, Kyushu University

Note: This paper is secondary publication, the first paper was published in the JART, vol. 70 no. 848: 49-54, 2023.

Key words: Liquid-crystal display, Aged deterioration, Luminance uniformity, Contrast-detail phantom, Image quality figure (IQF)

【Abstract】
The purpose in this study is to examine the effect of the luminance non-uniformity caused by the aged-deterioration of medical liquid-crystal displays (LCDs) for the low contrast detectability using a contrast-detail phantom. Two medical LCDs of the same-type with different operating times were used. The first was operated for 38,000 h (aged-deterioration LCD) and the second for 200 h (non-deterioration LCD). These LCDs were calibrated to the grayscale standard display function with a maximum luminance of 170 cd/m^2. Contrast-detail images acquired under the same exposure conditions were displayed on each LCD and an observer study was performed by ten radiological technologists. The average image quality figures of the aged-deterioration and non-deterioration LCDs were 74.2 and 70.4, respectively and a significant difference was seen (p = 0.036). Our results indicated that the luminance non-uniformity caused by aged-deterioration of the LCD may affect the low contrast detectability.

1 Introduction

In the past decade, liquid-crystal displays (LCDs) with cold-cathode fluorescent lamp (CCFL) backlights have increasingly been used, replacing the use of cathode ray tube monitors in medical settings as soft copy reading devices. However, according to investigations in Japan regarding the quality control of LCDs, the rate of performing quality control was low, implying that LCDs with degraded quality may be used in hospitals.[1)] Aged-deterioration of LCDs can lead to a decrease in the maximum luminance (L_{max}), change in chromaticity, and luminance non-uniformity.[2)] Takahashi et al. examined the relationship between the L_{max} and operating time of the display backlight over a three-year period for 249 LCDs (initial L_{max} setting: 240 cd/m^2, color temperature: 7,500 K, (RadiForce® RX210), EIZO Co., Ishikawa, Japan).[3)] They reported that the L_{max} of 39 of the LCDs were less than 170 cd/m^2 because of aged-deterioration.[3)] Akamine et al. examined the color temperature of two same type LCDs (RadiForce® RX210) with different operating times (under 10,000 hours and over 20,000 hours). They reported that the color temperature was different between these LCDs due to deterioration of phosphor in the CCFL and color filter.[4)]

There is a case study report that display performance will degrade with increasing time in use, which in turn may degrade diagnostic performance.[5)] To the author's knowledge, there are no previous reports in the literature regarding the effects of luminance non-uniformity, caused by the deterioration of the medical LCD, on soft copy reading. We assumed that the luminance non-uniformity may affect the low-contrast detectability. As a preliminary study for exploring the effects

(a) Aged-deterioration LCD (ADLCD)

(b) Non-deterioration LCD (NDLCD)

Fig. 1 The same type LCDs with different operation times displayed identical uniform test-patterns. The operating times of (a) and (b) were about 38,000 and 200 hours, respectively. A luminance non-uniformity was observed for the LCD with a longer operation time.

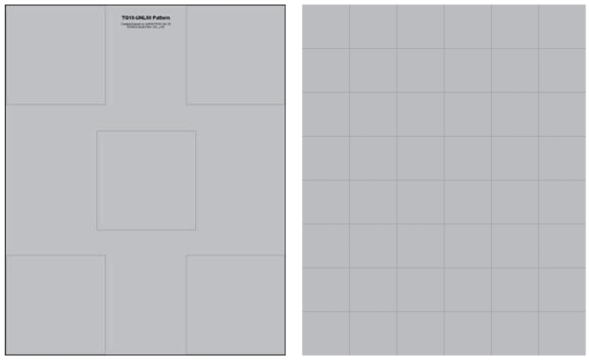

(a) (b)

Fig. 2 Test patterns used in this study. (a) and (b) are TG18-UNL80 test pattern and the original test pattern modified from TG18-UNL80 test pattern, respectively.

of the LCD luminance non-uniformity, we used the contrast-detailed (CD) phantom and compared the low-contrast detectability for two same type LCDs with different operating times. The purpose of this study was to examine the effect of luminance non-uniformity caused by aged-deterioration for the detectability of low-contrast signals.

2 Materials and Methods

A case study approach was used to perform a physical evaluation and observer study for medical LCDs (RadiForce® RX210, EIZO Co.) Two same type color LCDs with different operating times were used in this study. The first was operated for about 38,000 hours [aged-deterioration LCD (ADLCD)] and the second for about 200 hours [non-deterioration LCD (NDLCD)] (Fig. 1). Both LCDs were calibrated to the grayscale standard display function (GSDF) with a L_{max} of 170 cd/m^2 by using a quality-control software (RadiCS®, EIZO Co.) and a near-range luminance meter (RadiCS® UX1 Sensor, EIZO Co.).

First, we measured the luminance uniformity and variation of the luminance for the physical evaluation of the LCDs before performing an observer study to evaluate the low-contrast detectability of the LCDs.

2.1 Measurement of luminance for physical evaluation

In terms of the luminance non-uniformity of medical LCDs, American Association of Physicists in Medicine (AAPM) Task Group 18 (TG18) required that to measure luminance of five points in the test pattern displayed on an LCD (Fig. 2 (a)).[6] However, such test pattern cannot evaluate the entire screen. Therefore, an original test-pattern was modified based on the TG18-UNL80 test pattern. The test pattern had the same pixel value as the TG18-UNL80 test pattern and was divided into 48 measurement regions (Fig. 2 (b)); the luminance was measured corresponding to each rectangular region. The original test-pattern was displayed on the LCDs and the luminance was measured by use of a telescopic-type luminance meter (LS-100®, Konica Minolta Co., Ltd., Tokyo, Japan). The distance between the LCD and luminance meter was 150 cm. The ambient light at the center of the LCD measured by an illuminance meter (ANA-F9®, Tokyo Koden Co., Tokyo,

Japan) was 0.1 lux. Luminance measurement in a telescopic-type luminance meter is affected by stray light.[7, 8] To minimize the light emission from outside the focused area on the telescopic-type luminance meter, the region of the test pattern outside the measurement area was covered by solid fiberboard. The luminance was measured three times. The luminance uniformity is given by

$$\text{Luminance uniformity} = (Lm_{max} - Lm_{min}) / (Lm_{max} + Lm_{min}) \times 200; \quad (1)$$

where Lm_{max} and Lm_{min} are the measured maximum and minimum luminance including the reflected luminance. The luminance uniformity is calculated using only the Lm_{max} and Lm_{min}. To evaluate the luminance variation for the whole monitor screen, we also calculated the standard deviation (SD) of the luminance measured at 48 regions. Similarly, we measured luminance uniformity and the SD using TG18-UNL80 test pattern.

2.2 Observer study using CD phantom

The observer performance test was carried out with a CD phantom (Kyoto Kagaku Co., Ltd., Kyoto, Japan).[9] The CD phantom had signals (concave signals) of diameters ranging from 0.3 to 8.0 mm in 15 steps and depths from 0.3 to 8.0 mm in 15 steps. For the three largest diameters, there was a single signal in the center, similar to conventional CD phantoms. However, four-point selective CD phantoms were used for the remaining signals, comprising a signal in the center and in one of the corners. Three CD images were acquired. The exposure condition was 80 kV, 400 mA, and 25 ms and geometries are shown in Fig. 3. A computed radiography (CR) system (IP: ST-VN, IP reader FCR 5000®, Fujifilm Co. Tokyo, Japan) was used for the X-ray detector. The CD images in DICOM format were displayed on both the ADLCD and NDLCD. The display function of these LCDs was calibrated GSDF with a L_{max} of 170 cd/m^2. The illuminance of the center of these displays were set to 350 lux. This illuminance determined based on the actual measured illuminance at the center of this ADLCD, which was used in the clinical practice. The window level and window width were set to 512 and 1024, respectively. Ten radiological technologists (1−11 years of experiences) participated in the observer study. They could observe the CD images at any distance, for as long as needed. Each observer recorded the depth at which each signal size in the CD phantom could be recognized with 50% confidence. The image quality figure (IQF) was calculated from individual observer data by the following equation;

$$IQF = \sum_{i=1}^{i=15}(C_i \cdot D_{i,th}), \quad (2)$$

where C_i represents the depth value (contrast) of the object (visible hole) in the column *(i)*, and $D_{(i,th)}$ denotes the corresponding smallest visible diameter (threshold diameter) in the column *(i)*. A small IQF value indicates high detectability with a low-contrast signal.[9–11] A paired t-test analysis was performed to examine the mean differences of IQF values between ADLCD and NDLCD.

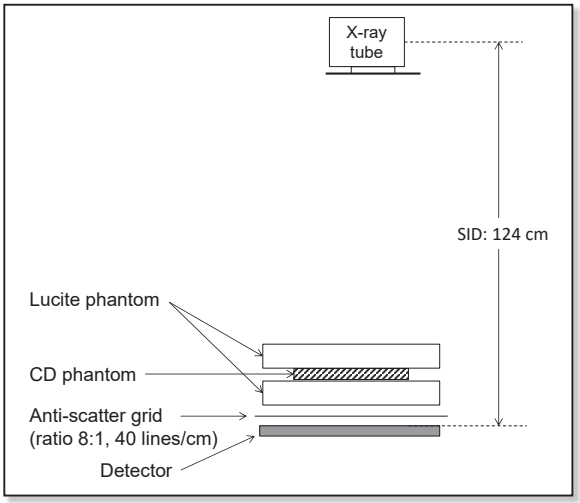

Fig. 3 Geometries for acquiring CD with 7-cm-thickness lucite phantoms.

3 Results

The results of the measured luminance using our original test pattern are shown in Figs. 4 (a and b). Table 1 provides the values of Lm_{max}, Lm_{min}, luminance uniformities, and SD of the luminance value using the original test pattern. The luminance uniformities of ADLCD and NDLCD were 77.8% and 25.4%, respectively. The ADLCD displayed a significant non-uniformity. The SDs of the measured luminance for the ADLCD and NDLCD were 9.30 and 3.15, respectively. There was a significant difference in the SDs between the ADLCD and NDLCD (F-test, $p < 0.01$). On the other hand, for using TG18-UNL80 test pattern, the luminance uniformities of ADLCD and NDLCD were 23.2% and 10.6%, respectively. The SDs of the measured luminance for the ADLCD and NDLCD were 5.12 and 2.5, respectively. There was not a significant difference in the SDs between the ADLCD and NDLCD.

For the observer performance test, the IQF values of the ADLCD and NDLCD were 74.2 ± 14.7 and 70.4 ± 14.4, respectively. There was a statistical difference in the IQF values for the ADLCD and NDLCD (Fig. 5) (paired t-test, $p = 0.036$).

4 Discussion

We measured the luminance uniformity as physical evaluation and IQF as low contrast detectability, using two same type LCDs with different operating times in order to investigate the effect of luminance non-uniformity due to aged-deterioration of the medical LCD.

For both test patterns (TG18-UNL80 test pattern and the original test pattern), the luminance uniformity of the ADLCD was poorer than that of the NDLCD because of the degradation of the backlight or impurities contained in the liquid crystal component

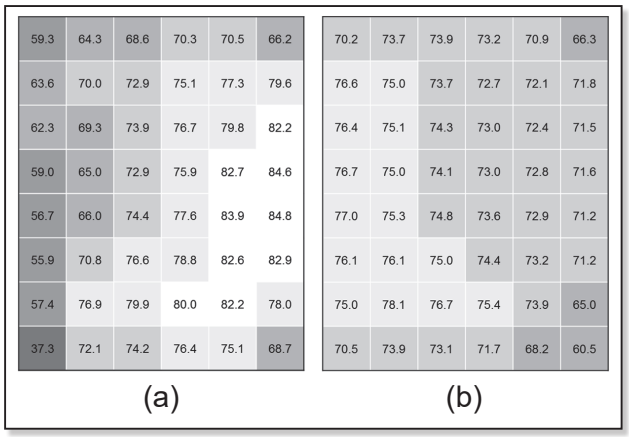

Fig. 4 Luminance values (cd/m^2) measured using the original test pattern (Fig. 2 (b)). (a) and (b) are the luminance values corresponding to small rectangular regions of the original test pattern (Fig. 2 (b)) displayed on the ADLCD and NDLCD, respectively.

Table 1 Results of physical evaluation for ADLCD and NDLCD using the original test pattern

	ADLCD	NDLCD
Lm_{max}	84.8 cd/m^2	78.1 cd/m^2
Lm_{min}	37.3 cd/m^2	60.5 cd/m^2
Luminance uniformity	77.8%	25.4%
SD of luminance value	9.30	3.15

SD; standard deviation, ADLCD; aged-deterioration LCD, NDLCD; non-deterioration LCD

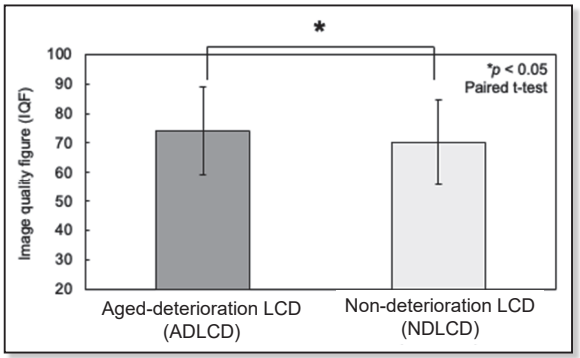

Fig. 5 Comparison of image quality figures (IQF) between aged-deterioration LCD and non-deterioration LCD.

(Fig. 4 and Table 1). The criteria for the acceptance test of the luminance uniformity showed that the value of luminance uniformity should be within 30%.[6, 12] When TG18-UNL80 test pattern was used, the results of both ADLCD and NDLCD were within this reference

value (23.2% and 10.6%, respectively). On the other hand, when our original test pattern was used, the results of only ADLCD exceeded this value (Table 1). The SD of the ADLCD was significantly higher than that of the NDLCD when the original pattern was used. This is because by increasing the number of measurement points for the luminance of the entire screen, the variation in luminance of the entire screen (non-uniformity), measured more accurately compared to using TG18-UNL80 test pattern.

There was a statistically significant difference between the ADLCD and NDLCD with the same L_{max} (170 cd/m^2) for IQF values (Fig. 5). We estimated that the reason for the higher IQF values of the ADLCD was because the region with the non-uniformity, in particular the black spot overlapping the signals of the CD phantom, resulted in low detectability of the low contrast signals.

In this study, we did not evaluate the chromaticity of the monitor in detail. Krupinski et al. reported that there is no significant difference in the diagnostic ability of breast biopsy virtual slide regions of interest for calibrated color LCDs and uncalibrated color LCDs.[13] In our study, we calibrated the LCDs before the experiment and it is considered that the change in chromaticity has less influence on the detectability of simple signals using monochrome images.

Only one LCD was used as the aged-deterioration sample; however, to our knowledge, there are no reports in the literature regarding the effects of luminance non-uniformity caused by the aged-deterioration of the LCD. This study revealed that the non-uniformity of the LCD may degrade the detectability of the low contrast signals.

By measuring the luminance uniformity regularly, degradation in low contrast detectability due to aged-deterioration can be detectable, however determining the luminance uniformity is difficult because the use of telescopic-type luminance meters for measuring luminance uniformity is time consuming, and scientific-grade 2D luminance colorimeters are too costly for most users in hospitals. Practical and easier methods such as using commercially available digital cameras[14], should be contained in constancy tests in certain guidelines and regular measurements of the luminance uniformity is required.[6, 12]

5 Conclusion

Because of either the degradation of the backlight or impurities contained in the liquid crystal component, the luminance uniformity of ADLCD (77.8%) was degrade compared to NDLCD (25.4%). There was a statistically significant difference between the ADLCD and NDLCD with the same L_{max} (170 cd/m^2) for low contrast detectability (paired t-test, p = 0.036). The detectability of low-contrast signals may be lower due to the effects of luminance non-uniformity caused by the aged-deterioration of the LCD.

Acknowledgments

The authors are grateful to all members in division of radiology, department of medical technology, Kyushu university hospital whose comments made enormous contribution to this study.

Funding

This research did not receive any specific grant from funding agencies in the public, commercial, or not-for-profit sectors.

Declarations Conflicts of interest

Not applicable.

Ethics approval

The observers of this study were explained about the outline and purpose of the study, the method of the experiment, and the possibility of presenting the results of the experiment at academic conferences and papers.

Informed consent

Not applicable.

References

1) T Shibutani, et al.: Current Situations and Problems of Quality Control for Medical Imaging Display Systems. Japanese Journal of Radiological Technology, 71(4); 356-361, 2015. (Japanese)
2) N. Hashimoto: Image display devices (3): LCD Monitor (Lecture of JSRT Member). Japanese Journal of Radiological Technology, 59(1); 21-28, 2003. (Japanese)
3) K Takahashi, et al.: Effective luminance deterioration of medical liquid crystal displays in clinical use. Radiological Physics and Technology, 10; 382-386, 2017.
4) H Akamine, et al.: Chromaticity and correlated color temperature of the white point in medical liquid–crystal display. Medical Physics, 39(8); 5127-5135, 2012.
5) LJ Caffery, et al.: The effect of time in use on the display performance of the iPad. British Journal of Radiology, 89(1063); 20150657, 2016.
6) E. Samei, et al.: Assessment of display performance for medical imaging systems. Report of the American Association of Physicists in Medicine (AAPM) Task Group 18, AAPM On-line Report No. 03, Med Phys, 2005.
7) J Morishita, et al.: Effect of test patterns on measurement of the luminance of LCD devices by use of a telescopic-type luminance meter. Radiological Physics and Technology, 1; 95-99, 2008.
8) T Shiiba, et al.: Effects of ambient-light correction in luminance measurements of liquid-crystal display monitors by use of a telescopic-type luminance meter. Radiological Physics and Technology, 3; 65-69, 2010.
9) T MAO, et al.: Manual: contrast-detail phantom Artinis CDRAD type 2.0. St. Radboud, The Netherlands: Project Quality Assurance in Radiology, Department of Radiology, University Medical Center Nijmegen, 1998.
10) M. McEntee, et al.: A comparison of low contrast performance for amorphous Silicon/caesium iodide direct radiography with a computed radiography: A contrast detail phantom study. Radiography, 13; 89-94, 2007.
11) S. Hatanaka, et al.: Comparison of viewing angle and observer performances in different types of liquid-crystal display monitors. Radiological Physics and Technology, 2; 166-174, 2009.
12) Japan Industries Association of Radiological Systems (JIRA): Japanese Engineering Standards of Radiological Apparatus (JESRA) X-0093*B-2017 quality assurance guideline for medical imaging display systems. JIRA, Tokyo; 2017.
13) E. A. Krupinski, et al.: Observer Performance Using Virtual Pathology Slides: Impact of LCD Color Reproduction Accuracy. Journal of Digital Imaging, 25(6); 738-743, 2012.
14) K Kawamoto, et al.: A method for evaluating luminance non-uniformity of displays by use of a commercially available digital camera. Radiological Physics and Technology, 10; 409-414, 2017.

Received June 17, 2022; accepted January 6, 2023

Effective scan parameter setting of Quiet Suite combined readout segmented multi-shot EPI DWI (qRESOLVE) for decrease of image distortion and acoustic noise with a 3T MRI scanner

KOBAYASHI Yoshikazu[1)], KANDA Toshimitsu[2)], SAITO Yoko[3)]

1) ShinSapporo neurosurgical hospital / Hirosaki University Graduate School of Health Sciences, Radiologic technologist
2) ShinSapporo neurosurgical hospital, Radiologic technologist
3) Department of Radiation Science, Hirosaki University Graduate School of Health Sciences, professor, Medical doctor

Note: This paper is secondary publication, the first paper was published in the JART, vol. 70 no. 850: 34-44, 2023.

Key words: Quiet Suite combined readout segmented multi shot EPI DWI (qRESOLVE), image distortion, acoustic noise, echo spacing, parallel imaging factor

【Abstract】
The purpose of this study was to determine effective scan parameter settings for decreasing image distortion and acoustic noise by scanning phantoms with various parameters using the Quiet Suite combined readout segmented multi-shot echo planar imaging (qRESOLVE) with a 3T MRI scanner. The distortion rate of the slit area in the phantom was calculated in the phantom experiment. Furthermore, peak sound pressure levels were calculated. The results showed that with a decrease in echo spacing (ES) and field of view (FOV), for a thin slice thickness, an increase in the parallel imaging factor (PIF) and matrix size (MS) were effective for decreasing image distortion ($p<0.017$). To decrease acoustic noise, an increase in ES, number of segments (SEG), repetition time (TR), and FOV, and a decrease in PIF and MS, were effective ($p<0.017$). With respect to routine clinical examinations, a decrease in ES and an increase in PIF were effective for decreasing image distortion, and with an increase in ES, a decrease in PIF and SEG were effective for decreasing acoustic noise.

Introduction

Diffusion-weighted imaging (DWI) using single-shot echo planar imaging (EPI) is useful for the diagnosis of acute cerebral infarction and brain tumors. However, it has the disadvantages of causing significant image distortion and very loud acoustic noise[1)]. Image distortion may degrade the diagnostic accuracy, and loud acoustic noise causes discomfort and anxiety in patients. Moreover, a decrease in acoustic noise is important to avoid hearing impairment. Siemens Healthineers has developed readout segmented multi-shot EPI DWI (RESOLVE：readout segmentation of long variable echo-trains) as an imaging method to improve image distortion. RESOLVE is a new multi-shot EPI DWI that segments the readout direction in k-space. RESOLVE decreases the readout time in k-space, which allows short echo spacing, and can be used in conjunction with parallel imaging methods. In addition, parallel imaging methods can be used to decrease dephasing and image distortion[2)]. However, RESOLVE has the disadvantages of loud acoustic noise resulting from the fast switching of the gradient field and short echo spacing. Recently, RESOLVE with the Quiet Suite method (qRESOLVE) was developed to decrease discomfort and avoid hearing impairment during routine clinical examination. qRESOLVE is an effective sequence that achieves silence by automatically optimizing the shape of the gradient field (the angle of the gradient field is decreased)[3,4)]. In this study, a phantom was scanned with various qRESOLVE parameters, and effective parameter settings for decreasing

image distortion and acoustic noise were investigated.

Materials and Methods

1. Equipment

An MRI scanner (MAGNETOM Skyra syngo VE11 3.0T (Siemens Healthineers)) was used. The coil was a 20 channels head/neck coil (Siemens Healthineers). A spherical phantom (Siemens Healthineers : D165{1.25gNaS04 × 6H20}) and Japanese Industrial Standards (JIS) phantom (Nikko Finds Industries : 95-1108Z type) were used.

2. Scan parameters

In qRESOLVE, the echo spacing (ES), parallel imaging factor (PIF), number of segments (SEG), phase partial fourier (PpF), repetition time (TR), matrix size (MS), slice thickness (ST), and field of view (FOV) were varied. The scan parameters are listed in Tables 1-1 through 1-8. The center of the phantom was set to the isocenter, and the scan plane was a transverse section. The phase encoding direction was set to the left-right direction, motion probing gradient (MPG) pulses were applied in three axes, and a monopolar three-scan trace was used in diffusion mode. The parallel imaging method used was generalized auto-calibrating partially parallel acquisitions (GRAPPA)[5].

3. Examination of distortion rate

The distortion rate is generally calculated using the area method[6]. However, in this study, ST, MS, and FOV also varied, and the image could not be subtracted. Therefore, the distortion rate was defined as in Eq. (1), based on a report by Kajisako et al.[7] qRESOLVE with various scan parameters (Tables 1-1 through 1-8) were evaluated in comparison with T_2-weighted images (T_2WI) (Table 2). The slit area in the JIS phantom was imaged for both sequences. Scans were performed 10 times to decrease sampling error, and the average value was calculated.

$$\text{Distortion rate}(\%) = (Wq/Wt) \times 100 \quad \cdots\cdot(1)$$

where Wq is the slit width measured by qRESOLVE and Wt is the slit width measured by T_2WI. As shown in Fig. 1, Wt and Wq were measured by drawing a straight line perpendicular to the slits at both ends. The closer the distortion rate is to 100, the less image distortion is present.

4. Examination of acoustic noise

4.1. Peak sound pressure level

A spherical phantom was scanned using qRESOLVE (Tables 1-1 through 1-8) with various scan parameters to measure acoustic noise. The measurement position of acoustic noise (●) is shown in Fig. 2. The measurement time was set to 1 min (because the scan time for DWI using single-shot echo planar imaging used in routine clinical examination is approximately 1 min). The maximum value during the measurement period was used as the peak sound pressure level (L_{peak}) (dB). Scans were performed 10 times to decrease sampling error, and the average value was calculated. An acoustic sound measurement system (Kenneth Inc. : YC-30) was used. The settings of the acoustic noise measurement system are as follows : the frequency-weighting characteristic was

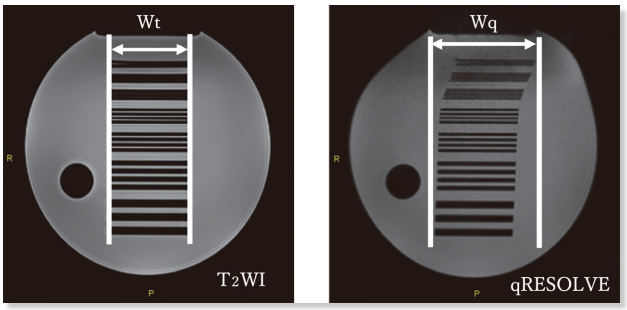

Fig. 1 Slit width measuring method

Straight lines were drawn at the slits on both ends ; Wt was measured on T_2WI, and Wq was measured using qRESOLVE.

Table 1-1 Imaging parameters of qRESOLVE with various ES values

ES (ms)	0.5	0.6	0.7	0.78	0.94	1
TR (ms)			4500			
TE (ms)	83	92	100	107	122	127
Band width (Hz/pixel)	620	465	372	318	250	228
FOV (mm)			220×220			
Slice thickness (mm)			5			
Slice gap (%)			20			
MS			192×192			
number of excitations			1			
SEG			7			
PIF			GRAPPA 2			
PpF			Off			
Fat suppression			CHESS			
b-factor (s/mm^2)			0, 1000			
Reacquistion mode			on			
Filter	Raw filter, Distortion Correction (2D), Prescin Normalize					

Table 1-2 Imaging parameters of qRESOLVE with various PIF values

PIF	2	3	4
TR (ms)		4500	
TE (ms)	122	94	81
Band width (Hz/pixel)	250	260	277
FOV (mm)		220×220	
Slice thickness (mm)		5	
Slice gap (%)		20	
MS		192×192	
number of excitations		1	
SEG		7	
ES (ms)		0.94	
PpF		Off	
Fat suppression		CHESS	
b-factor (s/mm^2)		0, 1000	
Reacquistion mode		on	
Filter	Raw filter, Distortion Correction (2D), Prescin Normalize		

Table 1-3 Imaging parameters of qRESOLVE with various SEG values

SEG	3	5	7	9	11
TR (ms)			4500		
TE (ms)	122	122	122	122	122
Band width (Hz/pixel)	521	326	250	207	176
FOV (mm)			220×220		
Slice thickness (mm)			5		
Slice gap (%)			20		
MS			192×192		
number of excitations			1		
PIF			GRAPPA 2		
ES (ms)			0.94		
PpF			Off		
Fat suppression			CHESS		
b-factor (s/mm^2)			0, 1000		
Reacquistion mode			on		
Filter	Raw filter, Distortion Correction (2D), Prescin Normalize				

Table 1-4 Imaging parameters of qRESOLVE with various PpF values

PpF	Off	7/8	6/8
TR (ms)		4500	
TE (ms)	122	101	81
Band width (Hz/pixel)		250	
FOV (mm)		220×220	
Slice thickness (mm)		5	
Slice gap (%)		20	
MS		192×192	
number of excitations		1	
PIF		GRAPPA 2	
SEG		7	
ES (ms)		0.94	
Fat suppression		CHESS	
b-factor (s/mm^2)		0, 1000	
Reacquistion mode		on	
Filter	Raw filter, Distortion Correction (2D), Prescin Normalize		

Table 1-5 Imaging parameters of qRESOLVE with various MS values

MS	128×128	160×160	192×192	226×226
TR (ms)		4500		
TE (ms)	94	108	122	137
Band width (Hz/pixel)	275	256	250	240
FOV (mm)		220×220		
Slice thickness (mm)		5		
Slice gap (%)		20		
number of excitations		1		
SEG		7		
PIF		GRAPPA 2		
ES (ms)		0.94		
PpF		Off		
Fat suppression		CHESS		
b-factor (s/mm^2)		0, 1000		
Reacquistion mode		on		
Filter	Raw filter, Distortion Correction (2D), Prescin Normalize			

Table 1-6 Imaging parameters of qRESOLVE with various TR values

TR (ms)	4030	4500	5000	5500	6000
TE (ms)			122		
Band width (Hz/pixel)			250		
FOV (mm)			220×220		
Slice thickness (mm)			5		
Slice gap (%)			20		
MS			192×192		
number of excitations			1		
SEG			7		
PIF			GRAPPA 2		
ES (ms)			0.94		
PpF			Off		
Fat suppression			CHESS		
b-factor (s/mm^2)			0, 1000		
Reacquistion mode			on		
Filter	Raw filter, Distortion Correction (2D), Prescin Normalize				

Table 1-7 Imaging parameters of qRESOLVE with various FOV values

FOV (mm)	100×100	150×150	200×200	250×250	300×300
TR (ms)			4500		
TE (ms)			122		
Band width (Hz/pixel)	277	260	250	241	237
Slice thickness (mm)			5		
Slice gap (%)			20		
MS			192×192		
number of excitations			1		
SEG			7		
PIF			GRAPPA 2		
ES (ms)			0.94		
PpF			Off		
Fat suppression			CHESS		
b-factor (s/mm^2)			0, 1000		
Reacquistion mode			on		
Filter	Raw filter, Distortion Correction (2D), Prescin Normalize				

Table 1-8 Imaging parameters of qRESOLVE with various ST values

ST (mm)	1	3	5	7	10
TR (ms)			4500		
TE (ms)			122		
Band width (Hz/pixel)			250		
FOV (mm)			220×220		
Slice gap (%)			20		
MS			192×192		
number of excitations			1		
SEG			7		
PIF			GRAPPA 2		
ES (ms)			0.94		
PpF			Off		
Fat suppression			CHESS		
b-factor (s/mm^2)			0, 1000		
Reacquistion mode			on		
Filter	Raw filter, Distortion Correction (2D), Prescin Normalize				

Table 2 Imaging parameters of T$_2$WI

	T$_2$WI
TR (ms)	4500
TE (ms)	88
Band width (Hz/pixel)	193
FOV (mm)	220×220
Slice gap (%)	20
MS	192×192
Slice thickness (mm)	5
number of excitations	1
PIF	no used
ES (ms)	9.8
Filter	Distortion Correction (2D), Prescin Normalize

set to C, and the time-weighting characteristic was set to Fast. Furthermore, we calculated the sound pressure level (dB) between the

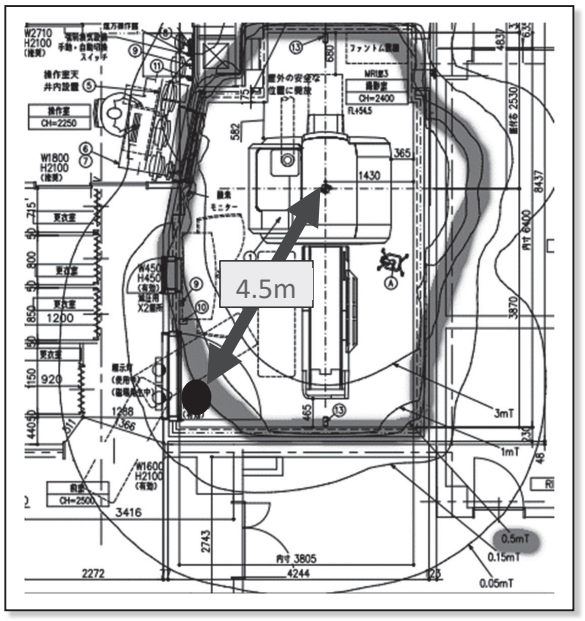

Fig. 2 Acoustic noise and time waveform measurement position

The black dot (●) shows the measurement position for acoustic noise and time waveform analysis. The distance from the center of the gantry was approximately 4.5 m and was located outside the five Gaussian lines (gray lines). The height of the measurement point was 1.3 m above the ground.

maximum and minimum of L_{peak} using various parameters and Eq. (2)[8] :

$$\text{Sound pressure level (dB)} = 20\log_{10}(A/Ao) \quad \cdots\cdots\cdots (2)$$

where A is the observed value and Ao is the reference value (20×10^{-6}[Pa]).

4.2. Time waveform analysis

The spherical phantom was scanned by qRESOLVE with various scan parameters (Tables 1-1 through 1-8) to analyze the time waveform of acoustic noise. The recording position of acoustic noise (●) is shown in Fig. 2. The recorded data was transferred to a personal computer (Microsoft Surface Pro3), and the time waveform was analyzed. A recording device for acoustic noise (TASCAM Inc. : DR-05X) was used. Frequency analysis software (NCH software Inc. : WavePad audio editing software) was used.

5. Statistical analysis

The distortion rate and acoustic noise (L_{peak}) obtained from the phantom experiment were evaluated to determine significant differences using the Friedman test. The signifacance level was set at 5%, and it was corrected using the Bonferroni method for multiple comparisons. EZR[9] was used for statistical analysis.

Results

1. Examination of distortion rate

1-1. Distortion rate with various ES values

The distortion rates with various ES values are listed in Table 3-1. The distortion rate increased with an increase in ES. There was a significant difference between ES values ($p<0.008$).

Table 3-1 Distortion rate with various ES values

ES (ms)	0.5	0.6	0.7	0.78	0.94	1
distortion rate (%)	115.8	118.3	121.3	123.4	128.2	130.6

1-2. Distortion rate with various PIF values

The distortion rates with various PIF values are listed in Table 3-2. The distortion rate decreased with an increase in PIF. There was a significant difference between PIF values ($p<0.017$).

Table 3-2 Distortion rate with various PIF values

PIF	2	3	4
distortion rate (%)	121.0	114.1	111.2

1-3. Distortion rate with various SEG values

The distortion rates with various SEG values are listed in Table 3-3. There was no change in the distortion rate with an increase in SEG. No significant difference was observed between any of the SEG values ($p>0.01$).

Table 3-3 Distortion rate with various SEG values

SEG	3	5	7	9	11
distortion rate (%)	119.2	119.2	119.2	119.3	119.3

1-4. Distortion rate with various PpF values

The distortion rates with various PpF values are shown in Table 3-4. The distortion rate decreased with a decrease in PpF. There was a significant difference between any PpF values ($p<0.017$).

Table 3-4 Distortion rate with various PpF values

PpF	Off	7/8	6/8
distortion rate (%)	120.9	121.5	123.6

1-5. Distortion rate with various TR values

The distortion rates with various TR values are shown in Table 3-5. No significant difference was observed between the TR values ($p>0.01$). TR did not affect the distortion rate.

Table 3-5 Distortion rate with various TR values

TR (ms)	4030	4500	5000	5500	6000
distortion rate (%)	120.9	120.9	120.9	120.8	120.9

1-6. Distortion rate with various MS values

The distortion rates with various MS values are shown in Table 3-6. The distortion rate decreased with an increase in MS. There was a significant difference between MS values ($p<0.013$).

Table 3-6 Distortion rate with various MS values

MS	128×128	160×160	192×192	226×226
distortion rate (%)	119.4	118.3	117.6	117.2

1-7. Distortion rate with various ST values

The distortion rates with various ST values are listed in Table 3-7. The distortion rate increased with increasing ST. There was a significant difference between ST values ($p<0.01$).

Table 3-7 Distortion rate with various ST values

ST (mm)	1	3	5	7	10
distortion rate (%)	113.0	114.4	118.4	120.2	123.0

Table 3-8 Distortion rate with various FOV values

FOV (mm)	100×100	150×150	200×200	250×250	300×300
distortion rate (%)	not measured	113.6	118.4	123.5	128.7

1-8. Distortion rate with various FOV values

The distortion rates with various FOV values are listed in Table 3-8. The distortion rate increased with an increase in the FOV. There was a significant difference between FOV values ($p<0.013$).

2. Examination of acoustic noise

2-1. Examination of L_{peak}

2-1-1. L_{peak} with various ES values

The results for L_{peak} with various ES values are shown in Table 4-1.With an increase in ES, L_{peak} decreased to 0.94 ms. There was a significant difference between all ES values except between 0.7 and 0.78 ms ($p<0.008$). Using this result, the phantom experiment was set to 0.94 ms (minimum value of L_{peak}). There was a level difference of 14.1 dB between the maximum (with an ES of 0.5 ms) and minimum (with an ES of 0.94 ms). According to Eq.(2), the sound pressure level with an ES of 0.5 ms was 5.1 times higher than that with an ES of 0.94 ms.

2-1-2. L_{peak} with various PIF values

The results for L_{peak} with various PIF values are listed in Table 4-2. L_{peak} increased with increasing PIF. There was a significant difference between PIF values ($p<0.017$). There was a level difference of 1.6 dB between the maximum (with a PIF of 4) and minimum (with a PIF of 2). According to Eq.(2), the sound pressure level with a PIF of 4 was 1.2 times higher than that with a PIF of 2.

2-1-3. L_{peak} with various SEG values

The results for L_{peak} with various SEG values are listed in Table 4-3. L_{peak} decreased with increasing SEG, and there was a significant difference between SEGs values ($p<0.01$). There was a level difference of 4.7 dB between the maximum (with a SEG of 3) and minimum (with a SEG of 11). According to Eq.(2), the sound pressure level with a SEG of 3 was 1.7 times higher than that with a SEG of 11.

Table 4-1 L_{peak} with various ES values

ES (ms)	0.5	0.6	0.7	0.78	0.94	1
L_{peak} (dB)	94.8	87.7	86.6	86.8	80.7	81.7

Table 4-2 L_{peak} with various PIF values

PIF	2	3	4
L_{peak} (dB)	82.2	83.2	83.8

Table 4-3 L_{peak} with various SEG values

SEG	3	5	7	9	11
L_{peak} (dB)	86.3	83.4	82.6	81.9	81.6

Table 4-4 L_{peak} with various PpF values

PpF	Off	7/8	6/8
L_{peak} (dB)	82.4	82.3	82.5

Table 4-5 L_{peak} with various TR values

TR (ms)	4030	4500	5000	5500	6000
L_{peak} (dB)	82.9	82.7	82.4	82.3	82.2

Table 4-6 L_{peak} with various MS values

MS	128×128	160×160	192×192	226×226
L_{peak} (dB)	82.1	82.1	82.8	82.5

Table 4-7 L_{peak} with various ST values

ST (mm)	1	3	5	7	10
L_{peak} (dB)	83.0	82.9	82.8	82.8	82.8

Table 4-8 L_{peak} with various FOV values

FOV (mm)	100×100	150×150	200×200	250×250	300×300
L_{peak} (dB)	82.9	82.7	82.4	82.3	82.2

2-1-4. L_{peak} with various PpF values

The results for L_{peak} with various PpF values are listed in Table 4-4. L_{peak} showed almost no change with decrease in PpF. There was no significant difference between any PpF values ($p>0.017$). There was a level difference of 0.2 dB between the maximum (with a PpF of 6/8) and minimum (a PpF of 7/8) with various PpF. According to Eq.(2), the sound pressure level with a PpF of 6/8 was 1.0 times higher than that with a PpF of 7/8.

2-1-5. L_{peak} with various TR values

The results for L_{peak} with various TR values

are shown in Table 4-5. L_{peak} decreased slightly with an increase in TR. There was a significant difference, except for between TR 5000 ms and TR 5500 ms and between TR 5500 ms and TR 6000 ms ($p<0.01$). There was a level difference of 0.7 dB between the maximum (with a TR of 4030 ms) and minimum (with a TR of 6000 ms) with various TR. According to Eq.(2), the sound pressure level with a TR of 4030 ms was 1.1 times higher than that with a TR of 6000 ms.

2-1-6. L_{peak} with various MS values

The results for L_{peak} with various MS values are shown in Table 4-6. L_{peak} increased slightly with increasing MS. There was a significant difference, except for between MS 128 × 128 and MS 160 × 160 ($p<0.013$). There was a level difference of 0.4 dB between the maximum (with a MS of 192 × 192) and minimum (with MS values of 128 × 128 or 160 × 160). According to Eq.(2), the sound pressure level with a MS of 192 × 192 was1.1 times higher than that with MS values of 128 × 128 or 160 × 160.

2-1-7. L_{peak} with various ST values

The results for L_{peak} with various ST values are shown in Table 4-7. L_{peak} was not affected by ST. There was no significant difference between any ST values ($p>0.01$). There was a level difference of 0.2 dB between the maximum (with a ST of 1 mm) and minimum (with ST values of 5, 7, or 10 mm). According to Eq.(2), the sound pressure level with a ST of 1 mm was 1.0 times higher than that with ST values of 5, 7, or 10 mm.

2-1-8. L_{peak} with various FOV values

The results for L_{peak} with various FOV values are shown in Table 4-8. L_{peak} decreased with increasing FOV. There was a significant difference, except for between FOV 200 × 200 mm and FOV 250 × 250 mm, and between FOV 250 × 250 mm and FOV 300 × 300 mm ($p<0.01$). There was a level difference of 0.7 dB between the maximum (with a FOV of 100 × 100 mm) and minimum (with a FOV of 300 × 300 mm) with various FOV. According to Eq.(2), the sound pressure level with a FOV of 100 × 100 mm was 1.1 times higher than that with a FOV of 300 × 300 mm.

2.2. Time waveform analysis

The time waveforms of acoustic noise measured with changes in various parameters are shown in Fig. 3-10. In the time waveform, the horizontal axis represents time (ms), and the vertical axis represents sound pressure (dB). Wada et al.[10] reported that the amplitude of the vertical axis of the time waveform increases as the acoustic noise increases. The results of this study showed that the amplitude of the time waveform decreased with increase in ES, FOV, and SEG, and slightly decreased with decreases in PIF and MS. The amplitude of the time waveform showed little change with any of the other parameters.

Discussion

Acoustic noise in MRI, especially in DWI using single-shot echo planar imaging, is very loud, and decreasing this noise is important for decreasing discomfort and anxiety during routine clinical examinations and preventing hearing impairment. In this study, we investigated the parameters of qRESOLVE that were effective for decreasing image distortion and acoustic noise.

First, we consider image distortion. With respect to ES, the distortion rate increased with an increase in ES. With an increase in ES, the bandwidth (BW) was automatically set to narrow, resulting in an increased phase dispersion and thus an increased distortion rate. Regarding the PIF, the distortion rate decreased with an increase in the PIF. When the reading time was shortened in the phase direction, the BW was automatically set to a

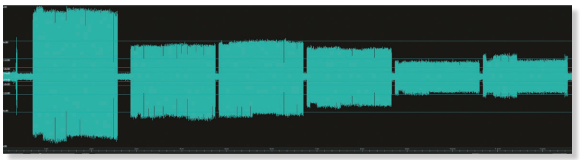

Fig. 3 Waveforms of qRESOLVE with various ES values (from left to right: 0.5, 0.6, 0.7, 0.78, 0.94, and 1.0 ms)

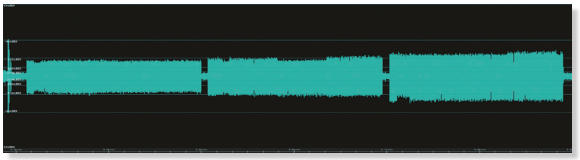

Fig. 4 Waveforms of qRESOLVE with various PIF values (from left to right: 2, 3, and 4)

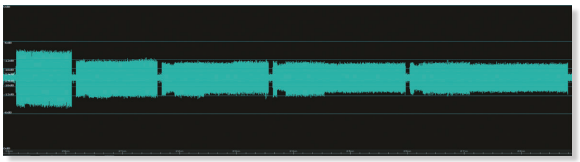

Fig. 5 Waveforms of qRESOLVE with various SEG values (from left to right: 3, 5, 7, 9, and 11)

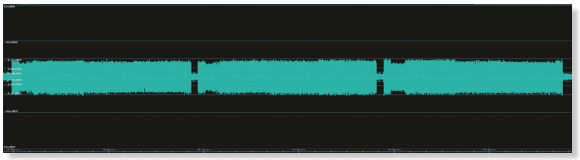

Fig. 6 Waveforms of qRESOLVE with various PpF values (from left to right: Off, 7/8, and 6/8)

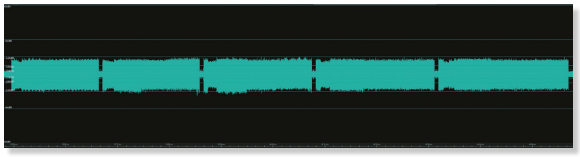

Fig. 7 Waveforms of qRESOLVE with various TR values (from left to right: 4030, 4500, 5000, 5500, and 6000 ms)

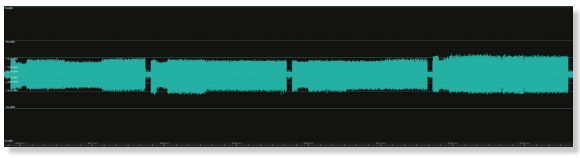

Fig. 8 Waveforms of qRESOLVE with various MS values (from left to right: 128×128, 160×160, 192×192, and 226×226)

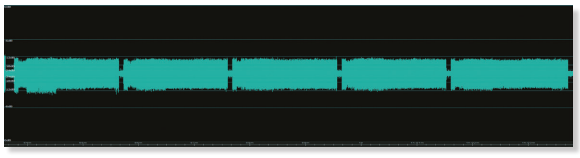

Fig. 9 Waveforms of qRESOLVE with various ST values (from left to right: 1, 3, 5, 7, and 10 mm)

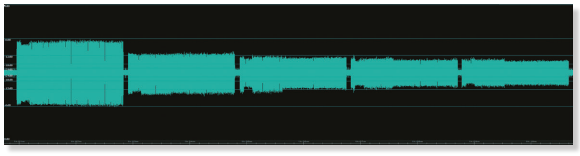

Fig. 10 Waveforms of qRESOLVE with various FOV values (from left to right: 100×100, 150×150, 200×200, 250×250, and 300×300 mm)

wide range, resulting in suppressed dephasing and thus a decreased distortion rate.

Concerning the SEG, with an increase in the SEG, the segment width decreased to divide k-space, thus decreasing the readout time. As a result, it is expected to be effective in suppressing dephasing and decreasing image distortion. However, there was no significant difference in the distortion rate between SEGs. With an increase in SEG, the reading time of each SEG decreased, but the BW was automatically set to a narrow range; thus, the distortion rate was not change. With respect to the PpF, the distortion rate decreased with an increase in PpF. Blurring was suppressed and the distortion rate decreased with an increase in the data filling of k-space, although the BW and echo time (TE) did not change with an increase in PpF. Regarding the TR, the distortion rate did not change with an increase in TR. The BW and TE did not change with increasing TR. Concerning MS, the distortion rate decreased with an increase in MS. The BW automatically narrowed with an increase in MS, but the magnetic field deflection in the voxel decreased, resulting in a decreased distortion rate[11]. With respect to ST, the distortion rate increased with increasing ST. The BW did not change with the ST thickness, but the magnetic field deflection in the voxel increased, resulting in an increased distortion rate[11]. Regarding the FOV, the distortion rate increased with increasing FOV. The BW automatically narrowed with an increase in

FOV, and the spatial resolution also increased. Therefore, the ES, PIF, MS, ST and FOV are effective parameters for decreasing the distortion rate. However, in routine clinical examinations, MS, ST and FOV change the spatial resolution. Thus, the MS, ST and FOV are not appropriate parameters. Furthermore, it is appropriate to set PpF to "off" to avoid image distortion resulting from blurring. Therefore, a decrease in ES and an increase in PIF are effective for decreasing image distortion.

Next, we consider acoustic noise. Concerning ES, L_{peak} decreased with an increase in ES. The BW was automatically set to narrow with an increase in ES, resulting in a decrease in the angle of the gradient field. With respect to the PIF, L_{peak} increased with an increase in the PIF. The intensity of the blip applied in the phase direction increased because of the wide interval of the collected data, resulting in an increase in the angle of gradient field. Regarding the SEG, L_{peak} decreased with an increase in SEG. The BW automatically narrowed with an increase in SEG, resulting in a decrease in the angle of the gradient field. However, the scan time increased threefold with an increase in SEG (from a SEG of 3 to a SEG of 11); thus, parameter settings with an increase in SEG should be avoided. Concerning the PpF, L_{peak} did not change with increasing PpF. The BW and TE did not change with increasing PpF. With respect to the TR, L_{peak} decreased slightly with an increase in TR. It was assumed that the BW and TE did not change, but acoustic sound was slightly lower in the longer TR than in shorter TR because the interval between acoustic sounds was wide and less affected by reverberation. Regarding the MS, L_{peak} increased slightly with an increase in MS. The BW automatically narrowed and TE increased. Generally, with a narrow in BW, resulting in a decrease in the angle of the gradient field and the acoustic noise is small. However, because the amplitude of the gradient increased simultaneously, L_{peak} was assumed to be increase. Concerning the ST, L_{peak} did not change with the thickness of ST. The BW and TE did not change with the thickness of ST. With respect to the FOV, L_{peak} decreased slightly with an increase in the FOV. With an increase in FOV, the BW was automatically set to narrow, resulting in a decrease in the angle of the gradient field. We calculated the sound pressure level difference between the maximum and minimum values of L_{peak} with various parameters using Eq.(2). The maximum value of L_{peak} was 5.1 times higher than the minimum value in ES, 1.1 times higher for FOV, 1.7 times higher for SEG, and 1.2 times higher for PIF. This suggests that an increase in ES is the most effective way to decrease acoustic noise. Individual differences in hearing are common. A decrease in acoustic noise is considered important to prevent hearing impairment. Furthermore, time waveform analysis of acoustic noise showed that an increase in ES, FOV and SEG, and a decrease in PIF and MS, are effective for decreasing the acoustic noise. Therefore, the effective parameters for decreasing acoustic noise are ES, PIF, SEG, TR, MS, and FOV. However, in routine clinical examinations, an increase in SEG prolongs scan time and increased the possibility of artifacts caused by body motion. Therefore, a parameter setting with an SEG of 9 or higher is not appropriate. With an increase in TR, the scan time increases and the image contrast changes, while with an increase in MS, ST, and FOV, the spatial resolution changes, so they are not appropriate parameters. Therefore, an increase in ES and SEG and a decrease in PIF are effective for decreasing acoustic noise. ES, PIF, and MS are common parameters employed for decreasing image distortion and acoustic noise. However, an increase in ES decreases acoustic noise and increases image distortion, whereas a decrease in PIF and MS decreases

acoustic noise and increases image distortion. Therefore, there is a trade-off relationship in the parameter setting, and further study is required. In the future, to determine the optimal scan parameter setting for decreasing image distortion and acoustic noise, we plan to evaluate the head MRI images of healthy volunteers.

Conclusion

In qRESOLVE, a decrease in image distortion was achieved with a decrease in ES and FOV, a thin slice thickness, and an increase in PIF and MS ($p<0.017$). Furthermore, a decrease in acoustic noise was achieved with an increase in ES, SEG, TR, and FOV and a decrease in PIF and MS ($p<0.017$). However, in routine clinical examinations, a decrease in ES and an increase in PIF are effective for decreasing image distortion, and with an increase in ES, and an increase in SEG and a decrease in PIF are effective for decreasing acoustic noise.

Conflict of interest

The author has no conflict of interest to declare.

Funding

The author received no specific funding for this work.

Acknowledgements

I would like to thank Professor Yoko Saito for her warm guidance and encouragement.

I would like to express my sincere appreciation.

References

1) M. E. Bastin: Correction of eddy current-induced artefacts in diffusion tensor imaging using iterative cross-correlation. Magn Reson Imaging, 17(7), 1011-1024, 1999.
2) D. A. Porter, et al.: High resolution diffusion-weighted imaging using readout-segmented echo-planar imaging, parallel imaging and a two-dimensional navigator-based reacquisition. Magn Reson Med, 62(2), 468-475, 2009.
3) O. Martin, et al.: Acoustic-noise-optimized diffusion-weighted imaging. Magn Reson Mater Phy, 28, 511-521, 2015.
4) R. Julie, et al.: Quiet Diffusion-Weighted Head Scanning: Initial Clinical Evaluation in Ischemic Stroke Patients at 1.5T. J. MAGN. RESON. IMAGING, 44(5), 1238-1243, 2016.
5) M. A. Griswold, et al.: Generalized Autocalibrating Partially Parallel Acquisitions (GRAPPA). Magn Reson Med, 47(6), 1202-1210, 2002.
6) Y. Kaneko, et al.: Using the area mismatch with SE images to evaluate the distortion of EPI. Japan Journal of Magnetic Resonance in Medicine, 36(3), 98-105, 2016.
7) M.Kajisako, et al.: Experience with Siemens' RESOLVE (readout segmented EPI DWI). Rad Fun,10(5), 11-14, 2012.
8) K. Kuno, et al.: Acoustic noise measurement and evaluation/dB and LAeq. Tokyo, Japan, Gihoudo publishing co., 28-31, 2006.
9) Y. Kanda : Investigation of the freely available easy-to-use software "EZR"(Easy R)for medical statistics. Bone Marrow Transplantation, 48, 452-458, 2013.
10) T. Wada, et al.: Analysis of the acoustic sound in MRI. Oto-Rhino-Laryngology, Tokyo, 42(1), 131-135, 1999.
11) T. Aoki, et al.: 3-Tesla MR Imaging of the pelvis. Japanisch-Deutsche Medizinische Berichte, 52(1), 47-52, 2007.

Regulations and Requirements for Submissions to the Journal of the Japan Association of Radiological Technologists

Submission Regulations

Revised: April 1, 2013
October 30, 2013
February 20, 2016
April 20, 2019
October 3, 2020
July 9, 2022
December 3, 2022

Objective

Article 1. These regulations are based on the operations defined in Article 4 of the articles on the incorporation of the Japan Association of Radiological Technologists (hereafter "the Association"). They stipulate the criteria for submissions to the Journal and informational magazines published by the Association (hereafter "the Journal, etc.").

Eligibility

Article 2.

2-1. Only members of this association are allowed to submit articles to the association's journal, etc.

2-2. However, the following requirements must be met in order to submit articles:

(1) Students of radiologic technology schools who have a member of this association as a co-author.

(2) Individuals with a foreign nationality who hold a radiologic technologist license.

(3) Non-members other than the above may submit articles by paying half of the association membership fee per article as a submission fee.

2-3. The submission fee stated in the preceding paragraph 3 will not be refunded regardless of whether the article is accepted or not.

2-4. Co-authors do not need to pay the submission fee.

Copyright

Article 3. The copyright of the published manuscript is based on rules regarding the management of the works of the Society.

Obligations

Article 4.

4-1. The topic of submitted manuscripts must belong to a relevant domain to technologies for prevention, diagnosis, and treatment related to radiation therapy, and manuscripts must be unpublished.

4-2. Submitted papers, whether for fundamental or applied research, must sufficiently consider bioethics, and authors must bear the ultimate responsibility for their content.

4-3. Fabrication, forgery, plagiarism, violation of the law, and other forms of wrongdoing are not allowed in submissions.

4-4. If the author has already reported similar content to that of the published manuscript or submitted it to another journal, the author is required to explain the difference from the manuscript in a separate document.

4-5. The author must disclose all information regarding conflicts of interest.

4-6. The author shall be held accountable for any misconduct regarding the content of the publication, and the Society shall not be involved at all.

Submissions

Article 5. The types of accepted submissions are categorized as follows:

(1) Original articles
Highly original research papers with clear objectives and conclusions.

(2) Review articles
Articles systematically summarizing a specific research domain from a particular perspective.

(3) Rapid communications
Reports of original research that must be published rapidly.

(4) Reports
Surveys of significance to the study of radiological technology or reports of interesting and

important cases.

(5) Notes

Articles on the development or evaluation of new equipment, techniques, products, etc.

(6) Technical material

Compilations of survey data or technical aspects, or anything that can serve as a reference for research and technology.

(7) Overview articles

A compilation of technologies, principles, or basic elements with reference to the literature. However, what was explained in the development and use of equipment and software constitutes a technical explanation.

(8) Miscellaneous

Other items approved by the editorial committee for publication, such as lecture transcripts, courses published as journal articles, and newspaper/magazine articles that were not published in Issues 1–7.

How to submit

Article 6.

6-1. Use the online posting system.

6-2. The author shall save the duplicate data of the submitted manuscript until the publication decision.

Formatting

Article 7. The explanation of the manuscript shall be provided according to the submission procedure specified separately.

Reception of submissions

Article 8. The reception date shall be the date on which the editorial board has determined to comply with this regulation.

Review

Article 9.

9-1. Received manuscripts will be reviewed carefully and impartially by peer-reviewers selected by the editorial committee.

9-2. Peer reviews are limited to two times. However, in the case of Article 5, items 7 and 8, in principle, peer review is not performed.

9-3. The acceptance or rejection of the manuscript will be decided by the editorial committee in consideration of the opinions of the reviewers, and the date will be the final acceptance date.

Corrections

Article 10.

10-1. In principle, the author must proofread the manuscript up to twice and return it by the designated date. If the deadline is breached, the school will be completed with the proofreading of the editorial board.

10-2. The correction of words and plates that were not included in the manuscript is not allowed.

Printing

Article 11.

11-1. 20 copies of the papers published in the Journal, etc., will be presented to their authors as an offprint.

11-2. The authors must bear the expenses of any additional offprints. If additional offprints are required, they must be requested by the time corrections are submitted.

Revision or repeal of regulations

Article 12.

12-1. This regulation will come into effect on April 1, 2012.

12-2. This regulation will come into effect on April 1, 2016.

12-3. This regulation will come into effect on April 20, 2019.

12-4. This regulation will come into effect on October 3, 2020.

12-5. This regulation will come into effect on July 9, 2022.

12-6. This regulation will come into effect on December 3, 2022.

Requirements for Submissions to the Journal of the Japan Association of Radiological Technologists

Revised: February 20, 2016
April 20, 2019
October 3, 2020
July 19, 2023

Based on Article 7 of the Submission Regulations of the Japan Association of Radiological Technologists, the following guidelines must be followed for manuscript submission:

1. How to write original articles, reviews, breaking news, reports, notes, materials, and explanations

1) Title and abstract

Enter the following items in the online posting system.

①List the author's name, institution, affiliation and occupation, and select the field of expertise. The author's qualifications should be as specified in the submission guidelines.

②Select the type of post.

③Provide the title in both Japanese and English, and include information about the co-authors. List the co-authors in the order of authorship. If a co-author is not a radiological technologist, their qualifications should be as specified in the submission guidelines.

④Summarize the abstract in Japanese and English within 300 characters (words).

⑤Enter the keywords in English. Keywords should be in noun forms and should be limited to five.

2) Text and figures/tables

Create the main text, including figures and tables, in a single file. Additionally, prepare figures and tables as separate files and submit them.

①The manuscript should be in Japanese or English.

Create the document using Word with A4 paper size. Use Mincho font for Japanese text and Times font for English text, both at 12 points. Set the line spacing to 18 points. Leave a margin of at least 2 cm on all sides (top, bottom, left, and right).

②The specified number of pages and excess page costs of the manuscript are as shown in the following table.

Type of submission	Number of pages (as published)	Fee for additional pages
Original articles	8	¥10,000 per page
Review articles	8	
Rapid communications	3	
Reports	3	
Notes	8	
Technical material	8	
Overview articles	8	
Technical overview articles	4–6	None
Miscellaneous	2 (strictly enforced)	

③As a general rule, academic terms should conform to Cabinet Notification No. 2 and JIS.

④The unit of quantity is the International System of Units (SI).

⑤Include page numbers and line numbers in the main text.

⑥Use ", " and ". " for punctuation.

⑦Use full-width characters for Katakana and half-width characters for English letters and numbers.

⑧The main text should be structured with headings such as Introduction, Methods, Results, Discussion, Conclusion, and References.

⑨For equipment, include the generic name, model, manufacturer, city, and country.

⑩Number the equations.

⑪The figures and tables created as separate files from the main text are of higher resolution and can be subjected to secondary processing in production.

⑫Number the figures and tables.

⑬Ensure that all figure and table numbers are referenced in the main text.

⑭For academic papers, write the titles of figures and tables, as well as the text within the tables, in English.

⑮Provide Japanese explanations for figures and tables.

⑯When reproducing figures and tables, clearly indicate the source and ensure that the author has obtained permission from the original source.

3) References

References should be listed in the order in which they appear, with the numbers in parentheses at the end of the referenced text.

The notation format is as follows.

①For magazines

Author names: Title (article title) Magazine name (abbreviation), volume, first-last page, year of publication.

②For a book

Author names: Book title, First-last page, publisher, year of publication.

③If there are two or more authors, enter only the first author and enter “other” and “et al.”

4) Trademark name

If a trademark name is required, write the trademark name in both parentheses after the common name and add ®.

5) Acknowledgments

Create a separate file from the main text for the acknowledgments.

2. Submission of copyright transfer agreement

(1) The first author and co-authors must agree to the contents of the copyright transfer agreement as specified in the copyright regulations.
(2) The copyright transfer agreement should be as specified in the copyright regulations, and the designated form available on the society's website must be used.
(3) The copyright transfer agreement must be signed by the first author and co-authors, and provided when the manuscript is submitted.

3. About secondary publication

(1) Obtain approval from the editorial departments of both the first and second journals.
(2) The period until the secondary publication should be decided through discussions between the editorial departments of both parties and the author.
(3) Secondary publications of treatises are intended for different types of readerships.
(4) The secondary publication of a treatise should faithfully reflect the content of the first treatise.
(5) Specify the source of the original treatise.
(6) Specify in the title that it is a secondary publication.

4. About technical commentary requested by the editorial board

The structure of the document should generally follow the sections (1) to (9) below.

(1) Abstract (100-150 words in Japanese and English)
(2) Keywords (3 words)
(3) Introduction:
(4) Purpose of explanation (overview)
(5) Main paper
(6) Comparison and consideration with previous research (development technology)
(7) Clinical usefulness
(8) Conclusion
(9) References

Journal of JART
-English edition 2024-

June 12, 2024

Issuer: Ueda Katsuhiko
Publisher: The Japan Association of Radiological Technologists
22F Mita Kokusai Building. 1-4-28,
Mita, Minato-ku, Tokyo. 108-0073
TEL: +81-3-4226-2211　FAX: +81-50-3153-1519
https://www.jart.jp

・Published by The Japan Association of Radiological Technologists

The Japan Association of Radiological Technologists
https://www.jart.jp